Pairing fluctuations in rapidly rotating nuclei

Y. R. Shimizu* and J. D. Garrett†

The Niels Bohr Institute, University of Copenhagen, DK-2100 Copenhagen Ø, Denmark

R. A. Broglia

The Niels Bohr Institute, University of Copenhagen, DK-2100 Copenhagen Ø, Denmark and Dipartimento di Fisica, Università di Milano, and Istituto Nazionale di Fisica Nucleare, Sezione di Milano, 20133 Milano, Italy

M. Gallardo

Departamento de Fisica Atomica, Molecular y Nuclear, Universidad de Sevilla, 41080 Sevilla, Spain

E. Vigezzi

Istituto Nazionale di Fisica Nucleare, Sezione di Milano, 20133 Milano, Italy

Empirical evidence for the existence of pair fluctuations in rapidly rotating nuclei in connection with the pair gap is reviewed. The quantities considered are single-particle energies (routhians) and alignments. While the cranked shell model in the presence of static pair correlations provides an accurate description of data at rotational frequencies below the critical frequency corresponding to the collapse of the static pair gap, conspicuous discrepancies are found in the region of and above the pairing phase transition. In particular, a group of excitations is observed displaying lower excitation energies and smaller alignments than those predicted by the cranked shell model. Such excitations can be characterized as behaving as if the correlations induced by the presence of a pairing condensate were not totally obliterated after the "phase transition." A theoretical model, based on the renormalization of the single-particle motion mixed by the coupling to pairing vibrations, is quite successful in explaining the overall trend of the data at rotational frequencies larger than the critical frequency. Smaller alignments and excitation energies are correlated with configurations displaying particle coupling schemes which profit most from fluctuations of the pair gap about its zero equilibrium value. While this model reproduces many of the experimental features, it still overpredicts the alignments by 2–3 units of $\hbar$ in the crossing region. Thus other degrees of freedom (both static and dynamic), e.g., deformations, also must play a role at large rotational frequencies.

CONTENTS

*Present address: Department of Physics, Kyushu University 33, Fukuoka, 812, Japan.

†Present address: Oak Ridge National Laboratory, Oak Ridge, Tennessee 37831.

I. INTRODUCTION

It is well established that nucleons in nonclosed shells can arrange their motion to produce collective nuclear rotations. The associated Regge trajectory reveals a moment of inertia only half that of a system of independent nucleons moving in a deformed potential. This reduced moment of inertia is well accounted for assuming that nuclei in their ground state are, as a rule, superfluid (Bohr, Mottelson, and Pines, 1958).

Extending the analogy between the metallic superconducting state (Bardeen *et al.,* 1957) and the nuclear ground state, Mottelson and Valatin (1960) predicted that the Coriolis and centrifugal forces in a rapidly rotating nucleus should be sufficiently strong to induce a transition from the condensed to the "normal" phase. It took a quarter of a century to test this prediction experimentally. Only recently have the heavy-ion accelerators, capable of producing the critical angular momentum for this phase transition, been coupled with arrays of high-resolution Compton-suppressed germanium detectors (Twin *et al.,* 1983; Herskind, 1985), necessarily to detect the electromagnetic radiation connecting the higher members of the rotational bands.

In a finite system such as the nucleus, one does not, of course, expect a transition with sharp singularities as in macroscopic systems (Bohr, 1976), and consequently the effect on the observables is more subtle (see, for example, Mutz and Ring, 1984). On the other hand, the finite nuclear system provides the possibility of studying such a phase transition in terms of the individual quantum states, in the presence of strong fluctuations of the order parameter.

Fittingly, the first breakthrough was the experimental observation by Johnson, Ryde, and Sztarkier (1971) of a rapid increase in the moment of inertia at large angular momentum, $I=10-16\hbar$. This phenomenon is often called "backbending," since the rotational frequency $\omega_{\rm rot}$ often decreases in the region of increasing moment of inertia J, producing a plot of $J(\omega_{\rm rot})$ that "bends back." This behavior was correctly interpreted by Stephens and Simon (1972) as the crossing of the ground-state rotational band by a band whose intrinsic configuration has a pair of excited, or "aligned," quasiparticles. In fact, the band crossing or "backbend" occurs for the rotational frequency at which the Coriolis and centrifugal forces compensate the effects of pairing correlations for a given pair of quasiparticles, as shown by Banerjee, Mang, and Ring (1973). Thus "backbending" is the result of the "blocking" of pairing correlations for a specific pair of time-reversed orbitals, not the collapse of the pairing gap as originally proposed by Johnson, Ryde, and Sztarkier (1971). Therefore, it can be considered the finite system analog of gapless superconductivity found in metallic superconductors (Goswami *et al.,* 1967; Grin, 1974; Lin, 1974; Chu *et al.,* 1975; Ragnarsson and Broglia, 1976).

Because of the low density of single-particle levels found around the nuclear Fermi surface, it takes about two band crossings (or the excitation of three to five quasineutrons or quasiprotons) to produce the transition to the statically (neutron or proton) unpaired phase. Evidence supporting the quenching of pair correlations at large angular momentum has been obtained recently; see, for example, Schuck *et al.* (1984), Bacelar *et al.* (1985), and Garrett (1985b).

The second turning point in the study of the nuclear pairing phase transition was the recognition by Egido, Mang, and Ring (1980a, 1980b) that pairing correlations vary smoothly in the vicinity of and above the critical rotational frequency, and by Broglia (1985) and Broglia *et al.* (1985, 1986) that pairing fluctuations are important near and above the critical frequency. These two effects have a common physical basis, namely, the finite number of nucleons in the nucleus. They are equivalent to the extent that the consequences of dynamical pairing fluctuations can be described in terms of an effective pairing gap.

The work of the Munich group, in particular was seminal in the study of pairing phase transitions of systems with a finite number of particles, where the fluctuations play a central role; this was in part because techniques were devised that allowed for detailed calculations of realistic situations (e.g., Egido *et al.,* 1985). Their main result is that fluctuations dramatically affect the sharp pairing collapse predicted by mean-field theories, a result that has received complete confirmation since.

In this context it is also important to mention that, while condensation only of Cooper pairs in s states of relative motion is observed in nuclei, clear evidence for a strong d-state pairing (quadrupole pairing) also exists, as indicated by Broglia, Bés, and Nilsson (1974) and Ragnarsson and Broglia (1976). The associated pairing correlations have been shown by Wakai and Faessler (1978), by Egido and Ring (1984), and by Diebel (1984) to be less affected by nuclear rotation than those arising from monopole pairing. In particular, Diebel concluded that quadrupole pairing is important in the calculation of the crossing frequencies between the ground-state band and the two-quasiparticle band. Recently it has been suggested by Bertsch, Broglia, and Schrieffer (1988) that superfluidity with nonzero angular momentum may be permitted in rotating nuclei, leading to a nuclear vortex. However, it appears that the associated excitation energy is too high to have observable consequences.

The most effective way to disentangle the roles played by static and dynamic pairing correlations close to the yrast line is by probing the nucleus with two-particle-transfer reactions in heavy-ion collisions where the target is Coulomb excited to states of high angular momenta (Dasso *et al.,* 1984; Broglia, 1985; Nazarewicz, Dudek, and Szymański, 1985; Egido and Rasmussen, 1987). These studies could reveal not only the magnitude, but also the phase of the transfer amplitude (Canto *et al.,* 1987; Nikam and Ring, 1987; Nikam, Ring, and Canto, 1987; Vigezzi *et al.,* 1988).

While for angular momenta smaller than the critical

momentum associated with pairing collapse it is expected that tunneling of s Cooper pairs essentially populates only the ground state of the target nucleus, for rotational frequencies higher than the critical, the tunneling strength will be distributed over a wide range of energies, associated with the fluctuations of the pairing gap around the zero equilibrium value (Broglia and Gallardo, 1985; see also Egido, Mang, and Ring, 1980a).

Situations similar to the one described above, but as a function of the rotational frequency in gauge space—i.e., Fermi energy or number of particles—are well established (see, for example, Broglia, Hansen, and Riedel, 1973, and references therein). On the other hand, although much progress has been made in the experimental study of Cooper tunneling following Coulomb excitation (Guidry, 1986; Butler *et al.*, 1987; Juutinen *et al.*, 1987; Wu *et al.*, 1987, 1988), no clear picture of pairing collapse has yet emerged from these studies, essentially due to the complexity of the associated heavy-ion reaction mechanism.

The dynamical interpretation of the stability of pairing correlations has a counterpart in infinite systems vis-à-vis the Meissner effect. The magnetic field is slowly expelled from the interior of a large metallic probe as the transition temperature is approached from above. This phenomenon, the analog of a reduction in the intrinsic alignment in the paired nucleus, is in conflict with theories that ignore fluctuations. Such theories predict that the internal field will drop off sharply to zero at the transition point. The onset of the Meissner effect has been observed by Gollub *et al.* (1969).

Pairing vibrations were suggested by Bohr and Mottelson and introduced in nuclear physics by Bés and Broglia (1966; see also Högaasen-Feldman, 1961). For nonnuclear superfluids these vibrations are hardly collective. In the treatment of Anderson (1958) they are associated with bound pairs appearing at the top of the pairing gap.

Pairing vibrations become strongly collective in near-closed-shell nuclei where, because of the large gap existing in these cases in the single-particle spectrum of states, the pairing interaction is unable to scatter time-reversed pairs of particles across the Fermi surface. Thus a clear distinction exists between particles and holes, and all the collectivity of the time-reversal response function is concentrated in the pair-addition and pair-removal modes. These modes, whose identity is not associated with a given isotope, can be viewed as elementary excitations. Pair vibrations were first observed by Bjerregaard *et al.* (1966) in the transfer of two neutrons (a single Cooper pair) leading to ^{208}Pb. Systematic evidence exists for this mode throughout the mass table (Broglia, Hansen, and Riedel, 1973).

In the case of rapidly rotating nuclei, in which the scattering of particle pairs is hindered by the poor overlap existing between time-reversed single-particle orbitals, the situation is quite different. While the system can display important pair fluctuations, as shown by the Munich group, the time-reversal strength is distributed over many states. Such a spectrum is typical of a collective mode in the presence of strong Landau damping (Pines and Nozières, 1966). A situation similar to this, although in the particle-hole channel, is found in the case of the paramagnon in liquid ^{3}He (Baym and Pethick, 1975). In fact, the paramagnon is not a real, but a virtual excitation with a diffusive motion. Although not directly observed in the absence of a magnetic field, it has important consequences for the specific heat (effective mass) of the system. Similarly, even if pairing vibrations in the unpaired regime of rapidly rotating nuclei cannot be observed directly, their effects can still be detected by the presence of configurations that systematically lie at lower excitation energies and display less alignment than predicted by the cranked shell model.

The effects of a fluctuating pairing gap have previously been considered at large rotational frequencies by the Copenhagen group (Broglia, 1985; Broglia and Gallardo, 1985; Broglia *et al.*, 1985, 1986; Szymański, 1985). These effects have also been studied in the case of the superdeformed band of ^{152}Dy (Nazarewicz *et al.*, 1987 Shimizu *et al.*, 1987). It was found that they affect in a major way a variety of properties, in particular, the $J^{(1)}$ moment of inertia, in keeping with the fact that the superdeformed configuration is associated with a large single-particle gap, which allows for well-developed pairing vibrations.

In this paper, the pairing vibrational model is applied systematically to the analysis of stably deformed ytterbium isotopes, $^{162-169}$Yb$_{92-99}$, for which the most complete set of experimental data exists at angular momenta where the static pairing gap is predicted to have collapsed. Another interest in reviewing this mass region is the existence of a variety of detailed calculations (e.g., Banerjee *et al.*, 1973; Chu *et al.*, 1975; Faessler *et al.*, 1976; Egido *et al.*, 1980a, 1980b; Bengtsson and Håkansson, 1981; Sugawara-Tanabe *et al.*, 1981; Egido and Ring, 1982a; Mutz and Ring, 1984; Egido *et al.*, 1985, 1986; Egido and Rasmussen, 1987). Stably deformed nuclei are chosen in order to isolate as much as possible the effects of pair correlations from the shape degrees of freedom. This cannot be totally accomplished, not even in the case of the ytterbium isotopes, as will be discussed below.

In Sec. III the pairing vibrational model (Bés and Broglia, 1966) is recast in the formalism of the response function discussed in Sec. II. The parameters entering the calculations are discussed in Sec. IV, and the model is applied to the high-spin data for the ytterbium isotopes in Sec. V. The predicted two-nucleon-transfer response functions are presented in Sec. VI, and the conclusions are collected in Sec. VII.

II. THE FORMALISM OF THE RESPONSE FUNCTION

In this section we briefly review the theory of the response function and indicate how to calculate the correlation energy of a many-particle system in terms of this formalism. For additional information the reader is referred to Pines and Nozières (1966), Fetter and Walec-

ka (1971), and Shimizu and Matsuyanagi (1984b, 1986).

The Hamiltonian describing the system,

$$H=H_0+V\ , \tag{2.1}$$

is the sum of an unperturbed single-particle term H_0 and a two-body residual interaction V. The associated eigenstates and eigenfunctions of H_0 and of H are denoted $E_0, |\Phi_0\rangle$ and $E, |\Psi\rangle$, respectively. From these quantities one can define the correlation energy

$$E_{\rm corr}=E-E_0\ . \tag{2.2}$$

Turning on the interaction adiabatically and using Feynman's theorem, one obtains

$$E_{\rm corr}=\int_0^1 d\lambda\langle\Psi(\lambda)|V|\Psi(\lambda)\rangle\ , \tag{2.3}$$

where $|\Psi(\lambda)\rangle$ is the eigenstate of the λ-scaled Hamiltonian $H(\lambda)=H_0+\lambda V$.

We now diagonalize the Hamiltonian (2.1) in the random-phase approximation. Furthermore, we write the residual interaction as a sum of separable multipole-multipole interactions,

$$V({\rm RPA})=-\tfrac{1}{2}\sum_\rho \chi_\rho \hat{Q}_\rho \hat{Q}^\dagger_\rho\ , \tag{2.4}$$

with

$$\hat{Q}_\rho=\sum_{\alpha<\beta} q_\rho(\alpha\beta)a^\dagger_\alpha a^\dagger_\beta+{\rm H.c.}=\hat{Q}^\dagger_\rho\ . \tag{2.5}$$

The vacuum state on which the quasiparticle creation operators $a^\dagger$ act is the eigenstate of H_0, $|\Phi_0\rangle$.

The unperturbed response matrix function associated with the interaction (2.4) is defined as

$$R_{\rho\sigma}(\omega)=\sum_{\alpha<\beta}\left[\frac{q^*_\rho(\alpha\beta)q_\sigma(\alpha\beta)}{E_\alpha+E_\beta-\omega}+\frac{q_\rho(\alpha\beta)q^*_\sigma(\alpha\beta)}{E_\alpha+E_\beta+\omega}\right], \tag{2.6}$$

where E_α is the unperturbed single-particle energy of H_0.

The random-phase approximation (RPA) response function is given by

$$\mathcal{R}=(1-R\chi)^{-1}R\ , \tag{2.7}$$

where $R\equiv(R_{\rho\sigma})$, $\mathcal{R}\equiv(\mathcal{R}_{\rho\sigma})$, and $\chi\equiv(\delta_{\rho\sigma}\chi_\rho)$.

Making use of the above definitions, one can write

$$\langle\Psi(\lambda)|V|\Psi(\lambda)\rangle_{\rm RPA}=-\tfrac{1}{2}\int_0^\infty d\omega\frac{1}{\pi}{\rm Im}\{{\rm Tr}[\mathcal{R}^{(\lambda)}(\omega)\chi]\}\ , \tag{2.8}$$

where $\mathcal{R}^{(\lambda)}$ is obtained from $\mathcal{R}$ by replacing χ by $\lambda\chi$ in Eq. (2.7).

To carry out the integral numerically we smooth the singularities of the integrand by analytically continuing the function $\mathcal{R}^{(\lambda)}(\omega)$, that is, by replacing ω with $\omega+i\delta$. This procedure also leads to the retarded form of the associated Green's function.

For practical reasons it is desirable to integrate over the adiabaticity parameter λ analytically. For this purpose we first diagonalize the unperturbed response matrix $R(\omega)\chi$ and obtain

$$A_p(\omega)+iB_p(\omega)\equiv\text{eigenvalue of }[R(\omega)\chi]\ . \tag{2.9}$$

When we define the function

$$\begin{aligned}T(\omega)&={\rm Im}\left[{\rm Tr}\int_0^1 d\lambda\,\mathcal{R}^{(\lambda)}(\omega)\chi\right]\\&=\sum_\rho\left[\arctan\left[\frac{A^2_\rho(\omega)+B^2_\rho(\omega)-A_\rho(\omega)}{|B_\rho(\omega)|}\right]\right.\\&\qquad\left.+\arctan\left[\frac{A_\rho(\omega)}{|B_\rho(\omega)|}\right]\right],\end{aligned} \tag{2.10}$$

Eq. (2.3) becomes

$$E_{\rm corr}=-\frac{1}{2\pi}\int_0^\infty d\omega\,T(\omega)\ . \tag{2.11}$$

The standard RPA expression for the correlation energy is [cf. Eq. (2.2)]

$$E_{\rm corr}=\frac{1}{2}\left[\sum_n\omega_n-\sum_{\alpha<\beta}(E_\alpha+E_\beta)\right], \tag{2.12}$$

where ω_n are the RPA eigenfrequencies. It can be shown that Eq. (2.11) coincides with Eq. (2.12) in the limit ${\rm Im}(\omega)=\delta\to 0$.

It should be mentioned that Eqs. (2.11) and (2.12) contain the mean-field contributions,

$$E_{\rm ex}=\langle\Phi_0|V|\Phi_0\rangle=-\tfrac{1}{2}\sum_\rho\chi_\rho\sum_{\alpha<\beta}q^*_\rho(\alpha\beta)q_\rho(\alpha\beta)\ , \tag{2.13}$$

i.e., the exchange (Fock) energy of the interaction V. Therefore the "real" correlation energy $\tilde{E}_{\rm corr}$, induced only by the dynamical effects, is

$$\tilde{E}_{\rm corr}=E_{\rm corr}-E_{\rm ex}\ . \tag{2.14}$$

The standard expression (Egido, Mang, and Ring, 1980b; Ring and Schuck, 1980) for $\tilde{E}_{\rm corr}$ is

$$\tilde{E}_{\rm corr}=-\sum_n\omega_n\sum_{\alpha<\beta}\varphi^*_n(\alpha\beta)\varphi_n(\alpha\beta)<0\ , \tag{2.15}$$

where $\varphi_n(\alpha\beta)$ is the backwards-going amplitude of the RPA solution. In the numerical applications we generally use $E_{\rm corr}$ rather than $\tilde{E}_{\rm corr}$, since we do not include the exchange energy into the single-particle estimate of energy E_0 (Hartree-Bogoliubov approximation; see Sec. III.A).

In actual situations the RPA equations display a high density of very closely spaced roots ω_n. Consequently the calculation of $E_{\rm corr}$ associated with Eq. (2.12) is rather tedious even for separable interactions. Making use of a finite averaging parameter $\delta={\rm Im}(\omega)$, we find that Eq. (2.11) leads to the desired result in an economic way. Equation (2.11) is general and can be used to calculate other correlation energies—for example, those associated with the quadrupole interaction acting in the particle-hole channel (Shimizu, 1987).

III. MODEL OF PAIRING FLUCTUATIONS

The different observables are calculated in a quasiparticle basis moving in a rotating system. The correlations between the quasiparticles are taken into account in the framework of the harmonic approximation (RPA) for each rotational frequency.

A. Self-consistent cranked BCS model

Since we are mainly concerned with the effect of pairing fluctuations in nuclei that display rather stable deformations, no self-consistency condition is imposed on the shape parameters. They remain fixed. The quasiparticles interact through a monopole pairing force that is diagonalized in the RPA. Only the lowest rotational bands associated with a specific parity π and signature[1] α, for which experimental information exists up to very high spins, are considered. The standard adiabatic quasiparticle basis described, for example, by Bengtsson and Frauendorf (1979) is used in the calculations. It is obtained by diagonalizing the Hamiltonian,

$$\begin{aligned}\hat{h}' &= \hat{h}_{def} - \Delta(\hat{P}^\dagger + \hat{P}) - \lambda\hat{N} - \omega_{\rm rot}\hat{J}_x \\ &= \sum_\mu E_\mu a_\mu^\dagger a_\mu + \sum_{\bar{\mu}} E_{\bar{\mu}} a_{\bar{\mu}}^\dagger a_{\bar{\mu}} \ , \end{aligned} \tag{3.1}$$

which is obtained by the standard Hartree-Bogoliubov procedure. In Eq. (3.1) $\hat{h}_{def}$ is the Nilsson Hamiltonian, $\hat{P}^\dagger = \sum_{i>0} c_i^\dagger c_{\bar{i}}^\dagger$ is the monopole pairing operator, and E_μ ($E_{\bar{\mu}}$) is the quasiparticle energy associated with the state of the signature $\alpha = \frac{1}{2}\,(-\frac{1}{2})$.

The unitary transformation between the Nilsson basis (with good signature) and the rotating quasiparticle states μ is given by

$$\begin{aligned} c_i &= \sum_\mu U_{i\mu} a_\mu + \sum_\nu \bar{V}_{i\nu} a_{\bar{\nu}}^\dagger \ , \\ c_{\bar{j}}^\dagger &= \sum_\mu V_{j\mu} a_\mu + \sum_\nu \bar{U}_{j\nu} a_{\bar{\nu}}^\dagger \ . \end{aligned} \tag{3.2}$$

The associated eigenvalue equation can be written as

$$\begin{bmatrix} \varepsilon - \omega_{\rm rot} j_x - \lambda & -\Delta \\ -\Delta & -(\varepsilon + \omega_{\rm rot} j_x - \lambda) \end{bmatrix} \begin{bmatrix} U & \bar{V} \\ V & \bar{U} \end{bmatrix} = \begin{bmatrix} U & \bar{V} \\ V & \bar{U} \end{bmatrix} \begin{bmatrix} E & 0 \\ 0 & -\bar{E} \end{bmatrix} , \tag{3.3}$$

where

$$\varepsilon = \delta_{ij}\varepsilon_i, \quad j_x = j_x(ij), \quad \Delta = \delta_{ij}\Delta \tag{3.4}$$

(Nilsson basis), and

$$E = \delta_{\mu\nu} E_\mu, \quad \bar{E} = \delta_{\mu\nu} E_{\bar{\mu}} \tag{3.5}$$

(rotating basis). The energy gap Δ and the chemical potential λ are self-consistently calculated at each rotational frequency, through the standard BCS equations

$$G\langle \hat{P}^\dagger \rangle = \Delta \ , \tag{3.6a}$$

$$\langle \hat{N} \rangle = N \ . \tag{3.6b}$$

B. Correlation energy and dealignment associated with pairing fluctuations

The unperturbed Hamiltonian appearing in Eq. (2.1) is

$$H_0 = E'_{\rm CBCS} + \hat{h}' \ , \tag{3.7}$$

where

$$E'_{\rm CBCS} = \langle \hat{h}_{def} - \omega_{\rm rot}\hat{J}_x \rangle - \Delta^2/G \tag{3.8}$$

is the standard cranked BCS routhian.

The residual interaction

$$V = -G\tilde{P}^\dagger \tilde{P} \ , \tag{3.9}$$

with

$$\tilde{P}^\dagger = \hat{P}^\dagger - \langle \hat{P}^\dagger \rangle \ , \tag{3.10}$$

can be expressed in the form (2.4) according to

$$V = -\tfrac{1}{2} G \sum_{\rho=\pm} \hat{S}_\rho \hat{S}_\rho - \frac{G}{2}(\hat{N} - \Omega_{\rm model}) \ , \tag{3.11}$$

with

$$\hat{S}_+ = \frac{1}{\sqrt{2}}(\tilde{P}^\dagger + \tilde{P}), \quad \hat{S}_- = \frac{i}{\sqrt{2}}(\tilde{P}^\dagger - \tilde{P}) \ . \tag{3.12}$$

The quantity $\Omega_{\rm model} = \sum_{i>0} 1$ is half the number of single-particle states in the model space considered. The second term in Eq. (3.11) is an absolute constant so that it is neglected in the following. The response matrix (2.6) has, in the present case, dimension 2×2 and matrix elements

$$R_{++}(\omega) = \sum_{\mu\bar{\nu}} \left[\frac{S_+^*(\mu\bar{\nu}) S_+(\mu\bar{\nu})}{E_\mu + E_{\bar{\nu}} - \omega} + \frac{S_+(\mu\bar{\nu}) S_+^*(\mu\bar{\nu})}{E_\mu + E_{\bar{\nu}} + \omega} \right] , \tag{3.13}$$

and similarly for $R_{+-}(\omega)$, $R_{-+}(\omega)$, and $R_{--}(\omega)$. The quantities $S_+(\mu\bar{\nu})$ and $S_-(\mu\bar{\nu})$ are defined by

$$\begin{aligned} S_+(\mu\bar{\nu}) &= \frac{1}{\sqrt{2}} \sum_{i>0} (U_{i\mu}\bar{V}_{i\nu} + V_{i\mu}\bar{U}_{i\nu}) \ , \\ S_-(\mu\bar{\nu}) &= \frac{i}{\sqrt{2}} \sum_{i>0} (U_{i\mu}\bar{U}_{i\nu} - V_{i\mu}\bar{V}_{i\nu}) \ . \end{aligned} \tag{3.14}$$

[1]Signature is the quantum number associated with a rotation of 180° about the rotational axis, i.e., is the eigenvalue of the signature operator, $R_x = \exp(-i\pi\hat{J}_x)$. A signature r can be defined as $r \equiv \exp(-i\pi\hat{J}_x) = \exp(-i\pi\alpha)$, where $I = \alpha$ Mod 2 and $\alpha = \pm 1/2$. The quantity α has been termed the "signature exponent" by Goodman (1974). Following Bengtsson and Frauendorf (1979) and others, we refer to α as the signature in the present review.

The pairing correlation energy is now calculated making use of Eqs. (2.7)–(2.11) and (3.13). The resulting total routhian is

$$E'_{\rm tot}=E'_{\rm CBCS}+E_{\rm corr}\ . \tag{3.15}$$

The associated angular momentum around the axis of rotation can be determined through the canonical relation

$$I_x^{(\rm tot)}=I_x^{(\rm sp)}+I_x^{(\rm corr)}\ , \tag{3.16}$$

where

$$I_x^{(\rm sp)}=-\frac{\partial E'_{\rm CBCS}}{\partial\omega_{\rm rot}} \tag{3.17}$$

and

$$I_x^{(\rm corr)}=-\frac{\partial E_{\rm corr}}{\partial\omega_{\rm rot}}\ . \tag{3.18}$$

C. Physical interpretation of $I_x^{(\rm corr)}$

It is instructive to examine the physical contents of the derivative expression for angular momentum appearing in Eqs. (3.16)–(3.18). The left-hand term of Eq. (3.17),

$$I_x^{(\rm sp)}=\langle\hat{J}_x\rangle_{\rm CBCS}\ , \tag{3.19}$$

is the expectation value of the angular momentum in the self-consistent cranked BCS state. The correlation contribution (3.18) to the angular momentum contains a variety of physical effects that go beyond those included in the RPA. This is natural because taking derivatives with respect to the angular momentum is equivalent to making insertions of the external field J_x in the corresponding field-theory diagrams.

Assuming that the mean field is independent of $\omega_{\rm rot}$, aside from the cranking term, we can express the quantity $I_x^{(\rm corr)}$ as the sum of three terms (see the Appendix),

$$I_x^{(\rm corr)}=I_x^{(\rm a)}+I_x^{(\rm b)}+I_x^{(\rm ex)}\ . \tag{3.20}$$

The quantity $I_x^{(\rm ex)}$ arises from the exchange contribution [see Eq. (2.13)]. The first and the second terms have been evaluated (Barranco *et al.*, 1987) within the framework of the nuclear field theory (Bortignon *et al.*, 1977), making use of the diagrams (a) and (b) shown in Fig. 1. The first is associated with RPA ground-state correlations, while the second is associated with renormalizations of the single-particle motion.

While the nuclear field-theory expressions for diagram (b) and $I_x^{(\rm b)}$ coincide, only diagonal terms ($\alpha=\beta$) appear in $I_x^{(\rm a)}$. This difference is not expected to bring any new physics into the problem. The term $I_x^{(\rm a)}$ can be written as

$$I_x^{(\rm a)}=\sum_n\sum_{\alpha<\gamma}[i_x(\alpha)+i_\gamma(\gamma)]\varphi_n^*(\alpha\gamma)\varphi_n(\alpha\gamma)\ , \tag{3.21}$$

where $i_x(\alpha)$ is the single-particle alignment ($\alpha=\mu$ or $\bar{\nu}$),

$$i_x(\alpha)=-\frac{\partial E_\alpha}{\partial\omega_{\rm rot}}\ , \tag{3.22}$$

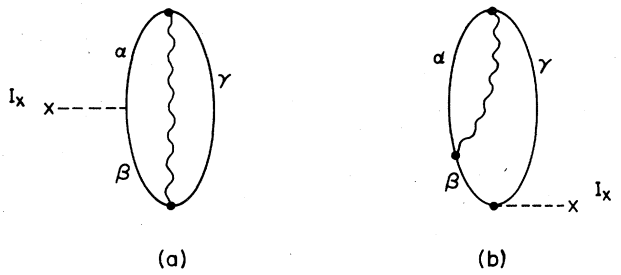

FIG. 1. Second-order processes in the coupling of vibrations (wavy lines) and quasiparticles (solid lines). The external field changing the motion of a quasiparticle as in (a) or exciting a two-quasiparticle state from the vacuum (b) is the angular momentum I_x.

assuming the mean field to be constant.

The process of Fig. 1(a) leads to an effective change of the BCS occupation numbers, depopulating states below the Fermi surface and populating states above it. For large values of $\omega_{\rm rot}$ in the lower portion of a major shell, this change in the occupancy parameters will lead to a dynamical quenching of the angular momentum, as the most aligned single-particle orbits lie below the Fermi level.

Diagram (b) leads to an effective change in the single-particle orbitals. In fact, both particles and holes are renormalized, due to coupling with the pairing modes, and acquire an effective mass. Levels below the Fermi energy become less bound, while those above it become more bound, the summed effect being an increase of the level density around the Fermi surface and, again, a depopulation of levels lying below ε_F; see, for example, Mahaux *et al.* (1985). Consequently, for nuclei in which the Fermi surface is in the lower portion of a shell, a net dynamical quenching of the angular momentum results.

While diagram (a) can be calculated by making use of the RPA solutions, to calculate diagram (b) one needs to go beyond the RPA, taking into account scattering vertices. The particle-vibration coupling Hamiltonian is, however, well determined once the RPA solution has been worked out, and both diagrams can be calculated with equal ease. They are also of the same order of perturbation. In fact, they constitute a set of sum-rule-conserving graphs, in the sense of the Ward identity (see, for example, Schrieffer, 1964).

In the present calculations the contribution of diagram (b) is, usually, much larger than that of diagram (a). This can be understood in terms of the value of the energy denominators (see the Appendix for details). For example, we find (see Sec. V.C) that the terms $I_x^{(\rm a)}$, $I_x^{(\rm b)}$ and $I_x^{(\rm ex)}$ contribute about 20%, 70%, and 10% of the total, respectively, for typical large rotational frequencies.

D. Limit $\omega_{\rm rot}=\omega_{\rm crit}$

It is instructive to study the limit in which the BCS pairing gap goes to zero. In this case (normal phase), the

RPA response matrix decouples into pair-addition and pair-removal components, that is,

$$\mathrm{Tr}\mathcal{R}=\mathcal{R}_A+\mathcal{R}_R \ . \tag{3.23}$$

The quantities $\mathcal{R}_A$ and $\mathcal{R}_R$ are calculated with the help of Eq. (2.7), making use of the unperturbed response function

$$R_A(\omega)=\left[\sum_{k\bar{k}'>\varepsilon_F}\frac{|M(k\bar{k}')|^2}{E_k+E_{\bar{k}'}-\omega}+\sum_{i\bar{i}'<\varepsilon_F}\frac{|M(i\bar{i}')|^2}{E_i+E_{\bar{i}'}+\omega}\right], \tag{3.24}$$

$$R_R(\omega)=\left[\sum_{i\bar{i}'<\varepsilon F}\frac{|M(i\bar{i}')|^2}{E_i+E_{\bar{i}'}-\omega}+\sum_{k\bar{k}'>\varepsilon_F}\frac{|M(k\bar{k}')|^2}{E_k+E_{\bar{k}'}+\omega}\right].$$

The quantities $M(k\bar{k}')$ and $M(i\bar{i}')$ are the matrix elements of the monopole pairing operator $\hat{P}^\dagger$. The quasiparticle energies are in the present case given by

$$E_\alpha=\begin{cases}\varepsilon_\alpha-\lambda, & \alpha=k,\bar{k}'>\varepsilon_F,\\ \lambda-\varepsilon_\alpha, & \alpha=i,\bar{i}'<\varepsilon_F\ ,\end{cases} \tag{3.25}$$

where k labels a particle state, while i is a hole state. The eigenvalues of the cranked Nilsson Hamiltonian $\hat{h}_{def}-\omega_{\mathrm{rot}}\hat{J}_x$ are denoted by ε_α.

In the vicinity of the critical frequency where the pairing collapses ($\omega_{\mathrm{rot}}\approx\omega_{\mathrm{crit}}$), a perturbative treatment of the BCS equation with respect to the parameter $\Delta\approx 0$ may be possible. Thus, in this limit, Eqs. (3.6) reduce to

$$\frac{1}{G}=R_A(\omega=0)=R_R(\omega=0)\ , \tag{3.26a}$$

$$0=\left.\frac{\partial R_A}{\partial\omega}\right|_{\omega=0}=\left.\frac{\partial R_R}{\partial\omega}\right|_{\omega=0}\ . \tag{3.26b}$$

Equation (3.26a) shows that the ω_{crit} for which $\Delta=0$ coincides with the critical rotational frequency for which the energy of the lowest pair-addition and pair-removal modes becomes zero. Moreover, Eq. (3.26b) fixes the value of the chemical potential at the critical frequency. It is thus natural to use the value λ determined by Eq. (3.26b) after the pairing collapse.

Equations (3.26) were obtained starting from Eqs. (3.6) under the assumption that

$$\Delta\ll(E_k+E_{\bar{k}'}),(E_i+E_{\bar{i}'})\ . \tag{3.27}$$

In realistic situations, the sharp crossing of a given configuration with the aligned quasiparticle states may cause a sudden collapse of the pairing gap. In such situations condition (3.27) may not be fulfilled, and the critical frequencies for which the pairing gap collapses and the energies of the lowest pairing vibration modes become zero may not coincide.

IV. DETAILS OF THE CALCULATIONS

The model discussed above has been applied to ytterbium isotopes with neutron number $N=92-99$. The parameters of the single-particle potential and of the residual interaction used in the calculations are discussed below, together with the accuracy of the approximations used in the linear-response (harmonic approximation) description of the correlation energy.

A. Parameters of the model

The Nilsson Hamiltonian is formulated as in Bohr and Mottelson (1975). The parameters of the $l\cdot s$ and l^2 terms, taken from Bengtsson and Ragnarssen (1985), depend on the main oscillator quantum number N_{osc}. The ytterbium isotopes with $N=92-99$ are predicted to have a sizable quadrupole deformation ε_2 and nearly zero hexadecapole distortion. These parameters are expected to be quite stable with respect to angular momentum and configurations (Bengtsson, 1980; Bengtsson *et al.*, 1983; Shimizu and Matsuyanagi, 1984a; Bengtsson and Ragnarsson, 1985). Note, however, the recent results of Bacelar *et al.* (1987), who measured lifetimes in ^{166}Yb and found that the $B(E2)$ values decreased significantly above $I=26\hbar$ in the yrast band. This variation can be correlated with a change in deformation (Garrett *et al.*, 1988), as discussed in Sec. V.E.2. Although sizable, it is considerably smaller than that expected for transitional nuclei in this mass region. We have checked the effects associated with these changes in deformation (Sec. V.E.2) and found that, although the $B(E2)$ values are significantly affected, they hardly change the energy spectra or the overall renormalization effect introduced by the coupling of the single-particle motion to pairing vibrations. Consequently, and aside from ^{166}Yb, we have used constant values of ε_2 for all rotational frequencies and configurations, and have set ε_4 and γ equal to zero. The isotopic dependence of ε_2 is taken from the systematics of Shimizu and Matsuyanagi (1984a) with a slight modification to fit the experimentally deduced values for ^{168}Yb. These parameters, collected in Table I, are also shown in Fig. 2.

The active subspace for the neutrons (protons) includes all levels associated with the $N_{\mathrm{osc}}=4,5,6$ (3,4,5) oscillator shells. In this space, particles interact with a monopole pairing force of strength

$$G_n=20.5/A\ \mathrm{MeV},\quad G_p=26/A\ \mathrm{MeV}\ . \tag{4.1}$$

The associated neutron pair gaps for the ground states of the ytterbium isotopes are compared in Fig. 2 with the experimental odd-even mass differences obtained from the most recent mass compilation (Wapstra and Audi, 1985). Monopole pairing strengths G_n, giving slightly larger Δ_n values than the odd-even mass differences, were chosen as a compromise with the prediction of the rotational frequencies of the band crossings—see Sec. V.G. This choice, however, is justified theoretically. Blocking effects in the odd-N isotopes are predicted (Nilsson and Prior, 1961) to produce about a 10% reduction in the odd-even mass difference for this mass region.

TABLE I. Quadrupole deformations and data sources for the ytterbium isotopes.

Nucleus	Neutron number	ε_2[a]	Experimental data sources
^{162}Yb	92	0.224	Mo *et al.* (1987)
^{163}Yb	93	0.232	Kownacki *et al.* (1983); Schuck *et al.* (1985)
^{164}Yb	94	0.240	Schuck *et al.* (1985); Jónsson *et al.* (1986)
^{165}Yb	95	0.245	Roy *et al.* (1982); Schuck *et al.* (1984, 1985)
^{166}Yb	96	0.250	Waluś *et al.* (1981); Beck *et al.* (1987)
^{167}Yb	97	0.254	Roy *et al.* (1982); Baceler *et al.* (1985)
^{168}Yb	98	0.258	Bacelar *et al.* (1985)
^{169}Yb	99	0.260	Bacelar *et al.* (1985)

[a] From systematics of Bengtsson (1980) and Shimizu and Matsuyanagi (1984a) slightly modified.

B. Accuracy of the linear-response approximation

The merit of the response function technique [Eqs. (3.13) and (2.6)–(2.11)] is that all the RPA roots consistent with the cranked BCS calculation can be taken into account in solving the pairing problem. This is important, since the strength G of the pairing force depends sensitively on the model space used in the cranked BCS calculation. In the present cases (see preceding subsection), the number of the RPA roots amounts to about one thousand.

The calculation of the response functions (3.13) [cf. Eq. (2.6)] is very economical when a complex energy $\omega+i\delta$ is utilized. The smooth dependence of the correlation energy, shown in Fig. 3, testifies to the stability with respect to the averaging parameter δ.

The accuracy of the results is demonstrated in Fig. 4, where the correlation energies for two configurations of ^{168}Yb calculated using Eqs. (2.12) and (2.11) with $\delta=80$ keV are shown as a function of the rotational frequency. The relative energies and frequency dependence are essentially the same in both calculations, except near the critical frequency, where the linear approximation itself is not valid. We have used $\delta=\mathrm{Im}(\omega)=80$ keV in all the results shown below.

C. Treatment of protons

The lowest proton band crossing is predicted to occur at $\hbar\omega_{\mathrm{rot}}=0.4$–$0.5$ MeV for all the isotopes considered. However, except for ^{162}Yb (Mo *et al.*, 1987), no proton crossing is observed in the experimental data up to $\hbar\omega_{\mathrm{rot}}\approx 0.6$ MeV. To account for this known deficiency in the calculations we have extrapolated the calculated quasiproton results for $\hbar\omega_{\mathrm{rot}}\lesssim 0.20$ MeV to larger frequencies, using the parametrization of Harris (1965),

$$I_x(\mathrm{proton})=J_0^{(p)}\omega_{\mathrm{rot}}+J_1^{(p)}\omega_{\mathrm{rot}}^3 . \tag{4.2}$$

The extracted Harris parameters $J_0^{(p)}, J_1^{(p)}$ are collected in Table II.

D. Dynamical and effective pairing gaps

Because the coupling of pairing vibrations to the nucleons is nonadiabatic (Bés *et al.*, 1970), it is not accurate to express the associated renormalization effects through a single effective parameter. Nonetheless, for a quantitative measure of the relative importance of dynamical and

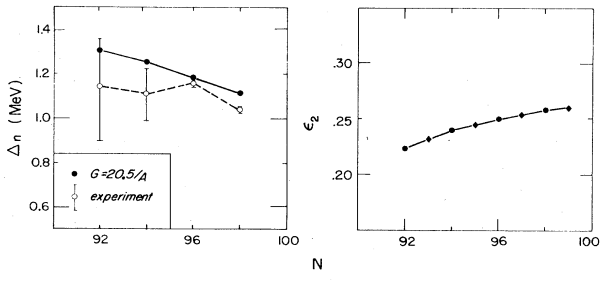

FIG. 2. Ground-state BCS neutron pairing gap Δ_n (left) for the different even-A ytterbium isotopes. The BCS equations (3.6) were solved for $G_n=20.5/A$ MeV and for neutron numbers $N=92$, 94, 96, and 98. The experimental odd-even mass differences, calculated using the third difference formulation of Bohr and Mottelson (1969) and the most recent compilation of nuclear masses (Wapstra and Audi, 1985), also are displayed. In the right-hand portion of the figure the quadrupole deformation parameters used in the calculations are shown.

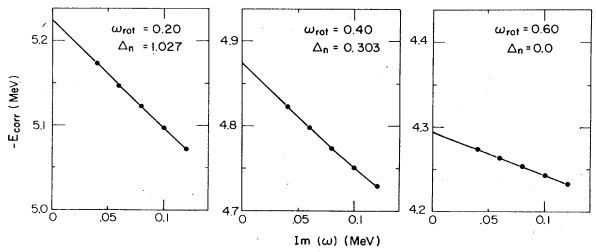

FIG. 3. Pairing correlation energies, E_{corr}, of the (+,0) configuration of ^{168}Yb as a function of the averaging parameter $\delta=\mathrm{Im}(\omega)$ are shown for three different values of the rotational frequency. The corresponding values of the static pair gap Δ_n calculated for each frequency are also given.

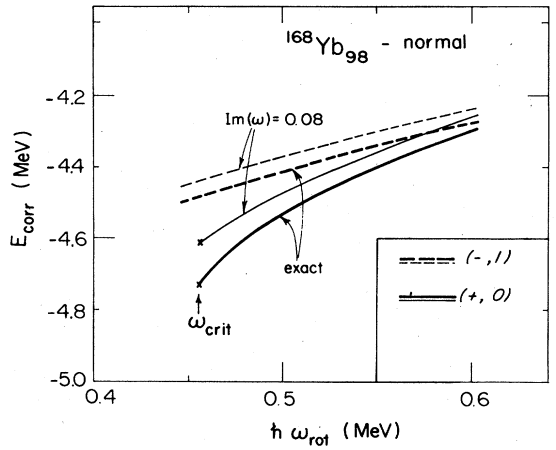

FIG. 4. Comparison of the correlation energy as a function of the rotational frequency for the (+,0) and (−,1) configurations of ^{168}Yb in the normal phase for $\delta=\mathrm{Im}(\omega)=80$ keV and 0. The curves labeled "exact" were calculated by the RPA dispersion relation and by summing up the contributions from each root. Within the framework of the linear approximation, these results are numerically "exact."

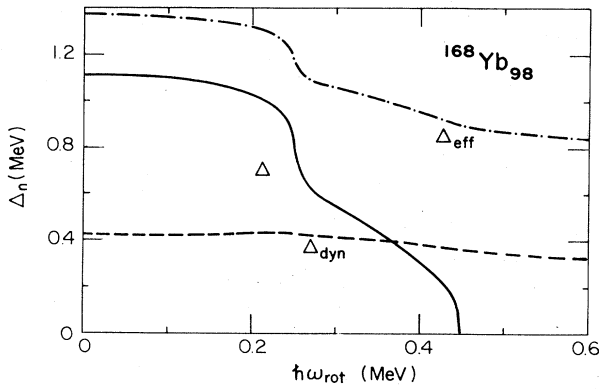

FIG. 5. Comparison of the calculated static (BCS) neutron pair gap Δ, dynamic neutron pair gap Δ_{dyn}, and effective neutron pair gap Δ_{eff} for the lowest $(\pi,\alpha)=(+,0)$ configuration of $^{168}Yb_{98}$. Δ, Δ_{dyn}, and Δ_{eff} are defined by Eqs. (4.4), (4.3), and (4.7), respectively. A comparison of Δ_{dyn} and Δ gives a measure of the relative importance of dynamic and static neutron pair correlations. The effective pair gap Δ_{eff} is constructed from the RPA solutions, containing both static and dynamical pairing effects, for comparison with the results of number-projected calculations; see Sec. IV.D.

static pairing correlations we define a "dynamical pairing gap" as

$$\Delta_{dyn}=\sqrt{G(-\tilde{E}_{corr})}\ . \tag{4.3}$$

It is noted that the contribution of the pairing force to the mean field, i.e., the exchange (Fock) energy, is not contained in this expression [see Eq. (2.14)]. The dynamic neutron pairing gap for ^{168}Yb is compared in Fig. 5 with the BCS pairing gap

$$\Delta=G\langle\hat{P}^{\dagger}\rangle_{BCS}\ . \tag{4.4}$$

The two quantities Δ and Δ_{dyn} have similar vlaues only for rotational frequencies between that of the two-quasineutron excitation ($\hbar\omega_{rot}\sim0.26$ MeV) and the critical frequency ($\hbar\omega_{rot}\sim0.45$ MeV) for which $\Delta\to0$. In the region of no quasiparticle excitations, i.e., $\hbar\omega_{rot}<0.26$ MeV, Δ is significantly larger than Δ_{dyn}. Consequently we do not expect pairing fluctuations to play a major role in the superfluid phase. This expectation is confirmed by the numerical results (Sec. V.E). The calculations also show that, for values of the rotational frequency where $\Delta\lesssim\Delta_{dyn}$, the situation is reversed and pairing fluctuations dominate.

It is important to underline the physical difference between the construct Δ_{dyn} [Eq. (4.3)] and the quantity Δ [Eq. (4.4)]. While Δ_{dyn} cannot be measured directly, the pairing gap Δ is specifically connected with two-nucleon-transfer processes. In fact, the cross section for the transfer of a Cooper pair between yrast states is proportional to $(\Delta/G)^2$ [see Broglia (1985), Broglia *et al.* (1985), and references therein].

In this context it is appropriate to discuss the conceptual difference between the static pairing gap Δ, Eq. (4.4), and the "pairing gap" calculated using number projection (Mang, 1975; Bengtsson and Håkonsson, 1981; Egido and Ring, 1982a, 1982b; Bengtsson and Zhang, 1984; Mutz and Ring, 1984; Canto *et al.*, 1985). The latter quantity Δ_{NP} is defined according to

$$\Delta_{NP}=G(_{NP}\langle0|\hat{P}^{\dagger}\hat{P}|0\rangle_{NP})^{1/2}\ , \tag{4.5}$$

where $|0\rangle_{NP}$ is the number-projected Hartree-Fock-Bogoliubov state. It should be noticed that $|0\rangle_{NP}$ contains the effects of pairing correlations that cannot be included in the simple mean-field approximation. In this sense, $|0\rangle_{NP}$ corresponds, roughly speaking, to the RPA vacuum state $|0\rangle_{RPA}$. In order to make the analogy more transparent, consider the explicit forms of both wave functions in the simple situation of the absence of rotation, where only the monopole pairing residual interac-

TABLE II. Harris parameters [Eq. (4.2)] fixed by fitting the calculated proton contribution to the angular momentum at $\hbar\omega_{rot}\sim0.2$ MeV. These values are used to extrapolate the proton contributions to larger rotational frequencies—see Sec. IV.C.

Nucleus	$J_0^{(p)}$ (MeV$^{-1}\hbar^2$)	$J_1^{(p)}$ (MeV$^{-3}\hbar^4$)
^{162}Yb	5.56	14.3
^{163}Yb	5.99	16.1
^{164}Yb	6.43	18.1
^{165}Yb	6.75	19.5
^{166}Yb	7.07	20.8
^{167}Yb	7.35	21.9
^{168}Yb	7.63	22.9
^{169}Yb	7.83	23.7

tion is taken into account and the pairing correlation is so weak that the BCS equation results in a zero static pairing gap (normal phase). In such a case, $|0\rangle_{\rm NP}$ and $|0\rangle_{\rm RPA}$ in the so-called quasiboson approximation take the following forms [Ring and Schuck (1980), pp. 342 and 343]:

$$|0\rangle_{\rm NP}=N\sum_{n=0}^{\infty}\frac{1}{(n!)^2}\left[\sum_{ph}\frac{V_pU_h}{U_pU_h}(C_p^{\dagger}C_{\bar{p}}^{\dagger})(C_{\bar{h}}C_h)\right]^n|{\rm HF}\rangle\ , \tag{4.6a}$$

$$|0\rangle_{\rm RPA}=N'\sum_{n=0}^{\infty}\frac{1}{n!}\left[\sum_{ph}Z_{ph}(C_p^{\dagger}C_{\bar{p}}^{\dagger})(C_{\bar{h}}C_h)\right]^n|{\rm HF}\rangle\ , \tag{4.6b}$$

where $|{\rm HF}\rangle$ is the Hartree-Fock state and $C_p^{\dagger}$ (C_h) is the particle (hole) creation operator. As can be clearly seen, both states take into account the *pp-hh* correlations coming from the pairing interactions. Note, however, that in the case of $|0\rangle_{\rm NP}$ the (U,V) factors in Eq. (4.6a) are not determined by the BCS equation, but instead are determined statically using the variational principle (variation after projection). In contrast, for $|0\rangle_{\rm RPA}$, the amplitudes Z_{ph} in Eq. (4.6b) are determined dynamically by solving the RPA equation.

Noticing that $|0\rangle_{\rm RPA}$ plays a similar role to that of $|0\rangle_{\rm NP}$, we can define the "effective pairing gap" $\Delta_{\rm eff}$, which is an analogous quantity to $\Delta_{\rm NP}$ in our BCS + RPA approach. The effective pairing gap $\Delta_{\rm eff}$ is defined by replacing $|0\rangle_{\rm NP}$ by $|0\rangle_{\rm RPA}$ and using a kind of symmetrization, i.e.,

$$\Delta_{\rm eff}=G[\tfrac{1}{2}({}_{\rm RPA}\langle 0|\hat{P}^{\dagger}\hat{P}|0\rangle_{\rm RPA}+{}_{\rm RPA}\langle 0|\hat{P}\hat{P}^{\dagger}|0\rangle_{\rm RPA})]^{1/2}\ . \tag{4.7}$$

The reason for the symmetrization is as follows: In the BCS + RPA formalism the quantities in Eq. (4.7) are calculated by using the complete set of the RPA eigenstates,

$${}_{\rm RPA}\langle 0|\hat{P}^{\dagger}\hat{P}|0\rangle_{\rm RPA}=|{}_{\rm RPA}\langle 0|\hat{P}|0\rangle_{\rm RPA}|^2+\sum_{n'\neq{\rm NG}}|{}_{\rm RPA}\langle n'|\hat{P}|0\rangle_{\rm RPA}|^2\ , \tag{4.8a}$$

$${}_{\rm RPA}\langle 0|\hat{P}\hat{P}^{\dagger}|0\rangle_{\rm RPA}=|{}_{\rm RPA}\langle 0|\hat{P}^{\dagger}|0\rangle_{\rm RPA}|^2+\sum_{n\neq{\rm NG}}|{}_{\rm RPA}\langle n|\hat{P}^{\dagger}|0\rangle_{\rm RPA}|^2\ , \tag{4.8b}$$

where $\sum_{n\neq{\rm NG}}$ means that the symmetry-conserving Nambu-Goldstone mode (the zero-energy pairing rotation) should not be included. The first, Eq. (4.8a), represents the part of the two-nucleon-transfer non-energy-weighted sum rule associated with the pickup of two nucleons from system A, while the second, Eq. (4.8b), is that corresponding to the stripping. Physically, there is no reason for preferring one to the other. The first terms in Eqs. (4.8a) and (4.8b) are approximated by

$$\begin{aligned}|{}_{\rm RPA}\langle 0|\hat{P}^{\dagger}|0\rangle_{\rm RPA}|^2&=|{}_{\rm RPA}\langle 0|\hat{P}|0\rangle_{\rm RPA}|^2\\&\approx|{}_{\rm BCS}\langle 0|\hat{P}^{\dagger}|0\rangle_{\rm BCS}|^2\\&\approx\left[\frac{\Delta}{G}\right]^2\ ,\end{aligned} \tag{4.9}$$

which is proportional to the two-nucleon-transfer cross section between members of the pairing rotational band. The second terms in (4.8a) and (4.8b) are the sum of the square of the spectroscopic amplitudes associated with the excitation of the pair-removal modes $[|n'\rangle=|n'(-2)\rangle]$ and of the pair-addition modes $[|n\rangle=|n(+2)\rangle]$ of system A. The first term in (4.8) with the approximation (4.9) measures the static distortion of the pair field, while the second gives the sum of the associated zero-point amplitudes. As the rotational frequency approaches $\omega_{\rm crit}$ the first term goes to zero and the zero-point amplitudes become relatively important.

Calculated values of Δ, $\Delta_{\rm dyn}$, and $\Delta_{\rm eff}$ for the $(\pi,\alpha)=(+,0)$ band of $^{168}{\rm Yb}_{98}$ are compared in Fig. 5. In this calculation of $\Delta_{\rm eff}$ the non-energy-weighted sum of the pair-transfer amplitudes appearing in Eq. (4.8a) is calculated by using the response function technique. This calculation is similar to that of Eq. (2.8) without λ integration, i.e.,

$$\tfrac{1}{2}\sum_{n\neq{\rm NG}}(|\langle n|\hat{P}^{\dagger}|0\rangle|^2+|\langle n|\hat{P}|0\rangle|^2)_{\rm RPA}=\frac{1}{2}\int_{\omega_{\rm cut}}^{\infty}d\omega\frac{1}{\pi}{\rm Im}[{\rm Tr}\mathcal{R}(\omega+i\delta)]\ . \tag{4.10}$$

Here $\mathcal{R}$ is defined through Eq. (2.7) in terms of the unperturbed pairing response function [see Eqs. (3.13) and (3.14)]. The low-energy cutoff $\omega_{\rm cut}$ is used for eliminating the contributions of the Nambu-Goldstone mode, which goes to zero energy at the critical frequency $\omega_{\rm crit}$, producing a divergence. As shown in Fig. 5, the behavior of $\Delta_{\rm eff}$ as a function of $\omega_{\rm rot}$ is quite similar to that of $\Delta_{\rm NP}$, which is shown in Fig. 6 (Egido *et al.*, 1985; see also Egido and

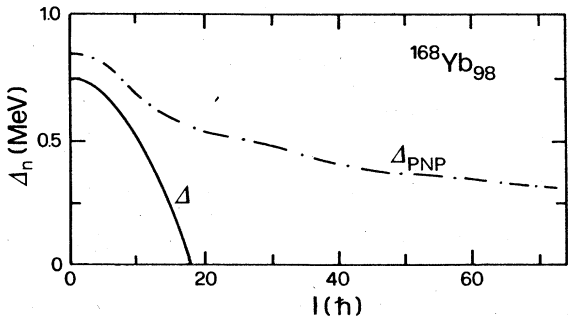

FIG. 6. The static (BCS) neutron gap Δ for the lowest configuration of $^{168}{\rm Yb}_{98}$, as calculated by Egido and Ring (1984), making use of the Kumar-Baranger Hamiltonian, compared with the pairing gap $\Delta_{\rm PNP}$ obtained by the same authors, using variation after particle number projection.

Ring, 1982a, 1982b). Moreover, the value of $\Delta_{\rm eff}$ is never quenched, staying at about 800 keV even after the static pairing has vanished. Although the quantity ${}_{\rm NP}\langle 0|\hat{P}^{\dagger}P|0\rangle_{\rm NP}$ in the definition of $\Delta_{\rm NP}$ [Eq. (4.1)] cannot be represented in the same way as Eq. (4.8), the analogy between $|0\rangle_{\rm NP}$ and $|0\rangle_{\rm RPA}$ in the simple case [see Eq. (4.6)] and the similar behavior of $\Delta_{\rm NP}$ and $\Delta_{\rm eff}$ as functions of $\omega_{\rm rot}$ suggest that the $\Delta_{\rm NP}$ contains a considerable part of the zero-point fluctuations. In other words, the static pairing gap Δ and the number projection gap $\Delta_{\rm NP}$ are conceptually different quantities and should not be confused. For instance, the value of $\Delta_{\rm NP}$ must not be used as the pairing gap parameter appearing in the usual cranked shell-model calculations. Similar results were obtained by Nazarewicz *et al.* (1985).

We can make an analogy between Eq. (4.5) and the case of surface distortions, in which the quadrupole fluctuations are measured in terms of the matrix element of the quadrupole operator

$$Q_{IP}=({}_{IP}\langle 0|\hat{Q}^2|0\rangle_{IP})^{1/2} . \tag{4.11}$$

Here $|0\rangle_{IP}$ is the projected state, and IP denotes angular momentum projection. Assuming $I=0$, one can write

$${}_{I=0}\langle 0|\hat{Q}^2|0\rangle_{I=0}=|{}_2\langle 0|\hat{Q}|0\rangle_0|^2+\sum_n |{}_2\langle n|\hat{Q}|0\rangle_0|^2 . \tag{4.11a}$$

The first term measures the transition within a quadrupole rotational band, being proportional to the static quadrupole moment of the system, while the second term is proportional to the transition probability connecting the ground state with the β or γ vibration. When the system becomes spherical, the first term is zero and the second gives the transition probability to the single-phonon quadrupole vibration.

Summing up, the pairing phase transition is associated with a spontaneous breaking of the symmetry and consequently with a violation of the particle number conservation law. The associated Nambu-Goldstone mode induces fluctuations of the order parameter that are precisely those needed to restore the symmetry, see Anderson (1958), leading to eigenstates of fixed particle number. The same result can be obtained by utilizing projected wave functions displaying correct transformation properties under rotations in gauge space.

E. The smoothening of the RPA correlation energy and dealignment

The RPA correlation energy $E_{\rm corr}$ defined by Eq. (2.11) or (2.12) may be discontinuous in two situations: (i) at band crossings and (ii) at the quenching of the static pair gap. In general, $I_x^{(\rm corr)}$ introduced in Eq. (3.18) is not defined at such points. In the case of band crossings, two situations can arise depending on the strength with which the crossing bands interact. If the interaction is weak, a sharp band crossing occurs. In this case the physical observable remains continuous if the so-called "diabatic quasiparticle basis" (Frauendorf, 1981) is followed. Calculations based on this prescription lead to sensible results (see, for example, Shimizu and Matsuyanagi, 1982, 1983, 1984a, 1985). In this paper we are mainly interested in the region of large rotational frequencies. Therefore we need not worry about sharp band crossings, since in this region the experimental routhians and alignments are also discontinuous, if one follows the yrast states.

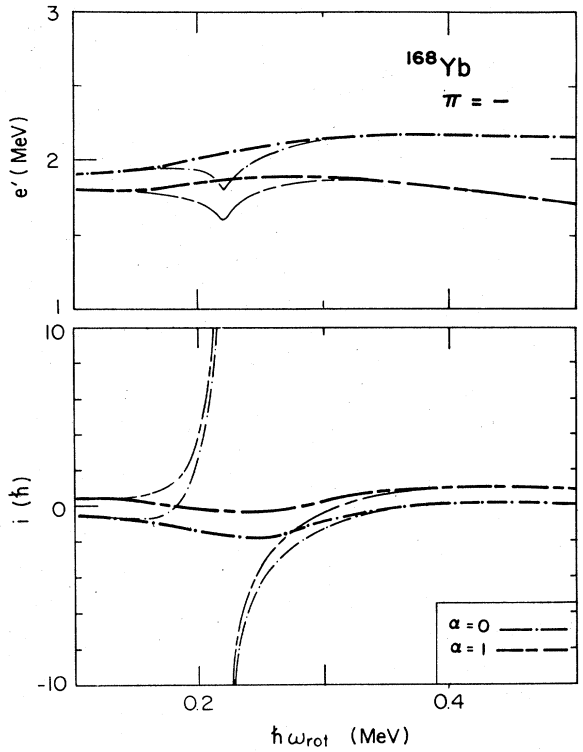

FIG. 7. Calculated routhians e' (top) and alignments i (bottom) for configurations of ^{168}Yb: dot-dashed curves, (-0); double-dashed curves, $(-,1)$. The light and heavy curves indicate the explicit calculations and the results of interpolation, respectively.

On the other hand, the strong-interaction situation, found, for example, in the first neutron crossing ("AB" crossing) in ^{168}Yb and in the superfluid-to-normal phase transition, poses a real difficulty to the RPA. The potential energy surface as a function of the gap parameter becomes flat; thus the harmonic picture is no longer valid. Number projection techniques (Mang, 1975; Faessler *et al.*, 1976; Bengtsson and Håkansson, 1981; Egido and Ring, 1982a, 1982b; Bengtsson and Zhang, 1984; Mutz and Ring, 1984; Canto *et al.*, 1985) can be used to overcome this problem. Likewise, the boson expansion approach leads to a satisfactory solution (Shimizu and Broglia, 1988).

In this paper we are interested in making a systematic comparison between theory and experiment and assessing the role of the dynamical pairing degrees of freedom. In

keeping with this goal, we shall use a simple interpolation procedure (Bes *et al.*, 1987). In Fig. 7 we show a typical example of such an interpolated routhian e' and single-particle alignment i.

V. DISCUSSION OF CALCULATED QUANTITIES AND COMPARISON WITH EXPERIMENTAL DATA

For some time both experimental evidence (Chapman *et al.*, 1983; Frauendorf, 1984; Garrett, 1984; Herskind, 1984; Bacelar *et al.*, 1985; Schuck *et al.*, 1985) and theoretical calculations (Agarwal *et al.*, 1983; Diebel, 1984) have indicated a quenching of static pair correlations for stably deformed nuclei at the largest rotational frequencies $\hbar\omega_{\rm rot}$. However, at these same values of $\hbar\omega_{\rm rot}$ certain specific configurations, e.g., the lowest $(\pi,\alpha)=(+,0)$ [and to a lesser extent the $(+,\frac{1}{2})$] configurations in rare-earth nuclei systematically are depressed in energy and have smaller moments of inertia relative to other configurations (Bacelar *et al.*, 1985; Garrett, 1985b; Zhang *et al.*, 1986). These experimental features are not predicted by cranking model calculations (Bengtsson and Frauendorf, 1979; Frauendorf, 1982). These results were successfully interpreted by Broglia *et al.* (1986) and Broglia and Gallardo (1985) as the coupling of the single-particle motion to pairing vibrations. The model, which is physically equivalent to that discussed in the preceding sections, was applied to the analysis of the experimental data associated with a couple of nuclei and only for $\omega_{\rm rot} > \omega_{\rm crit}$.

In the following subsections we apply the model described in Secs. III and IV over the complete range of rotational frequencies to the ytterbium isotopes ($Z=70$) with $N=92-99$. The high-spin data for this isotopic chain are the most complete available for well-deformed systems (see Table I).

Before proceeding to a comparison of the theory with experiment, it will prove instructive to consider the rotational frequency and configuration dependence of the unperturbed single-neutron states and of the pair matrix elements.

A. The unperturbed single-particle spectrum of states

The unperturbed single-neutron spectrum of states for a quadrupole deformation $\varepsilon_2=0.25$ is shown as a function of the rotational frequency in Fig. 8. This deformation, which represents an average value for this string of ytterbium isotopes (see Table I), was used for $^{166}Yb_{96}$ in the complete calculations. Most of the single-neutron features for neutron numbers of 95–99, discussed by Bacelar *et al.* (1985), are contained in this spectrum.

The deformation dependence of the single-neutron states in a nonrotating system (i.e., the Nilsson states) is shown in Fig. 9.

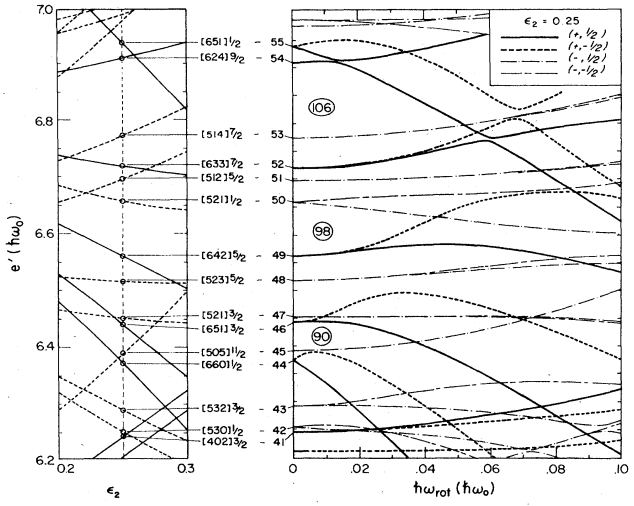

FIG. 8. Cranked shell-model energies for neutrons ($A\approx 165$) in the normal (unpaired) phase, as a function of the rotational frequency $\hbar\omega_{\rm rot}$. A quadrupole deformation ε_2 of 0.25 and modified-oscillator parameters from Bengtsson and Ragnarsson (1985) were used. To the left an enlarged portion of the corresponding Nilsson diagram, $\varepsilon_2=0.2-0.3$, is shown for orientation. The Nilsson model quantum numbers $[Nn_z\Lambda]\Omega$ and the level numbers used for identification in Fig. 10 are given for $\hbar\omega_{\rm rot}=0$ between the left and right portions of the figure: solid curve, $(\pi,\alpha)=(+,\frac{1}{2})$; short-dashed curve, $(\pi,\alpha)=(+,-\frac{1}{2})$; dot-dashed curve $(\pi,\alpha)=(-,\frac{1}{2})$; double-dashed curve, $(\pi,\alpha)=(-,-\frac{1}{2})$. In the Nilsson diagram, positive- and negative-parity configurations are denoted by solid and short-dashed curves, respectively.

B. Pairing matrix elements

Consider Eqs. (3.3) for the normal phase:

$$(\varepsilon-\omega_{\rm rot}j_x)G=\varepsilon^{\omega}G,\quad (\varepsilon+\omega_{\rm rot}j_x)H=\bar{\varepsilon}^{\,\omega}H\ . \tag{5.1}$$

The resulting eigenstates can be written as

$$|j\rangle=|\pi,\alpha=\tfrac{1}{2}\rangle=\sum_K G_K^j|K\rangle$$

and

$$|\bar{j}\rangle=|\pi,\alpha=-\tfrac{1}{2}\rangle=\sum_k H_{\bar{k}}^{\bar{j}}|\bar{K}\rangle\ .$$

The states $|K\rangle$ and $|\bar{K}\rangle$ are Nilsson states with good signature,

$$|K\rangle=\frac{1}{\sqrt{2}}[(-1)^{\Omega_\nu-1/2}|\nu,\Omega_\nu\rangle+|\overline{\nu,\Omega_\nu}\rangle] \tag{5.2}$$

and

$$|\bar{K}\rangle=\frac{1}{\sqrt{2}}[-|\nu,\Omega_\nu\rangle+(-1)^{\Omega_\nu-1/2}|\overline{\nu,\Omega_\nu}\rangle]\ . \tag{5.3}$$

These states are related by time reversal. The violation of this symmetry is measured by the deviation from unity

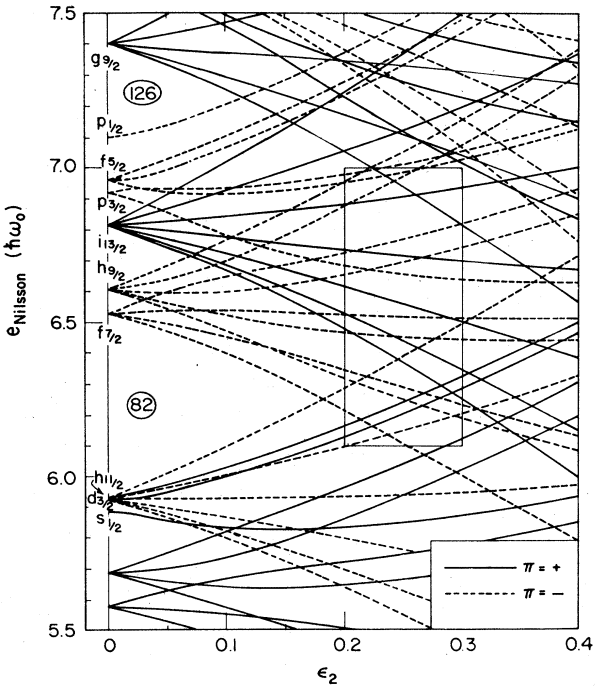

FIG. 9. Nilsson diagram showing the single-particle energies as a function of the quadrupole deformation ε_2. The modified-oscillator parameters of Bengtsson and Ragnarsson (1985) are used. The boxed area is shown enlarged in the left-hand portion of Fig. 8 together with the Nilsson model parameters for these configurations. Positive- and negative-parity configurations are denoted by solid and dashed curves, respectively.

of the matrix element of the pair-transfer operator

$$M(j\bar{j}')=\langle j\bar{j}'|\hat{P}^\dagger|0\rangle = \sum_{KK'} G_K^j H_{\bar{K}'}^{\bar{j}'} \langle K\bar{K}'|\hat{P}^\dagger|0\rangle \ . \tag{5.4}$$

The monopole pairing operator can be written as

$$\hat{P}^\dagger = \sum_{\nu_\alpha,\nu_\beta>0} \langle \bar{\nu}_\beta|\tau|\nu_\alpha\rangle C_{\nu_\alpha}^\dagger C_{\bar{\nu}_\beta}^\dagger \ , \tag{5.5}$$

where τ is the time-reversal operator. One can thus write

$$\langle KK'|\hat{P}^\dagger|0\rangle = \langle K'|\tau|K\rangle = \delta_{K'\bar{K}} \ . \tag{5.6}$$

We note that the pair field coincides with the transfer operator, which creates two particles in time-reversed states. From Eq. (5.6) one obtains

$$M(j\bar{j}')=\sum_K G_K^j H_{\bar{K}}^{\bar{j}'} \ , \tag{5.7}$$

which measures the pairing overlap between the orbitals j and $\bar{j}'$.

The resulting pair matrix elements $M(j\bar{j}')$ shown in Fig. 10 display conspicuous features. In particular for a high-J shell (e.g., the $i_{13/2}$ intruder orbit for rare-earth neutrons) they show a marked oscillatory behavior as a function of the rotational frequency when proceeding from the completely paired limit ($\omega_{rot}=0$) to the limit of

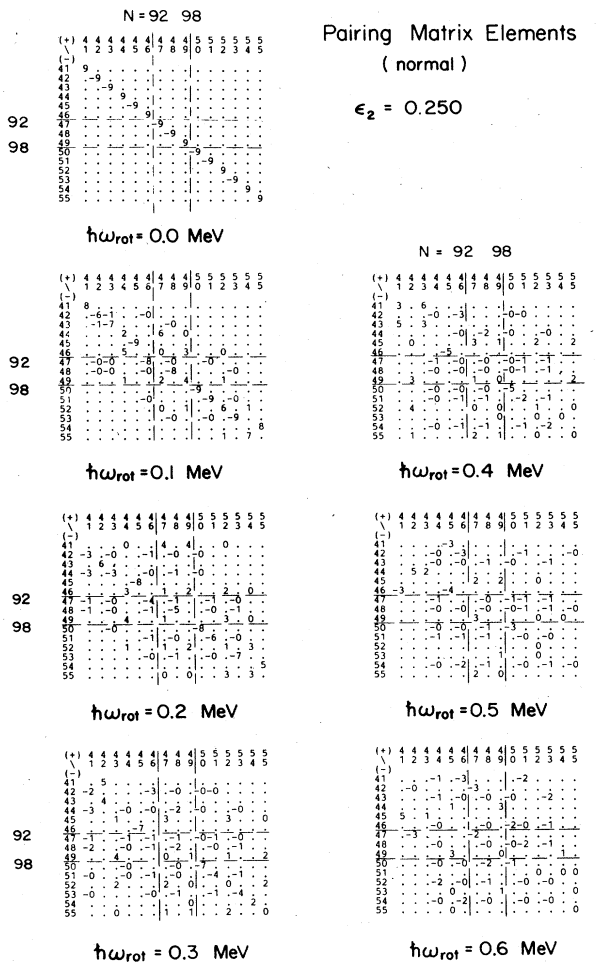

FIG. 10. Squared matrix elements of the pair operator [pairing overlaps; see Eq. (5.7)] between normal single-particle states associated with active configurations for the ytterbium isotopes. Values are tabulated as a function of the rotational frequency for $\varepsilon_2=0.25$. The labels $0,1,2,\ldots,9$ indicate values of M^2 between 0.01 and 0.1, 0.1 and 0.2, 0.2 and 0.3, . . . , 0.9 and 1.0. A dot indicates $M^2<0.01$. Minus and plus signs indicate matrix elements connecting negative- and positive-parity states, respectively. The numbers along the abcissa and ordinate count the signature $-\frac{1}{2}$ and $+\frac{1}{2}$ levels, respectively, starting with level number 1 at the bottom of the potential. This enumeration is shown for $\hbar\omega_{rot}=0$ in Fig. 8. The loci of the Fermi level for neutron numbers $N=92$ and 98 also are shown.

dominating Coriolis plus centrifugal force ($\omega_{rot}\to\infty$) (Broglia 1985; Broglia *et al.* 1985 1986; Nikam *et al.* 1986). This behavior is understood in terms of a semiclassical model (Vigezzi *et al.*, 1988) as well as a manifestation of the Berry phase (Nikam and Ring, 1987).

For a normal-parity state (e.g., the $N=5$ negative-parity neutron states in the rare-earth region), where several shell-model configurations contribute, the detailed behavior of the pair matrix elements $M(j\bar{j}')$ is more complicated, though the same general features are seen.

Two "hot" neutron orbits, which retain their paired character at quite large rotational frequencies, are encountered (see Fig. 10) near the Fermi level for the ytterbium nuclei considered in the analysis. The $\frac{11}{2}^-[505]$ orbital is near the Fermi level at $N=92$, and the $\frac{1}{2}^-[521]$ orbital is near Fermi level at $N=98$, see Figs. 8–19. These two orbitals, which retain sizable pair matrix elements up to $\hbar\omega_{\rm rot}=0.40$ MeV, will be important in many of the calculated properties considered in the ensuing discussion. The small j_x values for the $\frac{11}{2}^-[505]$ orbital, which is pure $h_{11/2}$, is a result of a large Ω. In contrast, the small value for the $\frac{1}{2}^-[521]$ orbital is a consequence of the small j value of this orbital, which at sizable deformations is dominantly $f_{5/2}$ and $p_{3/2}$ (see Fig. 9). The angular momentum vectors for these two orbitals are illustrated in Fig. 11, where they are also compared with that of a highly aligned $i_{13/2}$ orbital. It must be remarked that quadrupole pairing (Ragnarsson and Broglia, 1976; Wakai and Faessler, 1978; Diebel, 1984) is expected to modify the time-reversal properties, especially of the oblate $\frac{11}{2}^-[505]$ orbital (Garrett *et al.*, 1982; Peterson and Garrett, 1984), which has a different shape from the neighboring orbitals. The $\frac{11}{2}^-[505]$ orbital slopes upward on the Nilsson plot (Figs. 8 and 9), in contrast to the downward slopes of its neighbors.

C. Quasiparticle energies

Single-quasineutron energies (in the rotating frame—often called routhians), i.e., solutions of the eigenvalue problem (3.3), are shown as a function of rotational frequency in Fig. 12. The frequency-independent quadrupole deformation, $\varepsilon_2=0.25$, pair gap parameter, $\Delta=0.15\hbar\omega_0\approx 1.1$ MeV, and Fermi level, $\lambda=6.56\hbar\omega_0$, used in this calculation correspond approximately to the low-lying configurations of ^{166}Yb—see Table I and Fig. 8. The calculation of the single-quasineutron spectrum of states is essentially identical to a large number of other cranking, or cranked shell-model calculations shown in a variety of recent theoretical or experimental papers (see, for example, Bengtsson and Frauendorf, 1979; Riedinger *et al.*, 1980, Roy *et al.*, 1982, Bengtsson *et al.* 1986, Jónsson *et al.*, 1986). The alphabetic nonmenclature labeling the low-lying quasineutron configurations, also shown in this figure, is that commonly used in the literature; see, for example, Bengtsson and Frauendorf (1979) and Bengtsson *et al.* (1986). We shall often resort to a labeling of the states by the conserved quantum numbers of the intrinsic configuration (parity π and signature α), since such a labeling is also valid in the nonstatically paired regime. For quasiparticles, the following identifications can be made:

$$(\pi,\alpha)_n=\begin{cases}(+,\frac{1}{2})_1=A\ ,\\ (+,-\frac{1}{2})_1=B\ ,\\ (+,\frac{1}{2})_2=C\ ,\\ (+,-\frac{1}{2})_2=D\ ,\\ (-,\frac{1}{2})_1=E\ ,\\ (-,-\frac{1}{2})_1=F\ .\end{cases}$$

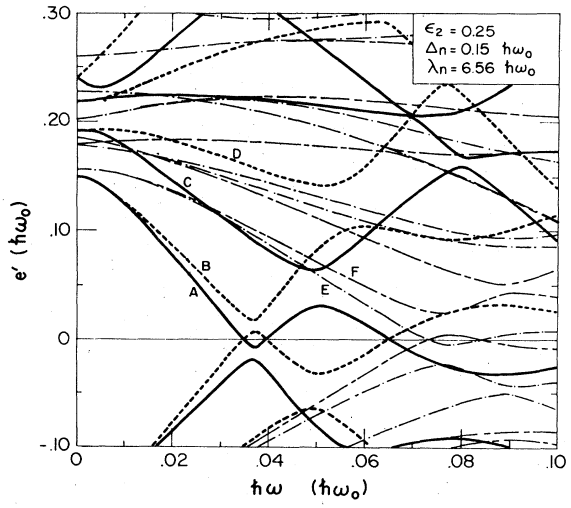

FIG. 12. Cranked shell-model quasiparticle energy diagram for neutrons ($A\approx 165$) in the superfluid phase as a function of the rotational frequency $\hbar\omega_{\rm rot}$. The parameters used in the calculation are given in the upper right-hand portion of the figure. Routhians e' are calculated for the following values of (π,α): solid curves, $(+,\frac{1}{2})$; short-dashed curves, $(+,-\frac{1}{2})$; dot-dashed curves $(-,\frac{1}{2})$; double-dashed curves, $(-,-\frac{1}{2})$. The alphabetic labeling given for a few of the low-lying orbitals and summarized in Sec. V.C of the text is that commonly used to denote quasineutron configurations in this mass region; see, for example, Bengtsson and Frauendorf (1979) and Riedinger *et al.* (1980).

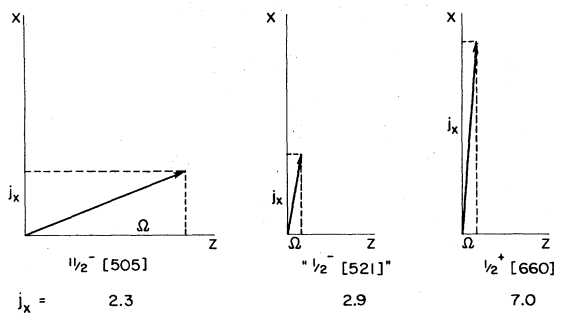

FIG. 11. Alignments of the intrinsic angular momentum j with respect to the nuclear symmetry axis z and the rotational axis x. Values are shown for the most aligned neutron configuration in this mass region, $\frac{1}{2}^+[660]$, and the two least aligned configurations near the Fermi surface for the light ytterbium isotopes considered in these calculations, $\frac{11}{2}^-[505]$, and "$\frac{1}{2}^-$"[521]. It is these two last configurations that retain large pairing matrix elements at large rotational frequencies; see Figs. 8 and 10. For the "$\frac{1}{2}^-$"[521] configuration, which is strongly mixed under rotation, $j=\frac{5}{2}$ and $\Omega=\frac{1}{2}$ were assumed. Values of j_x are also given.

A detailed discussion of the nomenclature and the correlation of theoretical quasiparticle orbitals to observed configurations is contained in Bengtsson and Garrett (1984) and Bengtsson *et al.* (1986).

D. Pair gaps and pair correlation energies

Self-consistent neutron pair gaps and RPA pair correlation energies are presented in Figs. 13, 15, 17, 19, 21, 23, 25, and 27 for the chain of ytterbium isotopes that are stably deformed and for which sufficient high-spin experimental data exist to allow a comparison in the region of the predicted quenching of the static neutron pair gap. The isotopes $^{162-169}Yb_{92-99}$ satisfy these criteria. Besides the normal static pairing gap, this series of figures shows the magnitude of Δ_{dyn}, as defined by Eq. (4.3). E_{corr}, the total RPA pair correlation energy, and E_{ex}, the exchange (or Fock) energy expressing the mean-field contributions to the RPA, are also given. These two quantities are defined in Eqs. (2.12) and (2.13), respectively.

For completeness, the calculated routhians and alignments, including and not including dynamical pairing effects, are compared in Figs. 14, 16, 18, 20, 22, 24, 26, and 28 with the corresponding experimental quantities for these same ytterbium systems, $^{162-169}Yb_{92-99}$. These quantities are discussed in Sec. V.E.

1. Pair gaps in the even-even ytterbium systems

A significant decrease of the neutron pair gap ($\approx$400 keV) is predicted, independent of the magnitude of Δ_n (at $\omega_{rot}=0$), at the frequency of the excitation of the most alignable pair of quasineutrons (i.e., at the *AB* quasineutron band crossing). The pair gap for the lowest $(\pi,\alpha)=(+,0)$ configurations, which becomes a two-quasineutron configuration after this crossing, decreases to the level of the lowest negative-parity configurations [$(-,1)$ or $(-,0)$] that also correspond to the excitation of two quasineutrons (*AE* or *AF*). Since the neutron pair-

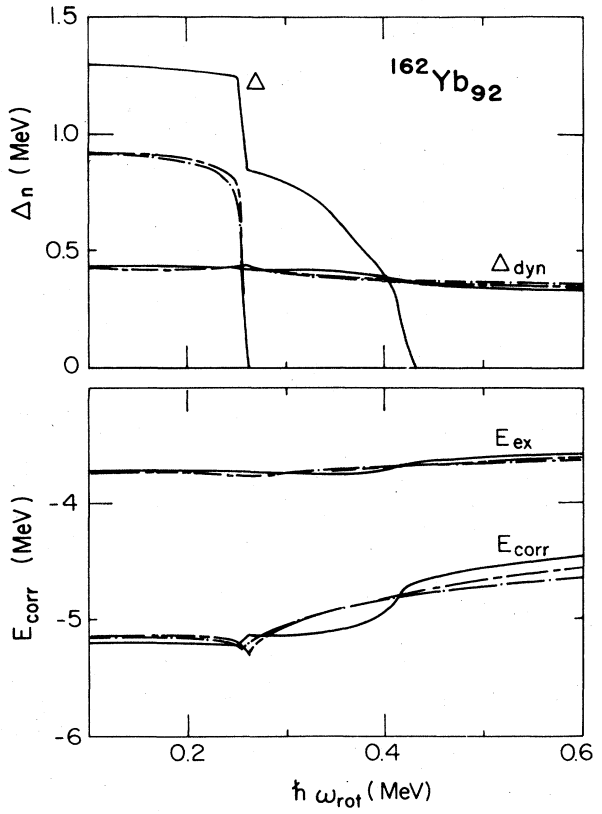

FIG. 13. Comparison of calculated static pair gaps Δ and dynamic pair gaps Δ_{dyn} (top portion) and of RPA correlation energies E_{corr} and exchange (Fock) energies E_{ex} (bottom portion) as a function of the rotational frequency $\hbar\omega_{rot}$ for a variety of configurations in $^{162}Yb_{92}$. Δ and Δ_{dyn}, defined by Eqs. (4.4) and (4.3), respectively, are discussed in Secs. IV.D and V.D.3. Likewise, E_{corr} and E_{ex} are defined by Eqs. (2.12) and (2.13), respectively, and are discussed in Secs. II and V.D.3. Configurations with $(\pi,\alpha)=(+,0)$, $(-,0)$, and $(-,1)$ are denoted by solid, dot-dashed, and double-dashed curves, respectively. A detailed discussion of this nucleus is given in Sec. V.E.2.

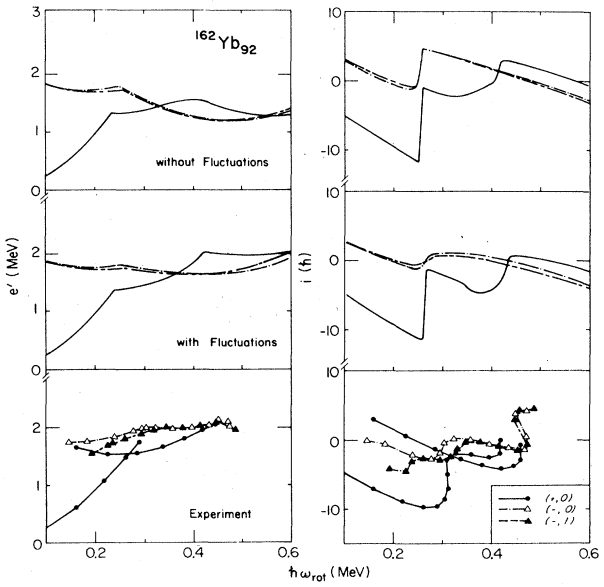

FIG. 14. Comparison of calculated and experimental routhians for various configurations in $^{162}Yb_{92}$: middle portion, with fluctuations; top portion, without fluctuations; bottom portion, experimental routhians e' (left-hand side) and alignments i (right-hand side). The corresponding static and dynamic pair gaps are shown in Fig. 13. Configurations are denoted as follows: solid lines and filled dots, $(+,0)$; dot-dashed lines and open triangles, $(-,0)$; double-dashed lines and filled triangles, $(-,1)$. The calculated and experimental values are referred to reference configurations with constant moments of inertia of 62 and 66 $\hbar^2$ MeV^{-1}, respectively. This nucleus is discussed in detail in Sec. V.E.2. The experimental data for ^{162}Yb are taken from Mo *et al.* (1987).

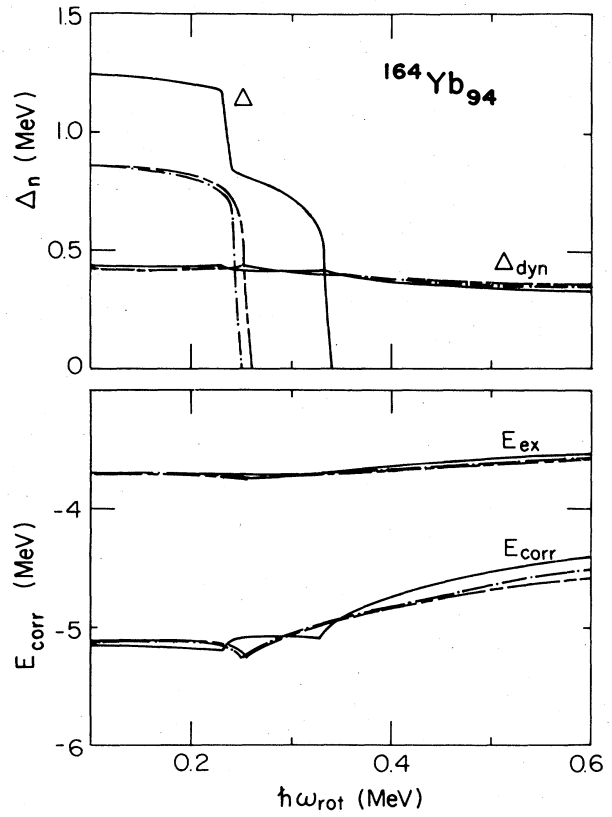

FIG. 15. Comparison of calculated static pair gaps Δ and dynamic pair gaps Δ_{dyn} (top portion) and RPA correlation energies E_{corr} and exchange (Fock) energies E_{ex} as a function of the rotational frequency $\hbar\omega_{rot}$ for a variety of configurations in $^{164}Yb_{94}$. See caption to Fig. 13 for additional information regarding the quantities plotted in this figure.

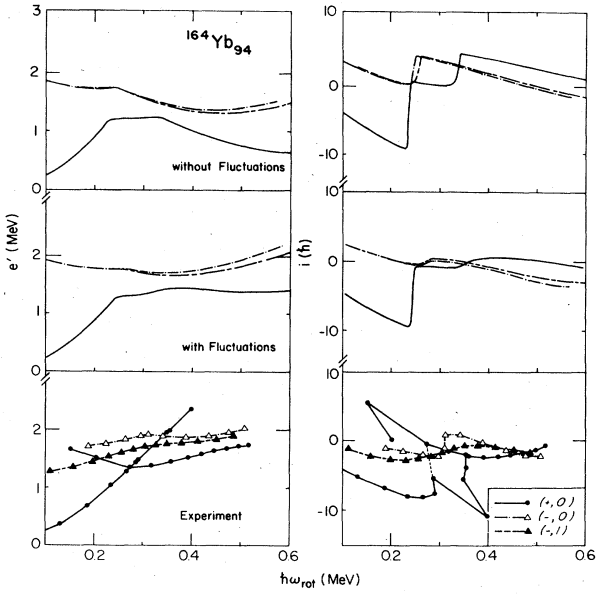

FIG. 16. Comparison of calculated and experimental routhians for various configurations in $^{164}Yb_{94}$: middle portion, with fluctuations; top portion, without fluctuations; bottom portion experimental routhians e' (left-hand side) and alignments i (right-hand side). The corresponding static and dynamic pair gaps are shown in Fig. 15. The experimental data for ^{164}Yb are taken from Schuck *et al.* (1985) and Jónsson *et al.* (1986). See the caption to Fig. 14 for additional information regarding definition of the quantities presented in this figure.

ing gap decreases as a function of N between $N=92$ and 98 (see Fig. 2), the relative decrease in Δ_n at this crossing is larger for the heavier ytterbium isotopes.

Above this band crossing a significant isotopic dependence is observed for the neutron pair gap. The value of Δ_n for (+,0) is predicted to decrease slowly up to about $\hbar\omega_{rot}=0.34$ MeV for $^{164}Yb_{93}$ and $^{166}Yb_{96}$ and then to plunge rapidly to zero. For $^{162}Yb_{92}$ and $^{168}Yb_{98}$ the (+,0) neutron pair gap parameter is observed to decrease more gradually above the *AB* crossing, finally disappearing at $\hbar\omega_{rot}\approx 0.45$ MeV. This behavior can be related to the survival of pair correlations in the $\frac{11}{2}^-[505]$ and $\frac{1}{2}^-[512]$ orbitals to rather large rotational frequencies—see Sec. V.B. The $\frac{11}{2}^-[505]$ and $\frac{1}{2}^-[521]$ "hot" orbitals are near the Fermi level at $N=92$ and 98, respectively.

The neutron pairing gaps for the negative-parity configurations are predicted to be nearly signature independent, as expected. The different negative-parity quasineutron orbitals (*E* and *F*) that give different signatures for these configurations when combined with orbital *A* are related by time reversal. Therefore occupying either orbital has a nearly identical effect on the pair gap.

The rapid quenching of the static neutron pair gap in the lowest negative-parity configurations of the even-even ytterbium isotopes apparently is associated with the fact that the excitation, or alignment, of the second most alignable pair of $i_{13/2}$ quasineutrons (*BC*) forming four quasineutron configurations (*ABCE* or *ABCF*) destroys the static neutron pair gap. It should be emphasized that above this frequency we can neither use the familiar quasiparticle language for neutrons nor talk of the alignment of a pair of quasineutrons. The neutron pair condensate from which the quasineutron pair is created simply does not exist in the absence of a static pair gap. Indeed, band crossings associated with excitations of pairs of quasineutrons apparently are absent at larger rotational frequencies (Garrett, 1988; Riley, Garrett, Simpson, and Sharpey-Schafer, 1988). The relation between the excitation of a pair of quasiparticles at a band crossing and the enhanced two-nucleon collective transfer between pair-correlated configurations (see Sec. VI) is noted. The occurrence of both effects depends on the existence of a pair condensate that can change particle number without changing structure, and from which the pair of quasiparticles can be created.

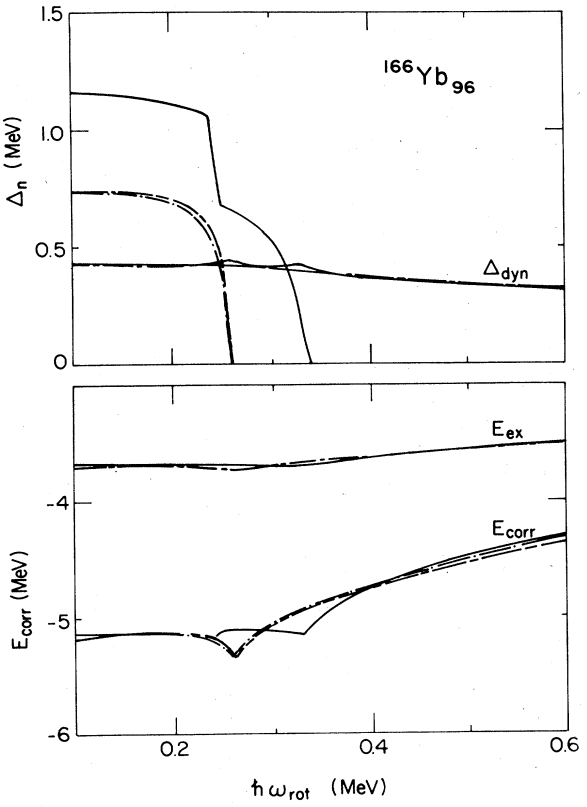

FIG. 17. Comparison of calculated static pair gaps Δ and dynamic pair gaps Δ_{dyn} (top portion) and RPA correlation energies E_{corr} and exchange (Fock) energies E_{ex} (bottom portion) as a function of the rotational frequency $\hbar\omega_{rot}$ for a variety of configurations in $^{166}Yb_{96}$. See caption to Fig. 13 for additional information regarding the quantities plotted in this figure.

A band crossing, however, will also be associated with the quenching of the static neutron pair gap if the frequency dependence of the two-quasineutron configurations (AE and AF) is significantly different from that of the lowest unpaired negative-parity configuration of the corresponding signature. This is expected to be the case, since moments of inertia are very sensitive to pair correlations. We wish to emphasize that this explanation of band crossing in the negative-parity sequences of these even-even isotopes is different from the conventional interpretation (see, for example, Bengtsson and Frauendorf, 1979; Riedinger *et al.*, 1980; Jónsson *et al.*, 1986) in terms of the alignment, or excitation, of a pair of quasineutrons. Of course, the routhians of these configurations, and hence the whole picture, will be somewhat modified by dynamical pairing effects. Such effects will smear, and perhaps shift, the band crossing; however, it should not alter its occurrence.

The quenching of the static neutron pair gap, for the negative-parity levels and the associated band crossing, is predicted at about the same rotational frequency as the AB crossing in these even-even isotopes. This is contrary to experiment. The frequencies of these band crossings are somewhat increased when dynamical pairing effects are included; however, they continue to be predicted too low in the full calculations; see Sec. V.G. The reduction of pair correlations in these negative-parity bands, and the associated reduction of the band crossing frequencies, by the occupation of the two excited quasineutrons ("blocking") is probably overestimated. On a relative scale, however, the isotopic dependence of the static pair collapse in the negative-parity configurations can be understood and is in agreement with experiment.

The fact that the quenching of the static neutron pair gap is predicted at lower rotational frequencies for the negative-parity configurations of $^{168}Yb_{98}$ than for such configurations in the other even-even ytterbium isotopes is understood. The $\frac{1}{2}^-[521]$ "hot" quasineutron is excited in the negative-parity configurations of ^{168}Yb. Indeed, the band crossing in the negative-parity sequences of ^{168}Yb is observed at a lower rotational frequency than for the other even-even ytterbium isotopes; see Sec. V.G, Bacelar *et al.* (1985), and Jónsson *et al.* (1986).

2. Pair gaps in the odd-*N* ytterbium systems

At the lowest rotational frequencies the static neutron pair gap parameter is nearly equal for negative- and positive-parity configurations in the odd-N ytterbium systems considered. The magnitude is about midway between that of the zero- and two-quasineutron configurations of the neighboring even-even ytterbium isotopes. These systematics can be explained as follows: At small rotational frequencies both the positive- and negative-parity configurations in the odd-N isotopes correspond to single-quasineutron excitations. In contrast, for the even-even ytterbium isotopes the low-lying positive-parity configurations have no excited quasineutrons, while the negative-parity configurations have two.

Significant decreases are predicted in the static neutron pair gap at the band crossings. In the negative-parity sequences the crossings correspond to the excitation of A and B quasineutrons (see Table III and Fig. 12). Quasineutron A is already excited in the positive-parity sequences; therefore the next most alignable pair of quasineutrons (B and C) is excited at the band crossing (see Grosse *et al.*, 1973). For the positive-parity configurations in $^{163}Yb_{93}$ and $^{167}Yb_{97}$ and the negative-parity configurations in $^{165}Yb_{95}$ and $^{169}Yb_{99}$ the excitation of this additional pair of quasineutrons is predicted to completely quench the static neutron pair gap. Thus the associated band crossings would be expected to correspond to crossings between single-quasineutron bands and unpaired bands. These crossings are predicted to occur at rotational frequencies nearly identical to that associated with three-quasineutron crossings in neighboring odd-N isotopes, where the static neutron pair correlations are not predicted to vanish for the three-

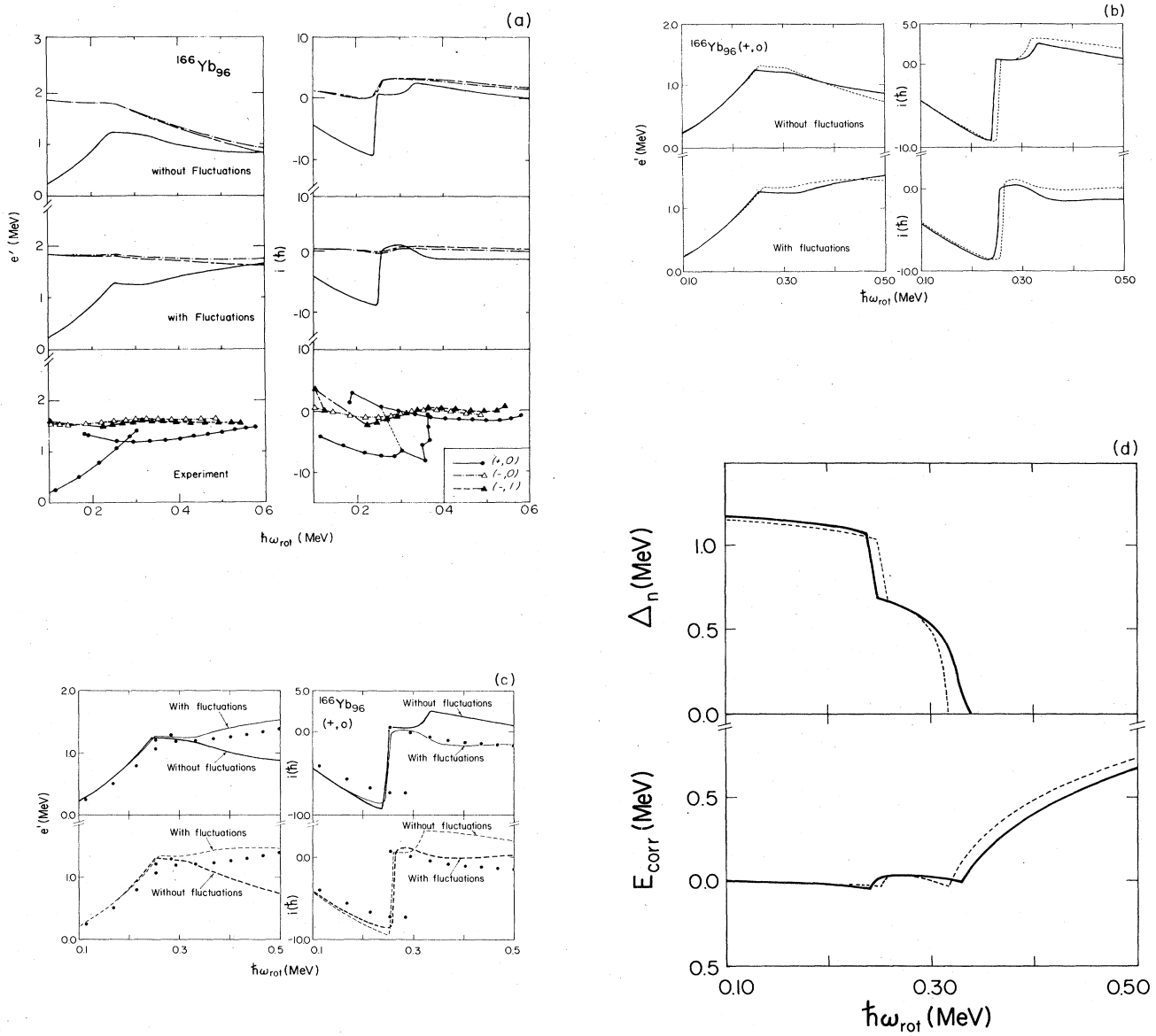

FIG. 18. (a) Comparison of calculated and experimental routhians for various configurations in $^{166}Yb_{96}$: middle portion, with fluctuations; top portion, without fluctuations; bottom portion, experimental routhians e' (left-hand side) and alignments i (right-hand side). The corresponding static and dynamic pair gaps are shown in Fig. 17. The experimental data for ^{166}Yb are taken from Waluś *et al.* (1981) and Beck *et al.* (1987). See the caption to Fig. 14 for additional information regarding the definition of the quantities presented in this figure. (b) Comparison of routhians and alignments for the (+,0) configuration in ^{166}Yb, calculated at a fixed deformation $\varepsilon_2=0.25$ (solid curves) and with the self-consistent value of $\varepsilon_2(\omega)$, shown in Table IV (dashed curves). (c) The routhians and alignments for the (+,0) configuration in ^{166}Yb with and without pairing fluctuations, compared with the experimental data: top portion, calculated with constant deformation; bottom portion, calculated with changing deformation. (d) Comparison of the energy gap Δ_n and the correlation energy $E_{\rm corr}$ for the (+,0) configuration of ^{166}Yb relative to the values at $\omega_{\rm rot}=0$: solid curve, calculated keeping the value of ε_2 fixed at $\varepsilon_2=0.250$; dashed curve, calculated using the self-consistent value. (e) Comparison of measured (Bacelar *et al.*, 1987) and calculated (Garrett *et al.*, 1988) $B(E2)/B(E2)_{\rm rot}$ ratios for the yrast decay sequence of ^{166}Yb. The predicted $B(E2)$ ratios correspond to the deformations of the minimum potential energy values [see Table V and Fig. 18(f)], calculated using the Warsaw Woods-Saxon code (Nazarewicz *et al.*, 1985). Calculations are shown corresponding to predicted static and particle-number-projected pair gaps. The predicted curves for $\hbar\omega_{\rm rot}>0.45$ MeV are dashed, indicating that effects corresponding to an unobserved quasiproton band crossing have been removed from the calculations as described in Garrett *et al.* (1988) and Nyberg *et al.* (1988). (f) Deformations of predicted minima in the potential energy surface for the yrast decay sequence of ^{166}Yb as a function of $\hbar\omega_{\rm rot}$. The numbers accompanying the data points are $\hbar\omega_{\rm rot}$ values in MeV. These minima were calculated (Garrett *et al.*, 1988) for full-strength neutron pair correlations and without proton contributions using the Warsaw Woods-Saxon code described by Nazarewicz *et al.* (1985).

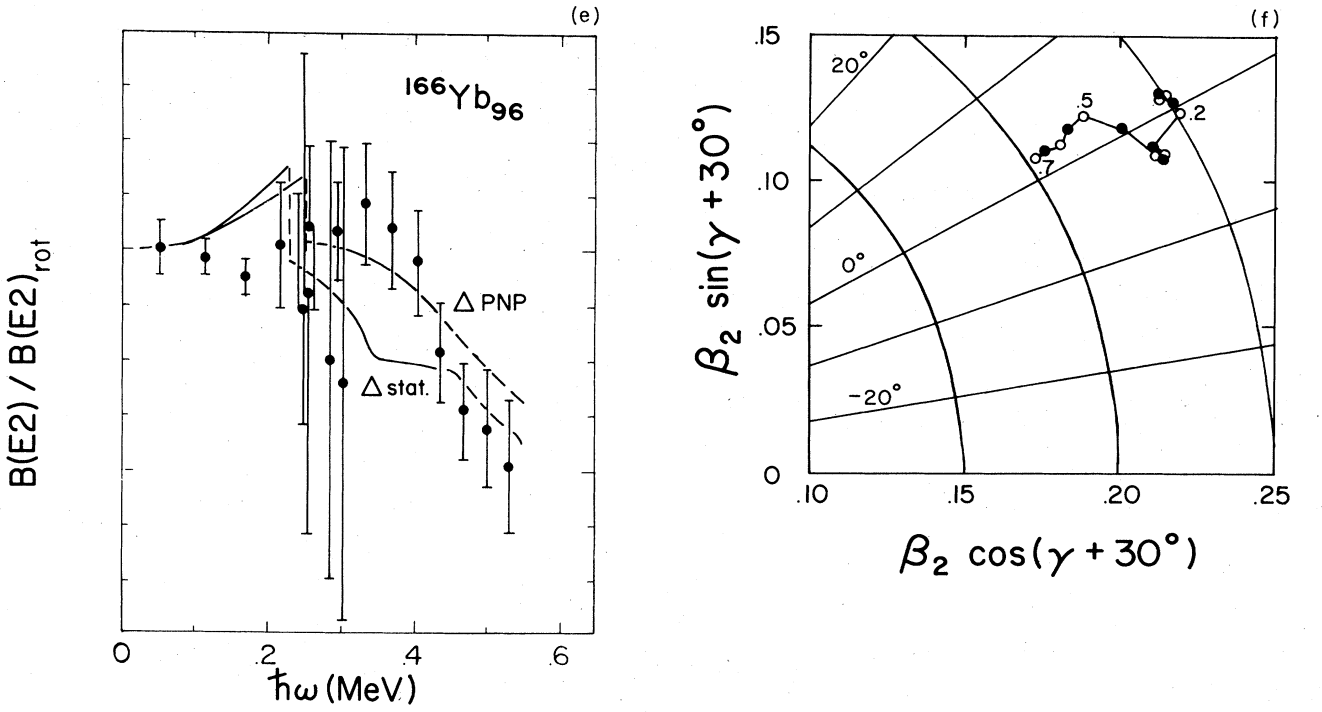

FIG. 18. (*Continued*).

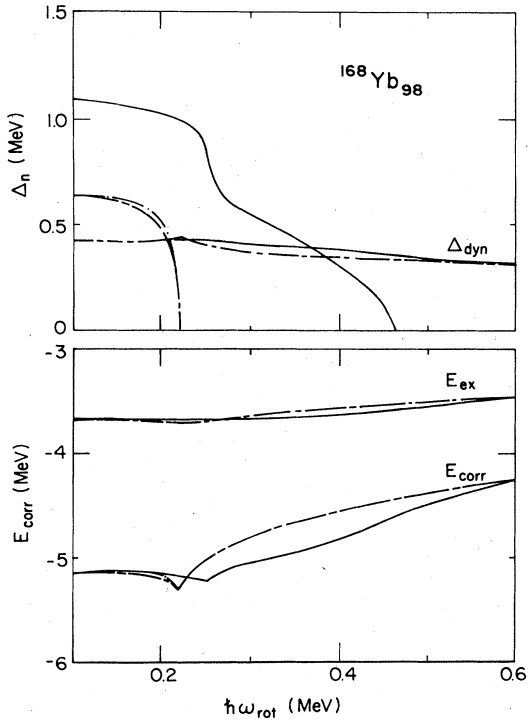

FIG. 19. Comparison of calculated static pair gaps Δ and dynamic pair gaps $\Delta_{\rm dyn}$ (top portion) and RPA correlation energies $E_{\rm corr}$ and exchange (Fock) energies $E_{\rm ex}$ (bottom portion) as a function of the rotational frequency $\hbar\omega_{\rm rot}$ for a variety of configurations in $^{168}Yb_{98}$. See caption to Fig. 13 for additional information regarding the quantities plotted in this figure.

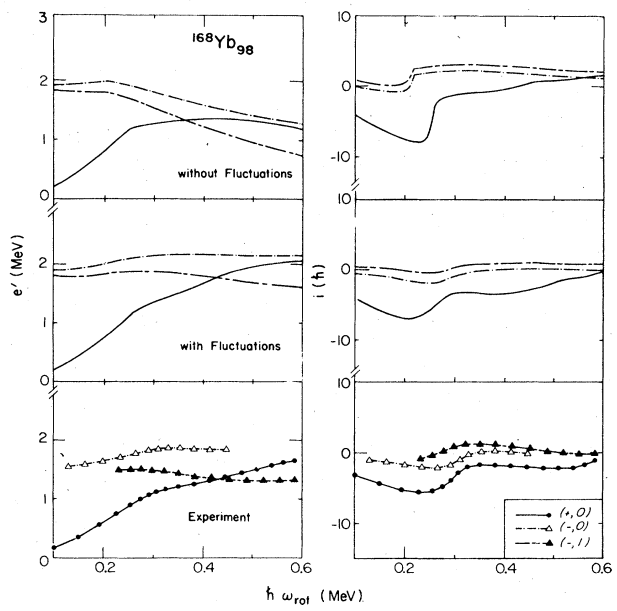

FIG. 20. Comparison of calculated and experimental routhians for various configurations in $^{168}Yb_{98}$: middle portion, with fluctuations; top portion, without fluctuations; bottom portion, experimental routhians e' (left-hand side) and alignments i (right-hand side). The corresponding static and dynamic pair gaps are shown in Fig. 19. The experimental data for ^{168}Yb are taken from Bacelar *et al.* (1985). See the caption to Fig. 14 for additional information regarding the definition of the quantities presented in this figure.

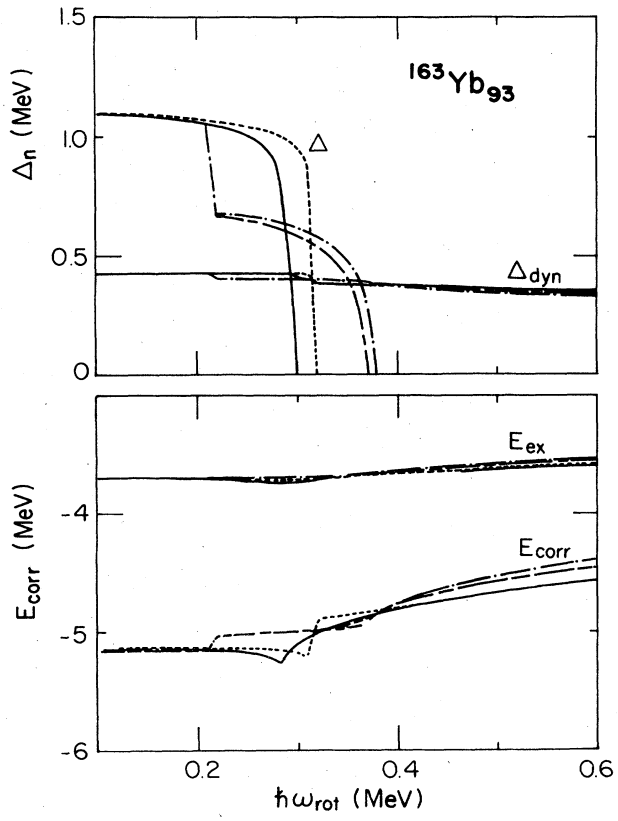

FIG. 21. Comparison of calculated static pair gaps Δ and dynamic pair gaps Δ_{dyn} (top portion) and RPA correlation energies E_{corr} and exchange (Fock) energies E_{ex} (bottom portion) as a function of the rotational frequency $\hbar\omega_{rot}$ for a variety of configurations in $^{163}Yb_{93}$. Δ and Δ_{dyn}, defined by Eqs. (4.4) and (4.3), respectively, are discussed in Secs. IV.D and V.D.3. Likewise, E_{corr} and E_{ex} are defined by Eqs. (2.12) and (2.13), respectively, and are discussed in Secs. II and V.D.3. Configurations are given for the following values of (π,α): solid curve, $(+,\frac{1}{2})$; short-dashed curve, $(+,-\frac{1}{2})$; dot-dashed curves, $(-,\frac{1}{2})$; double-dashed curve, $(-,-\frac{1}{2})$. This nucleus is discussed in detail in Sec. V.E.2.

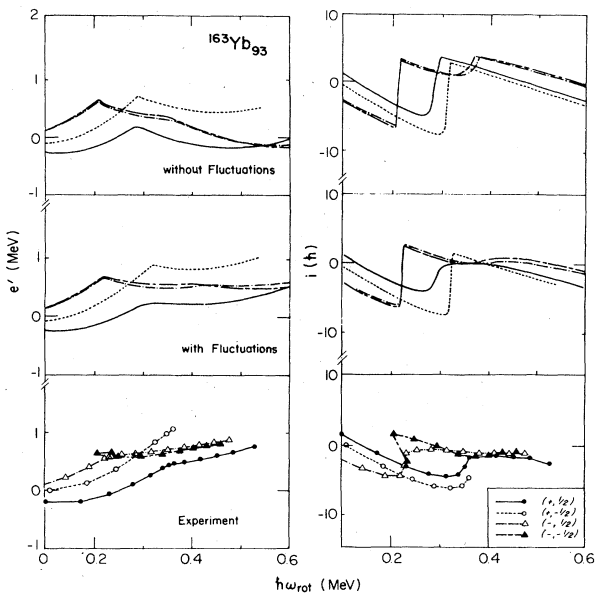

FIG. 22. Comparison of calculated and experimental routhians for various configurations in $^{163}Yb_{93}$: middle portion, with fluctuations; top portion without fluctuations; bottom portion, experimental routhians e' (left-hand side) and alignments i (right-hand side). The corresponding static and dynamic pair gaps are shown in Fig. 21. Configurations are denoted as follows: solid lines and filled circles, $(+,\frac{1}{2})$; dotted lines and open circles, $(+,-\frac{1}{2})$; dot-dashed lines and open triangles, $(-,\frac{1}{2})$; double-dashed lines and filled triangles, $(-,-\frac{1}{2})$. The calculated and experimental values are referred to reference configurations with constant moments of inertia of 62 and 66 $\hbar^2$ MeV^{-1}, respectively. This nucleus is discussed in detail in Sec. V.E.2. The experimental data for ^{163}Yb are taken from Kownacki *et al.* (1983) and Shuck *et al.* (1985).

quasineutron configurations. Thus it is probable that the predicted quenching of the static pair correlations for the negative-parity configurations in $^{165}Yb_{95}$ and $^{169}Yb_{99}$ and for the positive-parity configurations of $^{163}Yb_{93}$ and $^{197}Yb_{97}$ is associated with corresponding *AB* and *BC* or *AD* quasineutron alignments.

It is not surprising that the neutron pair correlations are predicted to be quenched in the three-quasineutron configurations of $^{169}Yb_{99}$. The $\frac{1}{2}^-[521]$ "hot" orbital is blocked, leading to reduced pair correlations for this decay sequence (see Fig. 27). We have no simple argument, however, explaining the predicted static neutron pair gap for some of the remaining three-quasineutron configurations and not for the others. The concept of a static neutron pair gap for these three-quasineutron configurations is ambiguous, since the magnitude of the static gap is of the order of the dynamic pair gap Δ_{dyn} (see Figs. 21, 23, 25, and 27).

3. The dynamic pair gap Δ_{dyn} and the RPA correlation energy E_{corr}

The total RPA correlation energy E_{corr}, the exchange Fock energy E_{ex}, and the dynamical pair gap Δ_{dyn}, which is proportional to the square root of the difference of these two correlation energies [see Eq. (4.3)], are predicted to be nearly independent of configuration and isotope. The magnitude of Δ_{dyn} decreases slowly from about 400–450 keV at $\hbar\omega_{rot}=100$ keV to 300–350 keV at 600 keV. This frequency dependence is slightly larger for the heavier ytterbium isotopes.

The relative magnitudes of the static neutron pairing gap Δ_n and the effective dynamic neutron pair gap Δ_{dyn} give an estimate of the relative importance of static and

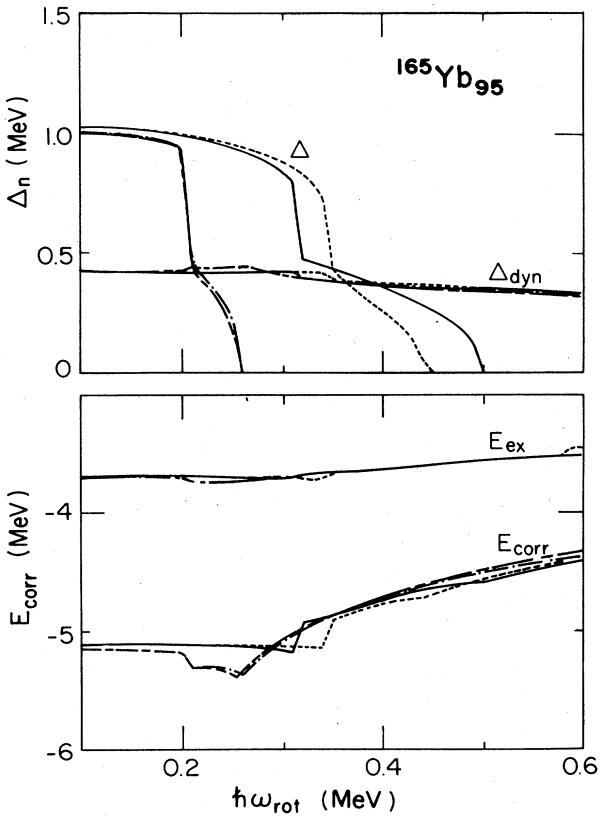

FIG. 23. Comparison of calculated static pair gaps Δ and dynamic pair gaps Δ_{dyn} (top portion) and RPA correlation energies E_{corr} and exchange (Fock) energies E_x (bottom portion) as a function of the rotational frequency $\hbar\omega_{rot}$ for a variety of configurations in $^{165}Yb_{95}$. See the caption to Fig. 21 for additional information regarding quantities plotted in this figure.

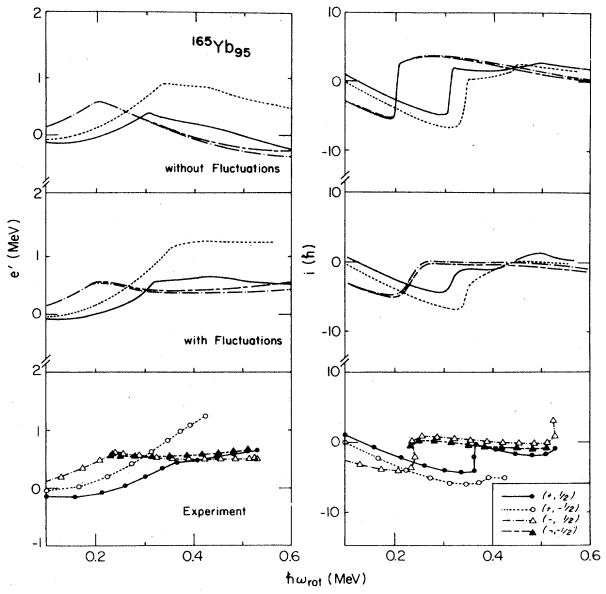

FIG. 24. Comparison of calculated and experimental routhians for various configurations in $^{165}Yb_{95}$: middle portion, with fluctuations; top portion, without fluctuations; bottom portion, experimental routhians e' (left-hand side) and alignments i (right-hand side). The corresponding static and dynamic pair gaps are shown in Fig. 23. See the caption to Fig. 22 for the definition of the various quantities plotted in this figure. The experimental data for ^{165}Yb are taken from Roy *et al.* (1982), Schuck *et al.* (1984, 1985).

dynamic neutron pair correlations. For example, it makes little sense to discuss the effects of the static pair gap when it is less than or of the order of the dynamic pair gap. The effects of the dynamic pairing correlations not only dominate at large rotational frequencies, but they continue to exist up to very large rotational frequencies (see Fig. 29).

As long as the static pairing gap has a sizable value ($\Delta \gtrsim \Delta_{dyn}$), the quantity E_{corr} is essentially constant as a function of $\hbar\omega_{rot}$. It acquires a marked dependence on $\hbar\omega_{rot}$ for values larger than the critical frequency at which the static pairing gap collapses. This dependence leads to a dealignment of the single-particle motion [see Eq. (3.18)]. Consequently the effects of the pairing fluctuations are much more important after the static pairing collapse.

The constancy of E_{corr} in the region of rotational frequencies where $\Delta > \Delta_{dyn}$ testifies to the rigidity of the pairing deformation. In this regime, a large fraction of E_{corr} is associated with pairing rotations, in particular, with the number-conserving collective mode.

E. Comparison of calculated and experimental routhians and alignments

Routhians (i.e., excitation energies in the rotating system) and alignments ($i = -de'/d\omega$) calculated with and without the effects of pair fluctuations are compared with the corresponding experimental quantities in Figs. 14, 16, 18, 20, 22, 24, 26, and 28. To magnify the details of the calculated and experimental routhians and alignments in the data figures, a "reference" configuration with constant moment of inertia has been subtracted. [See Frauendorf (1982), Bengtsson, Frauendorf, and May (1986), and Zhang *et al.* (1986) for detailed discussions of reference configurations.] Of course, this procedure preserves the relative spacing of the routhians and alignments. The calculated routhians and alignments, which in the region of the quenching of the static pairing gap have been smoothed as described in Sec. IV.E, are referred to a configuration with $J_0 = 62\ \text{MeV}^{-1}\hbar^2$. The effects of quasiprotons for the case of $^{168}Yb_{98}$ can be ascertained by comparing the calculated routhians and alignments of Fig. 20 with those of Fig. 30, which does not include quasiproton contributions. The main effect of the quasiprotons is a contribution to the moment of inertia. Note that the reference configuration for the calcu-

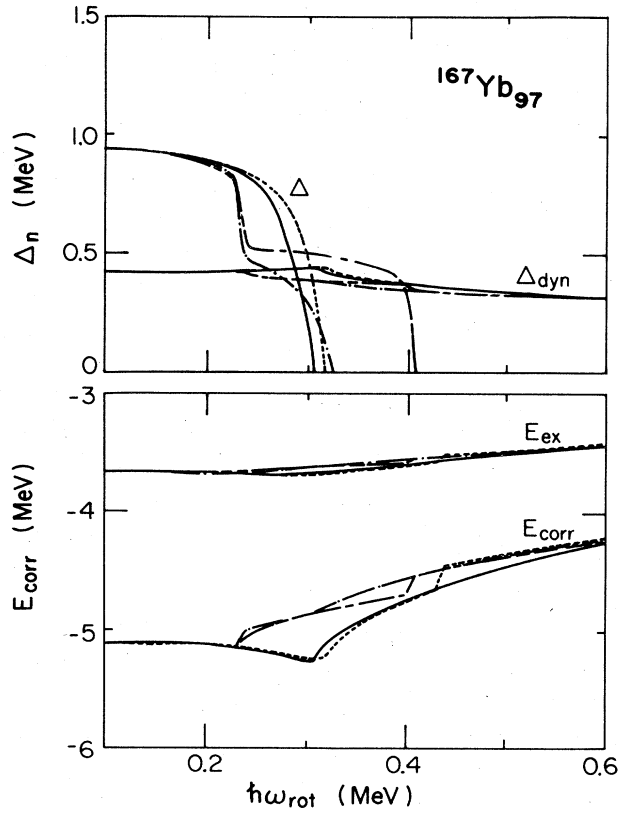

FIG. 25. Comparison of calculated static pair gaps Δ and dynamic pair gaps Δ_{dyn} (top portion) and RPA correlation energies E_{corr} and exchange (Fock) energies E_{ex} (bottom portion) as a function of the rotational frequency $\hbar\omega_{rot}$ for a variety of configurations in $^{167}Yb_{97}$. See the caption to Fig. 21 for additional information regarding the quantities plotted in this figure.

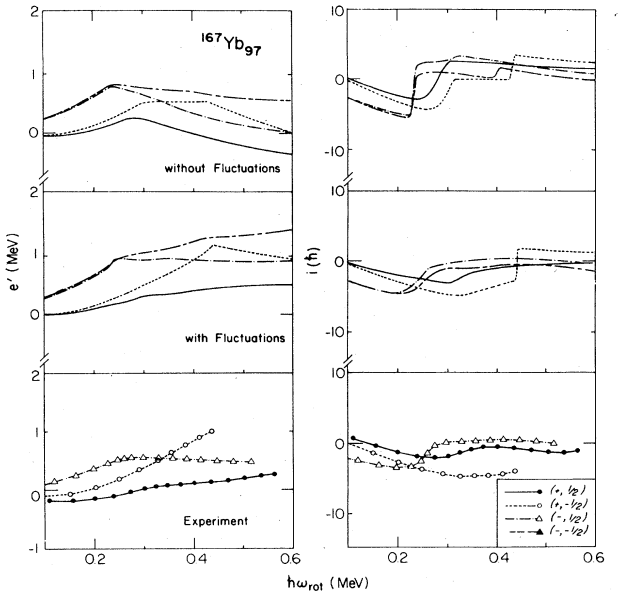

FIG. 26. Comparison of calculated and experimental routhians for various configurations in $^{167}Yb_{97}$: ; middle portion, with fluctuations; top portion, without fluctuations; bottom portion, experimental routhians e' (left-hand side) and alignments i (right-hand side). The corresponding static and dynamic pair gaps are shown in Fig. 25. See the caption to Fig. 22 for the definition of the various quantities plotted in this figure. The experimental data for ^{167}Yb are taken from Roy *et al.* (1982) and Bacelar *et al.* (1985).

lations of Fig. 30 has a moment of inertia $J_0=49$ MeV$^{-1}\hbar^2$, while 62 MeV$^{-1}\hbar^2$ is the moment of inertia for calculations including quasiprotons.

The experimental data, also referred to a constant moment-of-inertia reference ($J_0=66$ MeV$^{-1}\hbar^2$), are taken from the literature summarized in Table I. The experimental reference, about 85% of the rigid-body value for a deformed nucleus with a quadrupole deformation of $\varepsilon_2=0.25$, corresponds to the average moment of inertia of the negative-parity sequences at the largest rotational frequencies (Garrett, 1985b; Zhang *et al.*, 1986). The remaining 15% contribution to the moment of inertia corresponds to the reduction associated with proton pair correlations. Indeed the moments of inertia of the least-correlated configurations of the $N=90$ and 91 isotones above the proton band crossings approach the deformed rigid-body value (Garrett, 1985b).

There is a small difference, about 6%, between the theoretical ($J_0=62$ MeV$^{-1}\hbar^2$) and the experimental ($J_0=66$ MeV$^{-1}\hbar^2$) references. The moment of inertia for the ground state calculated by the Inglis formula with reasonable values of the deformation and pair gap parameters systematically underestimates the experimental value (Nilsson and Prior, 1961; Dudek *et al.*, 1980). In contrast, the moment of inertia calculated using the Nilsson potential without pairing overestimates the rigid-body value because of the momentum-dependent l^2 term (Andersson *et al.*, 1976; Neergård *et al.*, 1977; Bengtsson *et al.*, 1978). In the present calculations, the Nilsson potential is used, but the normal phase is realized only for neutrons. Moreover, the proton contribution is not treated fully microscopically in the high-frequency region (see Sec. IV.C). Therefore it is an open question why the theoretical reference underestimates the experimental one. In order to obtain the correct value, a more satisfactory treatment of protons is needed.

1. General effects of pair fluctuations on routhians and alignments

The general effect of pair correlations on the routhians is to give a more positive slope, i.e., less alignment

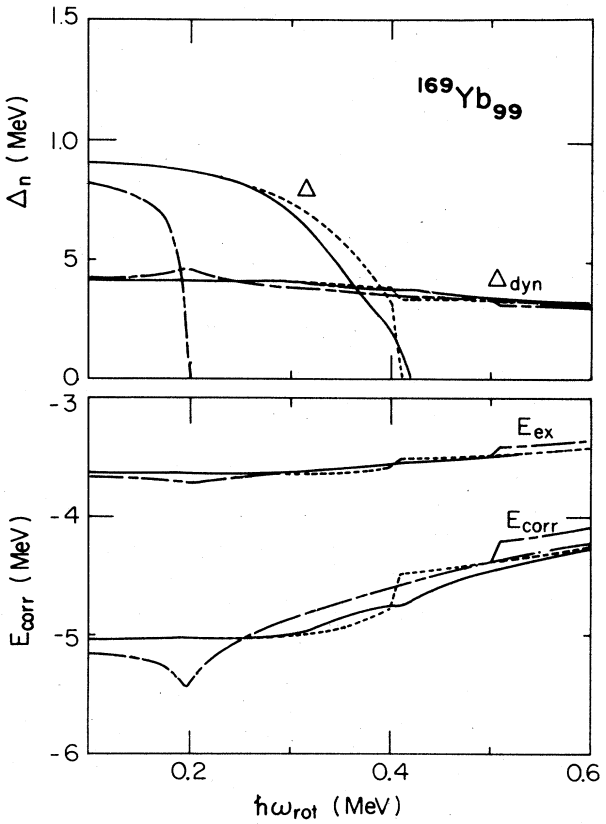

FIG. 27. Comparison of calculated static pair gaps Δ and dynamic pair gaps Δ_{dyn} (top portion) and RPA correlation energies E_{corr} and exchange (Fock) energies E_{ex} (bottom portion) as a function of the rotational frequency $\hbar\omega_{rot}$ for a variety of configurations in $^{169}Yb_{99}$. See the caption to Fig. 21 for additional information regarding quantities plotted in this figure.

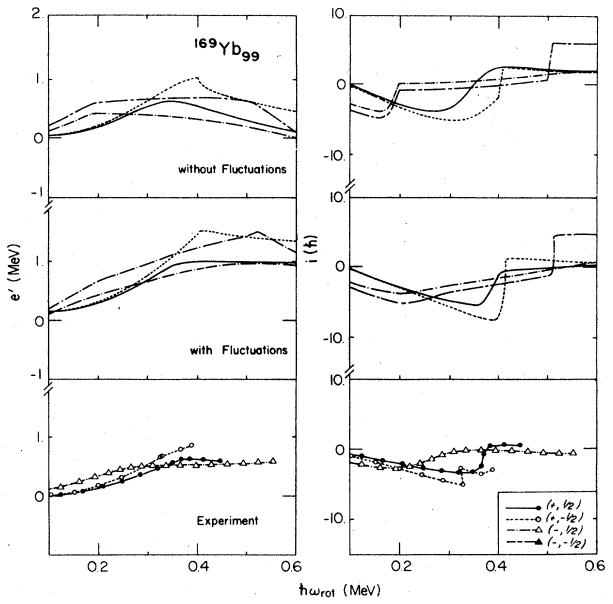

FIG. 28. Comparison of calculated and experimental routhians for various configurations in $^{169}Yb_{99}$: middle portion, with fluctuations; top portion, without fluctuations; bottom portion, experimental routhians e' (left-hand side) and alignments i (right-hand side). The corresponding static and dynamic pair gaps are shown in Fig. 27. See the caption to Fig. 22 for the definition of the various quantities plotted in this figure. The experimental data for ^{169}Yb are taken from Bacelar *et al.* (1985).

($i=-de'/d\omega$) and a smaller moment of inertia. The moment of inertia corresponds to the curvature of $e'(\omega_{rot})$. Let us consider as an example the case of the ground-state band of the even-even isotopes. In this case, the static pair gap is large. Hence the moment of inertia and the alignment are small. [The positive slope of the $e'(\omega_{rot})$ plot, i.e., $i<0$, is a result of a reference appropriate to nonstatistically paired neutron configurations.] Above the band crossing the slope of the (+,0) yrast sequence decreases as a result of increased alignment and momenta of inertia.

In addition to an unpaired spectrum of single-neutron states such as that shown in Fig. 8, two effects of pair correlations must be considered in a discussion of the routhians and alignments: (i) the self-consistent calculation of the static neutron pair gap and (ii) the role of pair fluctuations. Predictions of a larger static pair gap for the (+,0) sequence than for the negative-parity sequences in the even-even isotopes give a lower energy and a smaller alignment and moment of inertia for the (+,0) sequence. Pair fluctuations extend such features to larger rotational frequencies. Indeed, the systematically observed lower excitation energy and smaller alignment and moment of inertia for the (+,0) sequence than for either

TABLE III. Identification of quasineutron configurations with the various decay sequences.

	Decay sequence (π,α)	Quasineutron configuration[a] Below band crossing	Above band crossing
Even-even isotopes	(+,0)	0[b]	*AB*
	(−,0)	*AF*	*AFBC*[c]
	(−,1)	*AE*	*AEBC*[c]
Odd-*N* isotopes	$(+,\frac{1}{2})$	*A*	*ABC*[c]
	$(+,-\frac{1}{2})$	*B*	*BAD*[c]
	$(-,\frac{1}{2})$	*E*	*EAB*[c]
	$(-,-\frac{1}{2})$	*F*	*FAB*[c]

[a] Labeling of quasineutron configurations given in Fig. 12.
[b] Even-even ground-state vacuum configuration. No excited quasiparticles.
[c] Quasineutron configuration not valid when $\Delta\to 0$. See Sec. V.D.

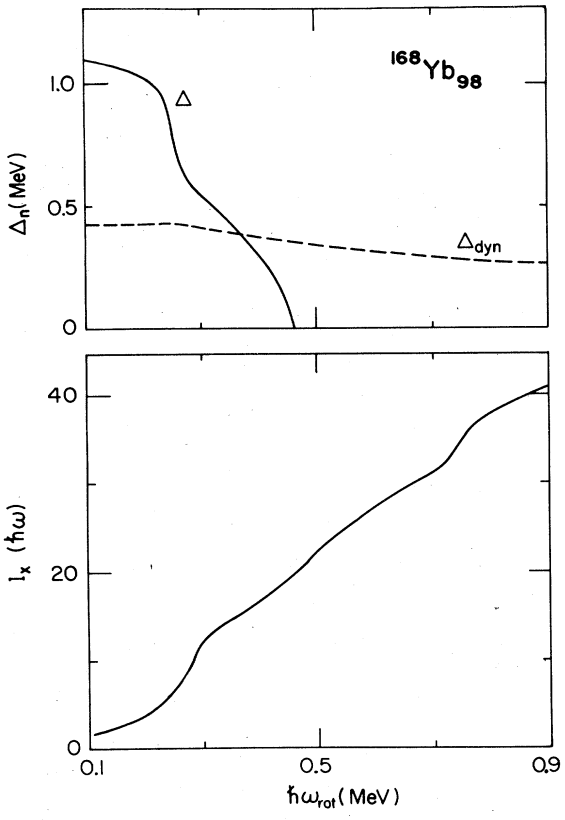

FIG. 29. The calculated static neutron pair gap Δ, dynamic neutron pair gap Δ_{dyn}, and total angular momentum component along the rotational axis I_x, for the lowest (+,0) configuration of $^{168}Yb_{98}$ are extended to large rotational frequencies, $\hbar\omega_{rot}=0.9$ MeV. [Δ and Δ_{dyn} are defined by Eqs. (4.4) and (4.3), respectively]. Note that Δ_{dyn} continues to large values of $\hbar\omega_{rot}$ and that the intrinsic alignment (see Fig. 31 and Sec. V.E) increases at large $\hbar\omega_{rot}$.

negative-parity sequence, (−,0) or (−,1), which extend to very large rotational frequencies (see Figs. 14, 16, 18, and 20), can be viewed as evidence for the existence of neutron pair fluctuations. Such effects will also shift possible crossings between the routhians of the (+,0) and the negative-parity sequences to larger rotational frequencies and will result in larger relative alignments for these crossings. The largest such effects will occur for a maximum separation in rotational frequency of the quenching of the static neutron pair gap for the (+,0) and negative-parity sequences, i.e., $^{168}Yb_{98}$.

Similar general arguments can be advanced for the odd-N isotopes. The effects, however, are more subtle. The configuration dependence of the static neutron pair gap is predicted neither to be as large nor to persist for as large a frequency range as for the even-even isotopes (see Figs. 21–28).

2. The routhians and alignments of even-even ytterbium isotopes

$^{162}Yb_{92}$ (Figure 14). The calculations with pair fluctuations predict the absolute magnitude of the (+,0) routhian reasonably well. The routhians of the negative-parity sequences at large rotational frequencies, however, are predicted 300–400 keV too low. Removing pair fluctuations from the calculations produces even poorer agreement. This significant discrepancy is attributed to the single-neutron spectrum of states (see Sec. V.E.4). The predicted band crossing in the (+,0) sequence at $\hbar\omega_{rot}=0.42$ MeV is not observed in experiment. The band crossing observed at $\hbar\omega_{rot}=0.46$ MeV, attributed to the excitation of a pair of quasiprotons, since it occurs in all sequences, is not included in these calculations. In summary, the agreement between theory and experiment for ^{162}Yb is the poorest of all the even isotopes studied. In the absence of pair fluctuations the disagreement is even worse.

$^{164}Yb_{94}$ (Figure 16). The calculations with pair fluctuations reproduce the experimental routhians and align-

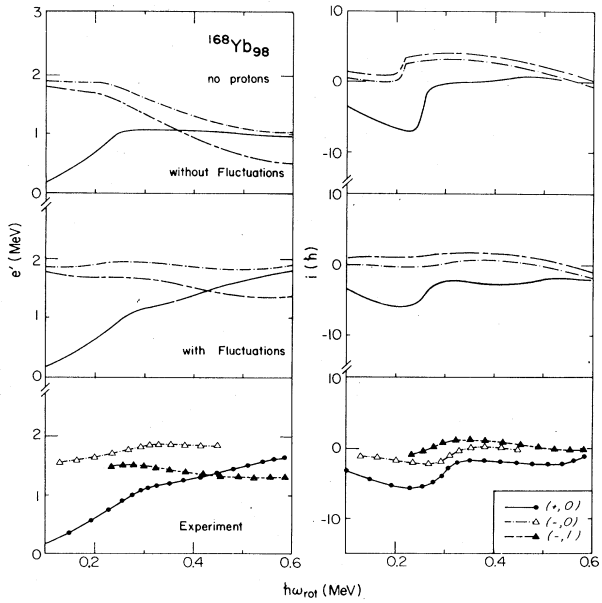

FIG. 30. Comparison of calculated and experimental routhians for various configurations in $^{168}Yb_{98}$ in the absence of proton contributions: middle portion, with fluctuations; top portion, without fluctuations; bottom portion, experimental routhians e' (left-hand side) and alignments i (right-hand side). The neutron static and dynamic pair gaps for this nucleus are shown in Fig. 19, and the corresponding calculations including static proton contributions are shown in Fig. 20. The calculated and experimental values are referred to reference configurations with constant moments of inertia of 49 and 66 $\hbar^2$ MeV^{-1}, respectively. The experimental data for ^{168}Yb are taken from Bacelar *et al.* (1985).

ments quite well, except for the (+,0) sequence at $\hbar\omega_{\rm rot} > 0.38$ MeV and the persistent problem in the lower-frequency portion of the negative-parity sequences, which is particularly bad for this isotope. The band crossing predicted in the (+,0) configuration at $\hbar\omega_{\rm rot} = 0.35$ MeV is not observed. Comparisons (Riley *et al.*, 1987) with heavier $N=94$ isotones (Dracoulis *et al.*, 1983; Chapman *et al.*, 1986; Frandsen *et al.*, 1986; Blume *et al.*, 1987) indicate that this crossing may occur in ^{164}Yb with a large interaction strength at larger rotational frequencies. This problem produces a large discrepancy in the alignments for the (+,0) sequence at large rotational frequencies. Both the predicted alignment and the energy splitting between the two signatures of the negative-parity sequences become progressively poorer at small rotational frequencies. This discrepancy for the $N=94$ isotones (Jónsson *et al.*, 1986; Blume *et al.*, 1987) has been attributed by Garrett (1984), Chapman *et al.* (1986), and Jónsson *et al.* (1986), to octupole correlations. Without neutron pair fluctuations both the predicted magnitude and relative spacings of the ^{164}Yb routhians are in poorer agreement with experiment.

$^{166}Yb_{96}$ (Figure 18). Lifetimes have been measured by Bacelar *et al.*, (1987) for the yrast configuration of ^{166}Yb. The $B(E2)$ values extracted from these experimental data can be understood in terms of a decrease in the quadrupole deformation of the nucleus [see Figs. 18(e) and 18(f)]. The associated values of the quadrupole deformation parameters are shown in Table IV (see Garrett *et al.*, 1988, and Nyberg *et al.*, 1988).

In keeping with these results, and in order to check the effect of deformation on pairing fluctuations, we have made two sets of calculations. In one, displayed in Fig. 18(a), the deformation parameter was kept constant. In another, the deformation was changed as a function of the rotational frequency [see Figs. 18(b)–18(d)]. In this case only the results associated with the (+,0) configuration are shown, since lifetimes have only been measured for the yrast configuration.

From the results shown in Figs. 18(b)–18(d) we see that deformation effects are rather small. In fact, they lead to changes of the order of 200 keV in the case of the routhians and of less than $1.5\hbar$ in the case of alignments. The systematic 200-keV discrepancy between the theoretical and experimental routhians at large rotational frequency is a result of the absolute value of the ground-state energy. The calculation of the energy of this configuration, which is taken as the zero for all routhians, is more uncertain than the relative value of the routhians in the less correlated regime. The effect of neutron pair fluctuations is a renormalization of the alignments and improves the agreement with the experimental values for $\hbar\omega_{\rm rot} = 0.26$–$0.32$ MeV. For both constant and changing deformation the corrections induced by vibrations of the pair field yield important corrections to routhians and alignments, leading to an overall consistency in the description of the experimental findings.

$^{168}Yb_{98}$ (Figure 20). The relative agreement between the calculated routhians, which include neutron pair fluctuations, and experiment is excellent; however, the ground-state calculation is about 400 keV too high—see the comments on the ground-state calculation for ^{166}Yb. Both the relative values of the routhians and the alignments, or moments of inertia, are significantly improved by including the effects of neutron pair fluctuations.

TABLE IV. Rotational frequency dependence of the deformation corresponding to the minimum potential energy for the yrast (+,0) decay sequence of ^{166}Yb. From Garrett *et al.* (1988).

$\hbar\omega_{\rm rot}$	ε_2	γ (deg)
0.00	0.261	4.0
0.05	0.261	3.9
0.10	0.268	3.5
0.15	0.264	2.9
0.20	0.267	1.9
0.25	0.251	2.4
0.30	0.247	2.0
0.35	0.236	4.8
0.45[a]	0.230	3.8
0.50[a]	0.225	6.4

[a] Equilibrium deformation obtained from excited quasiproton excitations due to the unphysically low $\hbar\omega_{\rm rot}$ of the predicted quasiproton band crossing; see Sec. IV.C. For detailed discussion, see Nyberg *et al.* (1988).

3. The routhians and alignments of odd-*N* ytterbium isotopes

$^{163}Yb_{93}$ (Figure 22). The calculations that include pair fluctuations are in very good agreement with the experimental data at small rotational frequencies and reproduce the relative spacing of the experimental routhians at large frequencies. However, at large rotational frequencies the experimental routhians slope upward, i.e., correspond to less alignment or a smaller moment of inertia. This is not predicted; however, an *ad hoc* larger reference moment of inertia could bring the calculations into agreement at large $\hbar\omega_{\rm rot}$. The observed alignments in all configurations at large rotational frequencies are the smallest measured for the odd-N ytterbiums considered. Similarly, these configurations are also less aligned than the negative-parity configurations in the even-even ytterbium isotopes at similar frequencies. Neither the observed crossings in the positive-parity sequences nor the predicted ordering of the signatures of the negative-parity sequences ("signature inversion") (Kownacki *et al.*, 1983) are correctly predicted. Indeed, the lowering of the $(-,-\frac{1}{2})$ and sequence relative to the $(-,\frac{1}{2})$ se-

quence, which also is unique for $N=93$, indicates a dominance of $f_{7/2}$ relative to $h_{9/2}$ in the wave function of these configurations (Kownacki *et al.*, 1983). The inclusion of configuration-dependent (self-consistent) pair correlations and pair fluctuations does not alter the relative signature splitting for this configuration, except at very large rotational frequencies. Including neutron pair fluctuations improves the agreement with data for the large-frequency moments of inertia and the crossings in the positive-parity sequences.

$^{165}Yb_{95}$ (Figure 24). Several experimental features are not predicted by theory. The relative positioning of the routhians at large rotational frequencies is not predicted correctly. Just as for $^{162}Yb_{92}$ the negative-parity states occur too low relative to the positive-parity states. This deficiency of the parametrization of the modified oscillator potentials of Bengtsson and Ragnarsson (1985) was noted previously and corrected by a small modification of the spin-orbit parameter for the $N=6$ neutron shell (Bacelar *et al.*, 1985). The rotational frequencies of the crossings in the positive-parity sequences are underpredicted, and the predicted crossing at $\hbar\omega_{\rm rot}=0.48$ MeV, the result of the quenching of the static neutron pair gap, is not observed up to $\hbar\omega_{\rm rot}=0.53$ MeV. Likewise the energy splitting between the $\alpha=\frac{1}{2}$ and $-\frac{1}{2}$ signatures of the positive-parity sequences is overpredicted. This discrepancy, which becomes even worse in $^{167}Yb_{97}$ and $^{169}Yb_{99}$, is resolved (Shastry *et al.*, 1987) in self-consistent shape calculations. Pair fluctuations, however, do improve the agreement for the moments of inertia, the rotational frequencies of the band crossing, and to a lesser extent the relative energies of the positive and negative sequences.

$^{167}Yb_{97}$ (Figure 26). The relative positions of the positive- and negative-parity sequences are predicted quite well; however, the signature splitting in the

TABLE V. Experimental estimates of apparent alignments and parameters assumed in the analysis.

Nucleus	(π,α)	K[a]	I range[b]	$\hbar\omega$ range[b]	i_0[c]
$^{162}Yb_{92}$	(+,0)				d
	(−,0)	2	22–28	0.35–0.43	5.2(0.2)
	(−,1)	2	23–24	0.37–0.45	5.0(0.4)
$^{163}Yb_{93}$	$(+,\frac{1}{2})$	0.5	22.5–30.5	0.38–0.49	1.2(1.4)
	$(-,\frac{1}{2})$	1.5	22.5–30.5	0.38–0.48	−1.1(0.2)
	$(-,-\frac{1}{2})$	1.5	23.5–29.5	0.40–0.47	−4.4(1.0)
$^{164}Yb_{94}$	(+,0)	0	22–32	0.39–0.50	−6.6(2.2)
	(−,0)	2	22–30	0.34–0.48	8.0(1.4)
	(−,1)	2	23–31	0.38–0.48	2.9(0.9)
$^{165}Yb_{95}$	$(+,\frac{1}{2})$	1.5	22.5–28.5	0.37–0.45	5.7(0.0)
	$(-,\frac{1}{2})$	2.5	22.5–28.5	0.36–0.42	2.1(0.2)
	$(-,-\frac{1}{2})$	2.5	21.5–29.5	0.35–0.45	1.6(0.4)
$^{166}Yb_{96}$	(+,0)	0	22–32	0.37–0.50	0.7(0.7)
	(−,0)	2	24–32	0.38–0.48	3.2(0.2)
	(−,1)	2	25–33	0.34–0.49	2.7(1.2)
$^{167}Yb_{97}$	$(+,\frac{1}{2})$	1.5	24.5–34.5	0.40–0.53	2.1(0.9)
	$(-,\frac{1}{2})$	0.5	24.5–34.5	0.39–0.51	2.2(2.4)
$^{168}Yb_{98}$	(+,0)	0	22–30	0.38–0.51	0.2(0.2)
	(−,0)	2	24–30	0.38–0.45	2.4(1.1)
	(−,1)	2	25–35	0.38–0.52	4.4(0.5)
$^{169}Yb_{99}$	$(-,\frac{1}{2})$	0.5	22.5–34.5	0.36–0.52	1.1(0.4)

[a] K value assumed in analysis.
[b] Angular momentum and rotational frequency range of data used in analysis.
[c] Apparent alignment (see Sec. V.F and Fig. 31). Uncertainty (in parentheses) extracted from data.
[d] Value varying rapidly in frequency range of interest.

positive-parity sequences is greatly underpredicted (see preceding paragraph). The absolute value of the routhians at large rotational frequencies is overpredicted by about 300 keV. As for $^{166}Yb_{96}$ and $^{168}Yb_{98}$, this feature is attributed to the ground-state calculation. Again, including pair fluctuations reduces the prediced alignments and moments of inertia at large rotational frequencies, which not only improves the absolute agreement with experiment at the large rotational frequencies for the reference choice but also produces an improved relative agreement for these quantities between small and large rotational frequencies.

$^{169}Yb_{99}$ (Figure 28). The comparison between experiment and theory is quite similar to that for ^{167}Yb. The relative energies of the routhians are well reproduced, but the absolute value at large rotational frequencies is predicted about 200 keV too large and the signature splitting for the positive-parity sequences is underpredicted except at large rotational frequencies. The effect of neutron pair fluctuations is not only to improve the agreement between experimental and theoretical alignments, but also to improve the relative energies of the positive- and negative-parity routhians. The reduction of the positive-parity routhian relative to that for the negative-parity sequence is a result of the "blocking" of the contributions of the "hot" orbital (see Secs. V.B and V.D) for the negative-parity sequence.

4. Summary of the experimental comparisons for individual isotopes

Including the effects of neutron pair fluctuations produces an improved agreement with experiment. Specifically, in the weakly and nonstatically paired region less alignment is predicted. The predicted reduction, as large as six units (more typically three to four units) in the vicinity of the quenching of the static pair gap, decreases to about one or two units at $\hbar\omega_{\rm rot}=0.6$ MeV. The pair fluctuations also smear the large rotational frequency band crossings and shift these crossings to larger frequencies. The sizable isotopic, configuration, and rotational frequency dependences of these effects depend on the detailed time-reversal response of the single-neutron configurations near the Fermi level.

Many of the remaining discrepancies between experiment and theory, identified in Secs. V.E.2 and V.E.3, are "old friends" attributed to effects not included in the present calculations: e.g., uncertainties in the spectrum of single-neutron states, configuration-dependent nuclear shapes, quadrupole pairing, quasiproton alignments, and octupole correlations.

F. Apparent alignment i_0

The total angular momentum of a nuclear state is a measurable quantity. The separation of the angular momentum into collective and single-particle (aligned) components, however, is ambiguous. Only the relative alignments between known configurations can be determined from experiment. Therefore the absolute alignment can only be obtained at small rotational frequencies in even-even isotopes where the experimentally measured ground-state configuration is a good approximation of the quasiparticle vacuum.

Another quantity related to the alignment can be extracted from experiment—the intercept on the $\omega_{\rm rot}=0$ axis of an extrapolated line with the local dynamic moment of inertia (Bohr and Mottelson, 1981),

$$J^{(2)}(\omega_{\rm rot})=dI_x/d\omega_{\rm rot} . \tag{5.8}$$

The definition of this quantity, i_0, which can be considered an apparent alignment, is illustrated in Fig. 31. Alternatively, the apparent alignment can be formulated (Garrett, 1985a; Riley *et al.*, 1987) in terms of the difference between the kinetic and dynamic moments of inertia $J^{(1)}$ and $J^{(2)}$, respectively,

$$i_0(\omega_{\rm rot})=\omega_{\rm rot}[J^{(1)}(\omega_{\rm rot})-J^{(2)}(\omega_{\rm rot})] , \tag{5.9}$$

where

$$J^{(1)}(\omega_{\rm rot})=I_x/\omega_{\rm rot} . \tag{5.10}$$

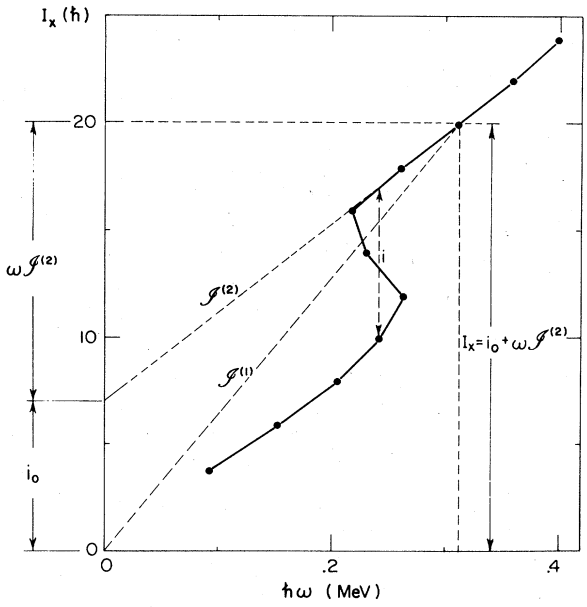

FIG. 31. Pedagogical figure illustrating the definition of apparent alignment (see Sec. V.F.). Apparent alignment (i_0), the $\omega_{\rm rot}=0$ intercept of an extrapolation of the local dynamic moment of inertia $J^{(2)}$, can be defined as the difference between the kinematic $J^{(1)}$, and dynamic moments of inertia—see Eq. (5.9). The various quantities entering this definition are indicated in the figure. The $I_x(\omega_{\rm rot})$ data shown for the ground-state $(-,\frac{1}{2})$ configuration of $^{159}Er_{91}$ are from Simpson *et al.* (1984).

This relation is obtained when the relation given for I_x in Fig. 31 is divided by $\omega_{\rm rot}$ and $J^{(1)}$ is inserted for $I_x/\omega_{\rm rot}$. Note that in general i_0 is frequency dependent. Thus the apparent alignment contains the same information as the difference between the kinetic and dynamic moments of inertia. Similarly, the condition of classical-like rotation (i.e., $I_x=\omega_{\rm rot}J^{(2)}$), which has been observed at large rotational frequencies for the (+,0) sequences of a variety of nuclei (Pakkanen *et al.*, 1982; Chapman *et al.*, 1983; Price *et al.*, 1983; Bacelar *et al.*, 1985), is equivalent to $i_0\equiv 0$ or equal kinetic and dynamic moments of inertia.

Apparent alignments extracted from experimental data and calculations for ytterbium isotopes are compared in Fig. 32. In some cases experimental and/or calculated i_0 are sensitive to the choice of $\hbar\omega_{\rm rot}$. Only the well-defined experimental cases are shown. The angular momentum and rotational frequency ranges for the experimental values of i_0 are given in Table V. The rotational frequency range for the calculated values is chosen to be 0.4–0.5 MeV, roughly corresponding to that of experimental values. The symbols are bracketed when the extraction of i_0 is ω dependent. In the extraction of these values the regions of obvious band crossing were avoided. Details of the criteria used to establish these experimental values are discussed by Riley *et al.* (1987).

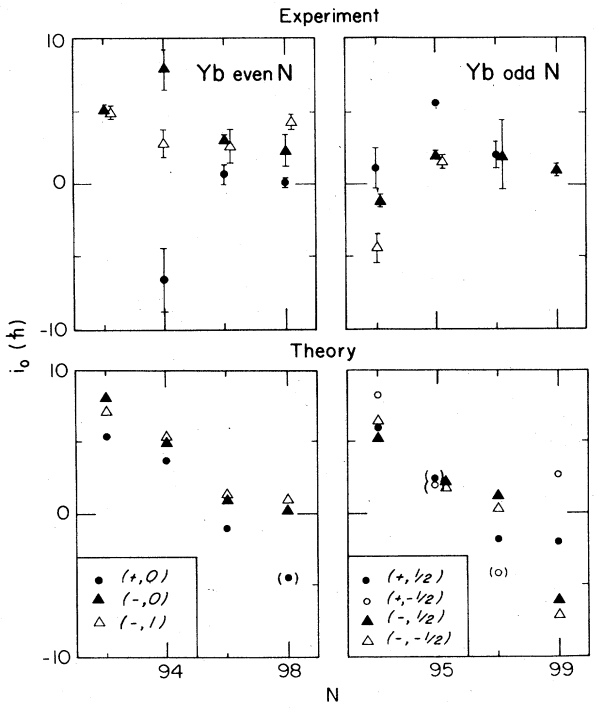

FIG. 32. Comparison of experimental (top) and calculated (bottom) apparent alignments i_0 for various configurations in even-A (left) and odd-A (right) ytterbium isotopes. The angular momentum and rotational frequency ranges for the experimental values are given in Table V. The frequency range for the calculated values, $\hbar\omega_{\rm rot}=0.4$–$0.5$, is chosen to correspond roughly to that of the experimental values. The quantum numbers identifying the decay sequence for which i_0 is extracted are given in the figure. Apparent alignment is defined in Sec. V.F and Fig. 31. Experimental and theoretical values are compared in Sec. V.F.

The apparent alignment is not systematically zero, nor is $i_0=0$ expected from calculations that include or do not include neutron pair fluctuations. If pairing fluctuations are neglected, the calculated values of i_0 are systematically larger than those shown in Fig. 32. The overall magnitude of the predictions is in reasonable agreement with experiment.

Certain systematic experiment trends are also predicted. The apparent alignment of the (+,0) configuration is systematically smaller than that of the negative-parity configurations of the same isotope or those of the neighboring odd-N isotopes. That is, for $\hbar\omega_{\rm rot}=0.35$–$0.50$ MeV, the most correlated configuration (see the routhians of Figs. 14, 16, 18, and 20) has the smallest apparent alignment. The isotopic dependence, however, is at variance with the predictions, indicating the presence of other frequency-dependent quantities that also contribute to the apparent alignment. For example, in $^{164}Yb_{94}$ octupole correlations for the (−,1) sequence (Jónsson *et al.*, 1986) and a strongly interacting band crossing for the (+,0) sequence (Riley *et al.*, 1987) are thought to be important.

G. Band crossing frequencies and critical frequencies of pairing collapse

The rotational frequency of the crossing between rotational bands based on different intrinsic configurations in a decay sequence is a well-defined experimental quantity (Bengtsson and Frauendorf, 1979; Garrett *et al.*, 1981; Garrett, 1983; Jónsson *et al.*, 1986). Though these crossings are shown in the experimental and theoretical routhians and alignment plots as a function of $\hbar\omega_{\rm rot}$ (Figs. 14, 16, 18, 20, 22, 24, 26, and 28), it seems appropriate to collect this information into a single plot—see Fig. 33.

1. The *AB* neutron crossings

The lowest-frequency band crossing in the (+,0) band $(-,\frac{1}{2})$ sequences is unambiguously associated with the alignment, or excitation, of the most alignable pair of $i_{13/2}$ quasineutrons (Stephens and Simon, 1972; Bengtsson and Frauendorf, 1979; Garrett *et al.*, 1981), i.e., those labeled A and B in Fig. 12—See Table III. Though the rotational frequency of this crossing (often called the AB crossing) is systematically underpredicted in the present calculations by 10–20 keV, the observed (Garrett *et al.*, 1981) reduction of the crossing frequency in the $(-,\frac{1}{2})$ sequence of the odd-N system is repro-

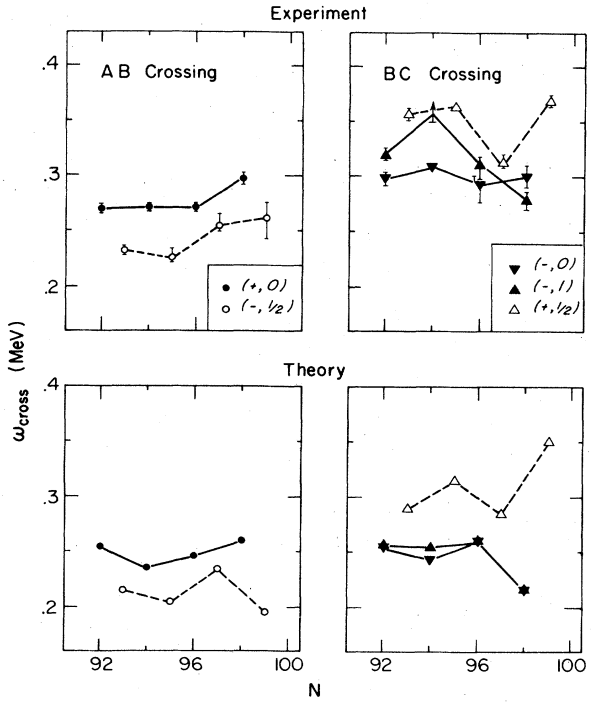

FIG. 33. Comparison of experimental (top) and calculated (bottom) band crossing frequencies corresponding to the alignment of pairs of $i_{13/2}$ of quasineutrons: left-hand portion, alignment of the lowest-frequency pair (AB crossing); right-hand portion, alignment of the next lowest-frequency pair (BC crossing). See Sec. V.G for definitions of the various band crossings and a discussion of the comparison between experiment and theory. The quantum numbers identifying the decay sequences in which the crossing occurs are given in the figure.

duced. This crossing frequency reduction is the result of the "blocking" of the pairing contributions from the occupied single-quasineutron orbital in the odd-N isotopes. That is, the crossing in the even-even system is a zero- to two-quasineutron crossing, whereas in the odd-N ytterbiums the crossing is between one- and three-quasineutron states. Improved absolute agreement for these crossing frequencies could be obtained by an *ad hoc* increase in the neutron monopole pairing strength G_n, at the expense of overpredicting the neutron pair gap Δ_n, as expressed by the odd-even mass difference; see Fig. 2. Indeed, the choice of $G_n = 20.5/A$ MeV was made as a compromise, to slightly overpredict the odd-even mass difference and to slightly underpredict these crossing frequencies—see Sec. IV.A.

In the present analysis only a monopole pairing force is included in the calculations. However, it is known (Wakai and Faessler, 1978; Diebel, 1984) that including the quadrupole pairing interaction increases the frequency of the crossing. The physical basis of this result is probably the fact that Cooper pairs associated with a quadrupole pairing force carry angular momentum and therefore are less sensitive to rotational effects.

2. The *BC* neutron crossings

In the low-lying negative-parity two-quasineutron bands of the even-even ytterbium isotopes and the low-lying positive-parity bands of the odd-mass ytterbium isotopes, one quasineutron of the most alignable pair of (A or B) is occupied. Therefore the excitation of the most alignable pair of quasineutrons (AB) violates (Grosse *et al.*, 1973) the Pauli principle. The excitation of another less alignable pair (e.g., the BC or AD pair shown in Fig. 12) at larger rotational frequencies is allowed—see Table III, and Bengtsson and Frauendorf (1979), and Riedinger *et al.* (1980).

In the presence of a static neutron pair gap with its associated quasineutron excitations, these quasineutron alignments correspond to crossings between two- and four-quasineutron bands in the even-even ytterbium isotopes and to crossings between one- and three-quasineutron bands in the odd-N isotopes. However, the self-consistent calculations of the neutron pair gap (see Sec. V.D and Figs. 13, 15, 17, 19, 21, 23, 25, and 27) predict that the static neutron gap should vanish for some of these three-quasineutron configurations and for all the four-quasineutron configurations. Therefore, as discussed in Sec. V.D, the band crossings predicted to occur in these decay sequences in some cases may be associated with crossings between statically paired quasineutron and unpaired neutron intrinsic configurations. This picture is further complicated by the presence of dynamical pair correlations in the absence of a stable static pair gap and by interactions between the various configurations.

The rotational frequencies of such band crossings in negative-parity sequences, $(-,0)$ and $(-,1)$, of the even-even ytterbium isotopes are compared with those of the lowest positive-parity sequence, $(+,\frac{1}{2})$, of the odd-N isotopes in the right-hand portion of Fig. 33. Except for the crossing in the $(-,1)$ sequence of $^{164}Yb_{94}$, where octupole correlations are thought to be important (Jónsson *et al.*, 1986) at large rotational frequencies, the relative configuration and isotopic dependence of the crossing frequencies are correctly predicted. However, the absolute magnitude of the crossing is systematically underpredicted by from 20 to 70 keV. If fluctuations in the neutron pair gap were ignored, the agreement would be even poorer—see Secs. V.D.1 and V.D.2.

The underprediction of these crossing frequencies is a serious deficiency of the model. Whereas an *ad hoc* increase of the neutron pair strength G_n would improve the situation for these crossings, the magnitude necessary to correct this discrepancy would overpredict both the odd-even mass differences and the frequency of the AB crossings (Garrett, 1982; Roy *et al.*, 1982). It is likely that including the quadrupole pairing interaction would alleviate the difficulty, as has been shown by Diebel (1984) for the AB crossing.

3. The frequencies of static neutron pairing collapse

In contrast to the band crossings discussed in the preceding paragraphs, the critical frequency associated with the collapse of the static neutron pair gap, ω_{crit}, is not well defined in the experimental routhians. There is experimental evidence (e.g., Garrett, 1984; Bacelar *et al.*, 1985; Zhang *et al.*, 1986) indicating that static neutron pair correlations are quenched at the largest rotational frequencies. However, both the frequency dependence of the pair gap and pair fluctuations "smooth" any discontinuity in the experimental routhians associated with this collapse.

Though an accurate experimental definition of ω_{crit} is at present difficult, this quantity does have a well-defined theoretical interpretation. Above this critical frequency the pairing is dominated by dynamical effects, including both a change in the two-nucleon transfer strength function from one characteristic of pair rotations to one characteristic of pair vibration and the disappearance of the band crossings corresponding to excitations of pairs of quasineutrons (see Sec. VI). Coulomb excitation combined with two-nucleon transfer may allow an experimental determination of ω_{crit}. It, must be admitted, however, that such data are neither easy to obtain nor easy to interpret.

Though band crossings are not a continuous function of rotational frequency, the systematic absence of quasiparticle crossings at large rotational frequencies argues for the normal phase. Indeed, no quasineutron band crossings are observed in the ytterbium isotopes at $\hbar\omega_{rot} > \hbar\omega_{crit}$. Neither are quasineutron band crossings observed (Riley, Garrett, Simpson, and Sharpey-Schafer, 1987) above the *BC* and *AD* crossings for recent studies of the erbium isotopes $^{159}Er_{91}$ and $^{160}Er_{92}$ (Deleplanque *et al.*, 1987; Simpson, Riley, James, *et al.*, 1987), even though these data extend to $\hbar\omega_{rot} \approx 0.70$ MeV (see Fig. 34).

The predicted values of ω_{crit}, as defined in Figs. 13, 15, 17, 19, 21, 23, 25, and 27, are collected in Fig. 35. The various features of these critical frequencies are discussed in Sec. V.E.

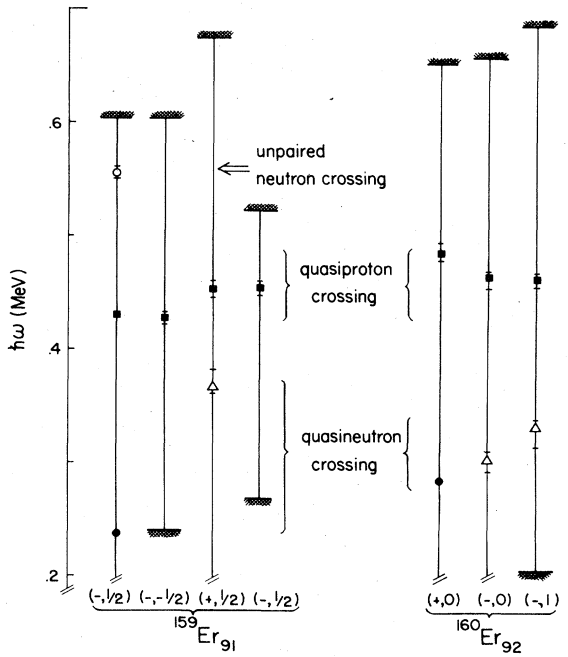

FIG. 34. Summary of band crossing frequencies $\hbar\omega_{cross}$ for the observed crossings in the decay sequences of $^{159}Er_{91}$ and $^{160}Er_{92}$. Crossings corresponding to the excitation of the lowest (AB) and second-lowest (BC) pair of quasineutrons are denoted by solid circles and open triangles, respectively. Those corresponding to the excitation of the lowest-frequency pair of quasiprotons (A_pB_p) are given as squares. While the only band crossing observed above $\hbar\omega_{rot}=0.39$ MeV, shown as an open circle, cannot be described as a quasiparticle excitation, it can be understood in terms of the expected spectrum of single-neutron states in the absence of static pair correlations; see Riley, Garrett, Simpson, and Sharpey-Schafer (1987). The limit of the experimental data for each configuration is indicated by the vertical lines. The data for ^{159}Er are taken from Simpson *et al.* (1984), Riley *et al.* (1984), and Deleplanque *et al.* (1987). The data for ^{160}Er are taken from Simpson *et al.* (1984), Simpson, Riley, Cresswell *et al.* (1987), and Simpson, Riley, James *et al.* (1987).

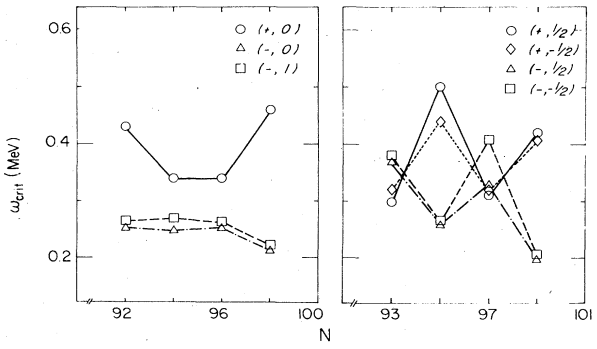

FIG. 35. Critical rotational frequencies ω_{crit} at which the static neutron pair gaps are predicted to collapse, shown for various configurations of even-A (left portion) and odd-A (right portion) ytterbium isotopes. The various configurations are identified in the figure. These systematics are discussed in Sec. V.G.3.

VI. THE TIME-REVERSAL RESPONSE TWO-NUCLEON-TRANSFER PROCESSES

Though pairing fluctuations smooth the correlation energy in the region of the transition between the normal and superfluid phases (see the preceding section), a marked change is predicted to occur in the two-nucleon-transfer response function with zero angular momentum ($L=0$) at ω_{crit}. Examples of these response functions [see Eq. (5.6)] are shown at a variety of rotational frequencies in Figs. 36, 37, and 38 for $^{164}Yb_{94}$, $^{167}Yb_{97}$, and $^{168}Yb_{98}$, respectively; the associated transfer processes are schematically summarized in Fig. 39.

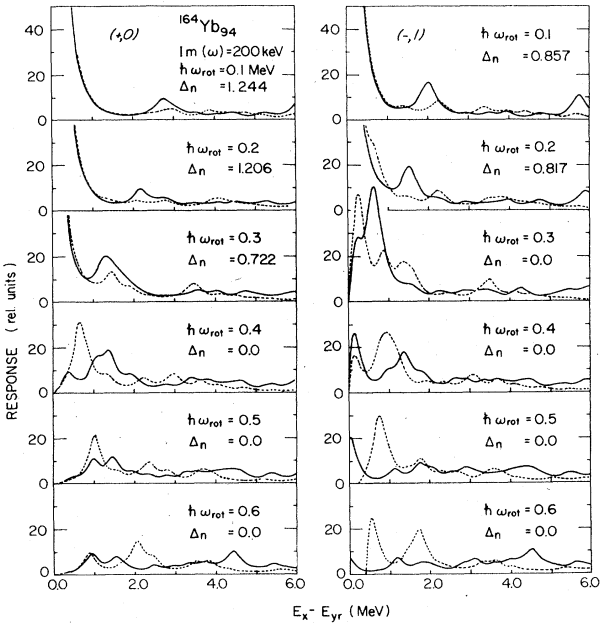

FIG. 36. Calculated two-neutron-transfer response functions for the lowest $(+,0)$ configuration (left portion) and lowest $(-,1)$ configuration (right portion), for $^{164}Yb_{94}$ shown as a function of the excitation energy relative to the yrast configuration, $E_x - E_{yr}$, for various values of the rotational frequency $\hbar\omega_{rot}$: solid curves, pair-addition modes; dotted curves, pair-removal modes. An averaging parameter $\mathrm{Im}(\omega)=200$ keV was used in these calculations. The corresponding static neutron pair gap Δ_n is given for each rotational frequency. The dramatic change in the response function, noted between the superfluid and normal phases, is discussed in Sec. VI.

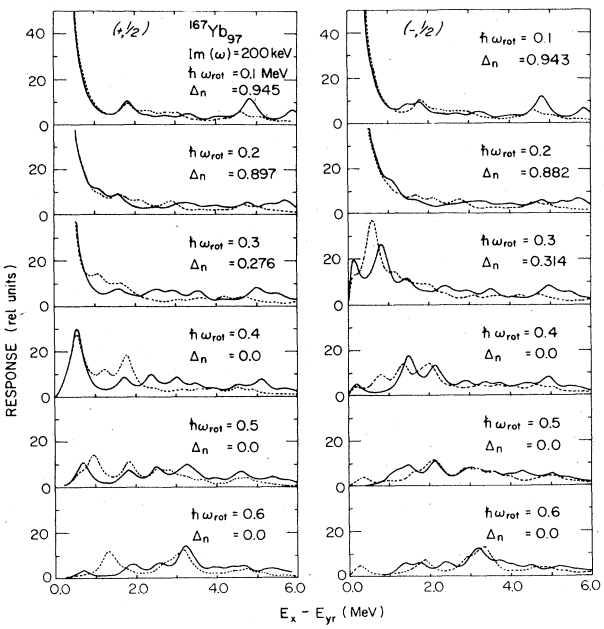

FIG. 37. Calculated two-neutron-transfer response functions for the lowest $(+,\frac{1}{2})$ configuration (left portion), and lowest $(-,\frac{1}{2})$ configuration (right portion), of $^{167}Yb_{97}$ shown as a function of the excitation energy relative to the yrast configuration, $E_x - E_{yr}$, for various values of the rotational frequency $\hbar\omega_{rot}$: solid curves, pair-addition modes; dotted curves, pair-removal modes. See also caption to Fig. 36.

For $\omega_{rot} < \omega_{crit}$ only the transitions between yrast states carry strength, while a strong fraction of the strength is expected to go into pairing vibrational states for $\omega_{rot} > \omega_{crit}$. This pattern is typical of a transition between pairing rotational and pairing vibrational schemes (Bés and Broglia, 1966; Broglia *et al.*, 1968, 1973) and reflects the transition from the superfluid to the normal phase.

A similar conclusion can be obtained from the results of Nikam *et al.* (1987). From Fig. 1 of this paper the ratio of two-particle-transfer cross sections connecting yrast states at $\hbar\omega \approx 0$ and 0.5 MeV is $|\langle A+2|S^{\dagger}|A\rangle|^2_{I=30} / |\langle A+2|S^{\dagger}|A\rangle|^2_{I=0} \approx (\frac{2}{6})^2 \sim 0.1$. This is typical of a superfluid-to-normal pairing phase transition.

However, we note that the pattern emerging from these results for the normal phase is quite different from that observed in closed-shell nuclei like ^{208}Pb, where a large single-particle gap exists between empty and occupied states and where the lowest pair-addition and pair-subtraction modes are the only low-lying collective states.

In the cases shown in Figs. 36–38 the pair-addition and pair-removal strengths are distributed over many

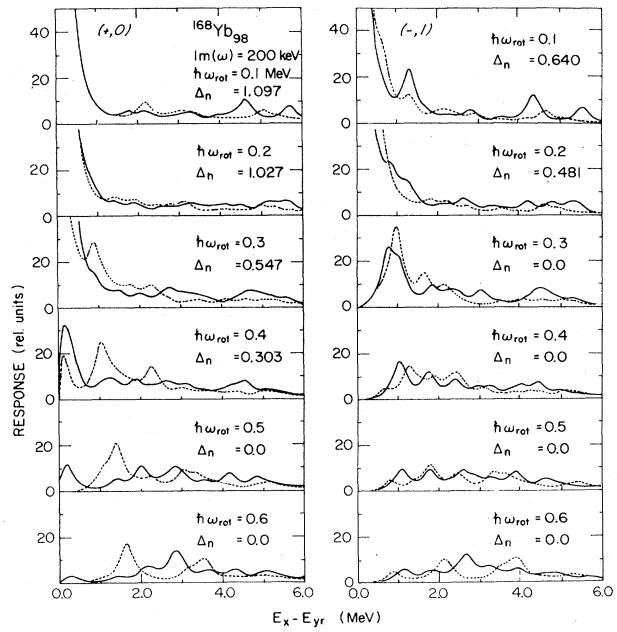

FIG. 38. Calculated two-neutron-transfer response functions for the lowest $(+,0)$ configuration (left portion) and lowest $(-,1)$ configuration (right portion) of $^{168}Yb_{98}$, shown as a function of the excitation energy relative to the yrast configuration, $E_x - E_{yr}$, for various values of the rotational frequency $\hbar\omega_{rot}$: solid curves, pair-addition modes; dotted curves, pair-removal modes. See also caption to Fig. 36.

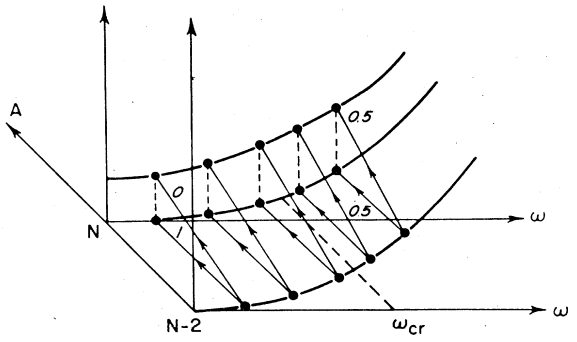

FIG. 39. Schematic figure, from Broglia and Gallardo (1985), depicting the rotating frequency dependence of two-neutron transfer from a nucleus with $N-2$ neutrons to one with N neutrons. The two ordinates denote excitation energies in nuclei with $N-2$ and N neutrons. The numbers indicate relative two-neutron-transfer strength to yrast and excited levels shown by the arrows. Below the critical frequency ω_{crit}, for the existence of static neutron pairing correlations, the transfer strength is concentrated in an enhanced yrast-to-yrast transition, whereas above it the transfer strength is divided between the yrast and two-particle, two-hole states.

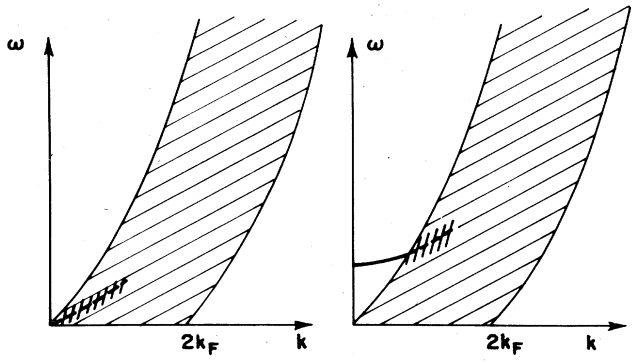

FIG. 40. Schematic representation of the dispersion relation associated with the paramagnon (left) and with the plasmon (right). The hatched area corresponds to unperturbed particle-hole excitations. The spin-spin interaction in ^{3}He giving rise to the spin vibration is attractive and the corresponding phonon encounters from the outset a continuous background. This is responsible for the existence of strong Landau damping. Conversely, in the plasma oscillations the residual interaction is repulsive. This, combined with the fact that the screening of the Coulomb field produced by the ions gives a finite mass (gap) to the plasmon, has the consequence that this mode moves away from the continuum of particle-hole states, and the only damping it has in the corresponding region of k values is due to the coupling to $2p$-$2h$ states. This coupling is very small because of the strong correlation existing between the particle and the hole in the plasmon.

states. This is because the collective pairing vibrations suffer very strong Landau damping.[2] That is, in the absence of a shell gap, the fluctuations of the pairing gap are trapped between closely spaced poles (unperturbed response function), and a transition almost on the energy shell can occur to uncorrelated two-particle or two-hole states. A situation similar to this one, although in the particle-hole channel, is the case of paramagnons (spin vibrations) in liquid ^{3}He. These excitations propagate in a continuum of uncorrelated particle-hole excitations and consequently are strongly damped (see Fig. 40).

It is expected that, in two-nucleon-transfer reactions between heavy ions, the deformed superfluid system will be Coulomb excited to the critical frequency before the pair of particles is transferred. Thus in principle it should be possible to observe the changes of the response function with ω_{rot} shown in Fig. 39. Results of experiments of this type are becoming available. Figure 41 shows results (Guidry, 1986; Juutinen *et al.*, 1987) for the two-nucleon pickup double differential cross section associated with the reaction $^{162}\text{Dy} \rightarrow {}^{160}\text{Dy}^*$ induced by ^{58}Ni and ^{116}Sn. Although much work remains to be done in connecting the experimental findings with the detailed nuclear structure properties of the nuclei involved in the reaction, it seems possible to interpret the main experimental pattern as shown in Fig. 42. In addition to the $L=0$ transfer associated with the excitation of pair vibrations and pair rotations, particle-hole states with a variety of angular momenta, for example, β and γ vibrations, octupole surface modes, etc., also will be excited. In Fig. 42(a) we have depicted the situation expected in the case of a target nucleus displaying a rather stable pairing gap as a function of the rotational frequency (hard superconductor), while in Fig. 42(b) is shown the situation for a nucleus displaying a weak pairing gap.

Before ending this section we believe a couple of remarks are in order. In fact, the question still exists whether the crucial frequencies for inducing the collapse of the pairing gap can be reached, even with the heaviest projectiles. Even if this is possible, the experiment will detect at best a transient phenomenon, instead of a "standard" phase transition. The collision time for bombarding energies of a few MeV per nucleon is $\approx 10^{-21}$ sec. Typical values of the pairing gap Δ are about 1 MeV, also leading to a characteristic time of the order of 10^{-21} sec. Thus the question is the following: will the critical field have enough time in such a reaction to destroy the pair correlations?

VII. SUMMARY

In rapidly rotating nuclei a pairing phase transition is expected, typically for rare-earth nuclei at frequencies of

[2]In nuclei, because of the finite density of particle-particle and hole-hole levels in which the pairing modes can decay, one could better talk about splitting of the original strength.

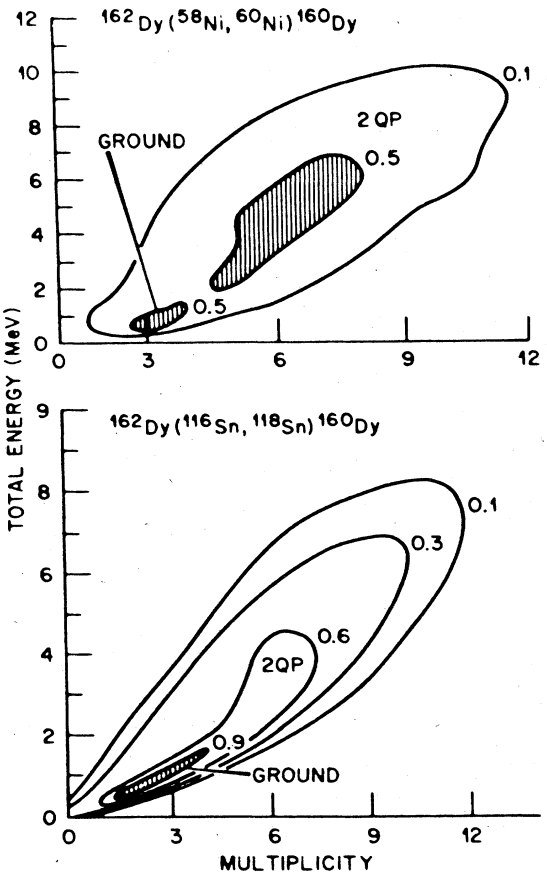

FIG. 41. Comparison of the measured total excitation energy as a function of the γ-ray multiplicity (proportional to the angular momentum) for the two-neutron-transfer reaction $^{162}\mathrm{Dy} \rightarrow {}^{160}\mathrm{Dy}^*$ induced by 345-MeV ^{58}Ni (top) and 637-MeV ^{116}Sn (bottom). The figure is taken from Guidry (1986).

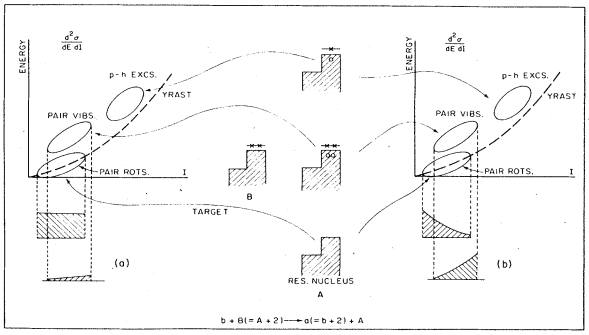

FIG. 42. Schematic representation of two particle pickup processes populating even-even nuclei in the presence of (a) a strong pairing gap and (b) a weak pairing gap. Although the target nucleus is assumed to be superfluid at small anglular momentum, it is represented as a normal system with two particles in the level just above the Fermi energy for the $A = B - 2$ system. This coupling, which eventually is reached at large angular momentum, is used to indicate the three types of states that can be excited in the final nucleus by two-nucleon transfer, namely, the yrast states (pair rotations), pair vibrations ($2p$-$2h$ states), and particle-hole excitations. The intensity distributions as a function of angular momentum expected in the presence (and absence) of strong pairing correlations are indicated for pair rotations and pair vibrations by the projected spectra in the left (and right) positions of the figure.

0.3–0.4 MeV. It could be specifically probed in the transfer of two particles after Coulomb excitation, in a collision between heavy ions. The neutron pair condensate, apparently, ceases to exist after the excitation of a few (three to five) quasineutrons. No single parameter aside from possibly the two-nucleon-transfer cross section definitively characterizes this phenomenon. Neither is it always associated with quasiparticle excitations. Instead, a variety of effects appear in the gradual change of the coupling scheme taking place as a function of $\hbar\omega_{\mathrm{rot}}$ in the vicinity of the pair phase transition. Some of these processes are depicted in Fig. 43 for the yrast configuration of $^{168}\mathrm{Yb}_{98}$, a typical even-even rare-earth isotope.

A decrease of the static neutron pair gap to about half of its value at $\hbar\omega_{\mathrm{rot}} = 0$ is associated with the band crossing corresponding to the excitation of a pair of $i_{13/2}$ quasineutrons. This crossing occurs at $\hbar\omega_{\mathrm{rot}} \approx 0.27$ MeV for a typical light even-even rare-earth isotope. For larger frequencies the magnitude of the pairing matrix elements continues to decrease as the time-reversed states become progressively more orthogonal, leading to an effective screening of the pairing coupling constant. The quenching of the static neutron pairing gap becomes total at $\hbar\omega_{\mathrm{rot}} \approx 0.3$–$0.4$ MeV, without, in general, the occurrence of any further distinct band crossing.

At frequencies above that of the pairing phase transition, pairing fluctuations are found to be important. In contrast, they play essentially no role for those frequencies for which the pairing gap has a sizable value.

These results for pair correlations are little affected by the changes in deformation taking place as a function of the rotational frequency, at least in the ytterbium isotopes. This is because the fluctuations of the pairing gap, which are strongly dependent on the average density of pairs of single-particle levels with opposite signature around the Fermi energy, are rather insensitive to the actual quantum numbers of the associated orbitals. This result does not imply that changes in the deformation with angular momentum are not important. What it says is that pairing fluctuations are very strong in nuclei rotating with frequencies above the critical frequency for which the pairing gap collapses. It thus confirms what was already known from the systematic study of two-particle-transfer reactions of normal systems like the lead isotopes close to their ground state.

At rotational frequencies larger than the critical value, pairing fluctuations lead to dynamical changes in the occupation of single-particle orbitals, resulting in a decrease of the alignment. This dealignment, which is borne out by experiment, is as large as six units (more typically

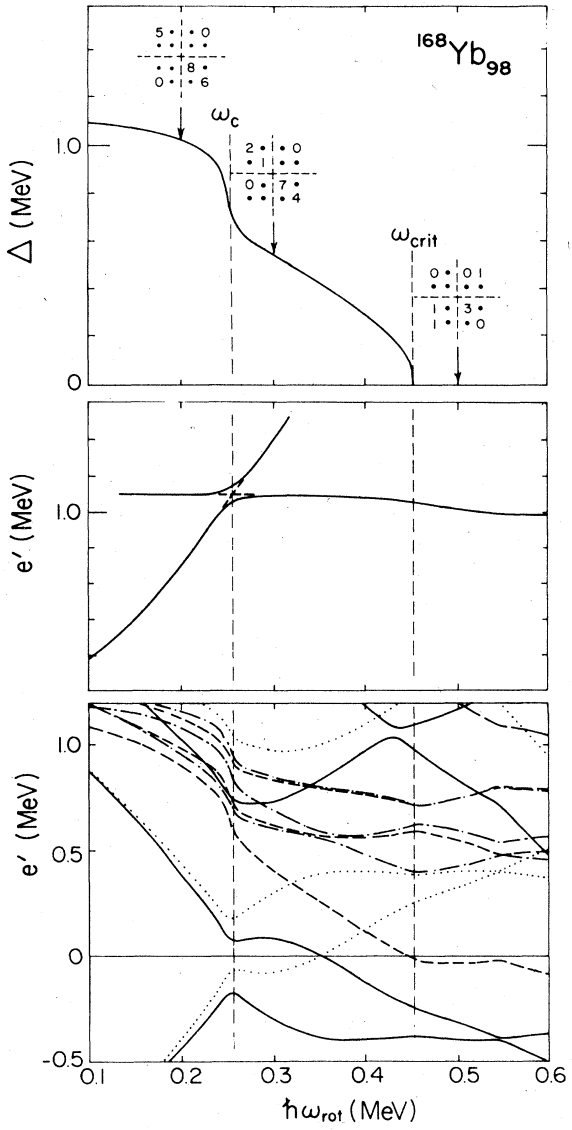

FIG. 43. Schematic figure showing predicted frequency dependences in the region of the "decline and fall" of the static neutron pair gap: top, the static pair gap; middle, the routhian (rotating-frame excitation energy); bottom, spectrum of single-neutron states. The parameters shown correspond to the yrast configuration of $^{168}Yb_{98}$, a typical mid-rare-earth even-even nucleus, and do not include the effects of pairing fluctuations. Calculated values of the squared matrix elements of the pair operator [see Fig. 10 and Eq. (5.7)] are also shown in the upper portion of the figure, for configurations near the $N=98$ Fermi level at $\hbar\omega_{rot}=0.2$, 0.3, and 0.5 MeV. The spectrum of single-neutron states (bottom portion) differs from that shown in Fig. 12, since the neutron pairing gap is varied as a function of $\hbar\omega_{rot}$ for the present calculation. The predicted band crossing frequency ($\hbar\omega_{cross}$), corresponding to the excitation of a pair of $i_{13/2}$ quasineutrons, and the predicted critical frequency ($\hbar\omega_{crit}$) for the disappearance of the static neutron pair gap are also indicated for reference. Similar predictions for this and other configurations and isotopes of ytterbium are shown in Figs. 13–30 and are discussed in Sec. V.E.

three to four units) for the ytterbium isotopes near the critical frequency and decreases to one or two units at the largest rotational frequencies ($\hbar\omega_{rot}\approx 0.6$ MeV). The configurations displaying a coupling scheme most resembling that described by the BCS wave function, e.g., the lowest $(\pi,\alpha)=(+,0)$ configuration, are most strongly affected by fluctuations of the pair density. At the same rotational frequency, other configurations, e.g., $(-,0)$ and $(-,1)$, are considerably less affected by pairing fluctuations. In the limit of small rotational frequencies, these configurations evolve to two-quasiparticle states relative to the $(+,0)$ vacuum configuration. Consequently the associated coupling schemes exploit pair correlations less favorably than do the coupling schemes of the lowest $(+,0)$ configuration.

The two-neutron-transfer strength is also predicted to be modified by pairing fluctuations. This strength, which in the static paired region is concentrated in the yrast-yrast transition, for $\omega_{rot}>\omega_{crit}$ is spread over a variety of low-lying states, no simple distinguishable neutron pair vibrational mode being predicted. Detailed experimental information on these processes is badly needed to check the predictions quantitatively.

The pairing vibrational model has a number of successes to its credit, but is not quantitatively correct in several cases. Other effects, like changes in deformation with rotational frequencies or state-dependent pairing correlations—e.g., quadrupole pairing—are likely to play a role.

ACKNOWLEDGMENTS

Discussions with T. Bengtsson, M. A. Riley, and F. Barranco are acknowledged. One of the authors (Y.R.S.) is indebted to the Nishina Memorial Foundation for the financial support for his stay at the Niels Bohr Institute from September 1985 to March 1986. This project has been executed with a grant of the Commemorative Association for the Japan World Exposition and was supported by the Danish Natural Science Research Council.

APPENDIX: APPROXIMATE EXPRESSION OF $I_x^{(corr)}$

In order to derive the explicit form of $I_x^{(corr)}$ defined by Eq. (3.18), we start from Eq. (2.12),

$$E_{corr}=\frac{1}{2}\left[\sum_n \omega_n-\sum_{\alpha<\beta}E_{\alpha\beta}\right],\quad E_{\alpha\beta}\equiv E_\alpha+E_\beta\ . \tag{A1}$$

As is usual, the RPA eigenvalue equation is expressed in the matrix notation by

$$\mathbb{K}\begin{bmatrix}\psi_n\\ \varphi_n\end{bmatrix}=\omega_n\begin{bmatrix}\psi_n\\ -\varphi_n\end{bmatrix}, \tag{A2}$$

where $\psi_n(\alpha\beta)$ and $\varphi_n(\alpha\beta)$ are the forward and the backward amplitudes and $\mathbb{K}$ is the RPA energy matrix. In the separable-force representation of the residual interaction

equation (2.4), the RPA energy matrix is expressed as

$$\mathbb{K}=\mathbb{K}_0+\mathbb{K}_I \ , \tag{A3}$$

with

$$\mathbb{K}_0(\alpha\beta;\mu\nu)=\begin{bmatrix} E_{\alpha\beta}\delta_{\alpha\mu}\delta_{\beta\nu} & 0 \\ 0 & E_{\alpha\beta}\delta_{\alpha\mu}\delta_{\beta\nu} \end{bmatrix} ,$$
$$\mathbb{K}_I=\begin{bmatrix} A & B \\ B^* & A^* \end{bmatrix} \tag{A4}$$

$$A(\alpha\beta;\mu\nu)=-\sum_\rho \chi_\rho q_\rho(\alpha\beta)q_\rho^*(\mu\nu) \ ,$$
$$B(\alpha\beta;\mu\nu)=-\sum_\rho \chi_\rho q_\rho(\alpha\beta)q_\rho(\mu\nu) \ . \tag{A5}$$

To derive Eq. (A1), the eigenenergy should be expressed as

$$\omega_n=X_n^\dagger \mathbb{K} X_n, \quad X_n=\begin{bmatrix} \psi_n \\ \varphi_n \end{bmatrix} . \tag{A6}$$

Thus by using the Feynman theorem we have

$$I_x^{(\mathrm{corr})}=-\frac{1}{2}\left[\sum_n (X_n^\dagger \mathbb{K}' X_n)-\sum_{\alpha<\beta} E'_{\alpha\beta}\right] . \tag{A7}$$

Here the primes indicate the derivative with respect to the rotational frequency ω_{rot}. The first term on the right-hand side of Eq. (A7) is decomposed into two parts according to Eq. (A3). The evaluation of the first term leads to

$$\begin{aligned}\sum_n (X_n^\dagger \mathbb{K}_0' X_n)&=\sum_n \sum_{\alpha<\beta} E'_{\alpha\beta}[\psi_n^*(\alpha\beta)\psi_n(\alpha\beta) \\ &\quad +\varphi_n^*(\alpha\beta)\varphi_n(\alpha\beta)] \\ &=\sum_{\alpha<\beta} E'_{\alpha\beta}+2\sum_n \sum_{\alpha<\beta} E'_{\alpha\beta}\varphi_n^*(\alpha\beta)\varphi_n(\alpha\beta) \ ,\end{aligned} \tag{A8}$$

where in the third line we have used the completeness relation of the RPA amplitudes. The second part arising from $\mathbb{K}_I$ of Eq. (A5) can be calculated similarly, and we obtain

$$\begin{aligned}\sum_n (X_n^\dagger \mathbb{K}_I' X_n)&=\sum_{\alpha<\beta} A'(\alpha\beta;\alpha\beta) \\ &\quad +2\sum_\rho \sum_n \left[\Lambda_\rho^*(n)\sum_{\alpha<\beta} q'_\rho(\alpha\beta)\varphi_n(\alpha\beta) \right. \\ &\quad \left. +\mathrm{H.c.}\right] ,\end{aligned} \tag{A9}$$

where $\Lambda_\rho(n)$ is the particle-vibration coupling vertex defined by

$$\Lambda_\rho(n)=\chi_\rho \sum_{\alpha<\beta}[q_\rho^*(\alpha\beta)\psi_n(\alpha\beta)-q_\rho(\alpha\beta)\varphi_n(\alpha\beta)] . \tag{A10}$$

Finally, from Eqs. (A7)–(A9) we have

$$I_x^{(\mathrm{corr})}=I_x^{(\mathrm{a})}+I_x^{(\mathrm{b})}+I_x^{(\mathrm{ex})} , \tag{A11}$$

with

$$I_x^{(\mathrm{a})}=-\sum_n \sum_{\alpha<\beta} E_{\alpha\beta}^*\varphi_n^*(\alpha\beta)\varphi_n(\alpha\beta) , \tag{A12a}$$

$$I_x^{(\mathrm{b})}=-\sum_n \sum_\rho \sum_{\alpha<\beta}[\Lambda_\rho^*(n)q'_\rho(\alpha\beta)\varphi_n(\alpha\beta)+\mathrm{H.c.}] , \tag{A12b}$$

$$\begin{aligned}I_x^{(\mathrm{ex})}&=-\tfrac{1}{2}\sum_{\alpha<\beta} A'(\alpha\beta;\alpha\beta) \\ &=\tfrac{1}{2}\sum_\rho \sum_{\alpha<\beta} \chi_\rho[q'_\rho(\alpha\beta)q_\rho^*(\alpha\beta)+\mathrm{H.c.}] .\end{aligned} \tag{A12c}$$

So far no approximations have been made. In order to make the connection to the diagrammatic expression, we neglect the self-consistency of the mean field and consider the single-particle potential to be a constant function of ω_{rot}. In this approximation, the derivatives are easily evaluated. It can be shown that

$$E'_\alpha=-J_x^{(B)}(\alpha\alpha)=-i_x(\alpha) , \tag{A13}$$

$$q'_\rho(\alpha\beta)=\frac{1}{2}\left[\sum_\gamma q_\rho^{(B)}(\alpha\gamma)\frac{J_x^{(A)}(\gamma\beta)}{E_\gamma+E_\beta}-(\alpha\leftrightarrow\beta)\right] , \tag{A14}$$

where the matrix elements $J_x^{(A)}$, $J_x^{(B)}$, etc., are defined by

$$\hat{J}_x=\sum_{\alpha<\beta}[J_x^{(A)}(\alpha\beta)a_\alpha^\dagger a_\beta^\dagger+\mathrm{H.c.}]+\sum_{\alpha\beta} J_x^{(B)}(\alpha\beta)a_\alpha^\dagger a_\beta \ . \tag{A15}$$

Similarly for the one-body operator $\hat{Q}_\rho$ entering in the separable-force representation of V

$$\hat{Q}_\rho=\sum_{\alpha<\beta}(q_\rho^{(A)}a_\alpha^\dagger a_\beta^\dagger+\mathrm{H.c.})+\sum_{\alpha\beta} q_\rho^{(B)}(\alpha\beta)a_\alpha^\dagger a_\beta \ . \tag{A16}$$

Here $q_\rho \equiv q_\rho^{(A)}$ in Eq. (2.5). Notice that only the first term in Eq. (A16) is taken into account in the RPA order. Moreover, the forward and backward amplitudes are expressed by

$$\psi_n(\alpha\beta)=\sum_\rho \frac{\Lambda_\rho(n)q_\rho(\alpha\beta)}{E_\alpha+E_\beta-\omega_n} ,$$
$$\varphi_n(\alpha\beta)=-\sum_\rho \frac{\Lambda_\rho(n)q_\rho^*(\alpha\beta)}{E_\alpha+E_\beta+\omega_n} \ . \tag{A17}$$

Now it is easy to see, by combining Eqs. (A12) and (A13)–(A17), that three terms of $I_x^{(\mathrm{corr})}$ in Eq. (A11) correspond to diagrams in Fig. 1 (see Sec. III.C and Barranco *et al.*, 1987).

REFERENCES

Agarwal, Y. K., J. Recht, H. Hubel, M. Guttormsen, D. J. Decman, H. Kluge, K. H. Maier, J. Dudek, and W. Nazarewicz, 1983, Nucl. Phys. A **399**, 1999.
Anderson, P., 1958, Phys. Rev. **112**, 1900.
Andersson, G., S. E. Larsson, G. Leander, P. Möller, S. G.

Nilsson, I. Ragnarsson, S. Åberg, R. Bengtsson, J. Dudek, B. Nerlo-Pomorska, K. Pomorski, and Z. Szymański, 1976, Nucl. Phys. A **268**, 205.
Bacelar, J. C., C. Ellegaard, J. D. Garrett, G. B. Hagemann, B. Herskind, A. Holm, C.-X. Yang, J.-Y. Zhang, P. O. Tjøm, and J. C. Lisle, 1985, Nucl. Phys. A **442**, 509.
Bacelar, J. C., A. Holm, R. M. Diamond, E. M. Beck, M. A. Deleplanque, J. Draper, B. Herskind, and F. S. Stephens, 1987, Phys. Rev. C **35**, 1170.
Banerjee, B., H. J. Mang, and P. Ring, 1973, Nucl. Phys. A **215**, 366.
Bardeen, J., L. N. Cooper, and J. R. Schrieffer, 1957, Phys. Rev. **108**, 1175
Barranco, F., M. Gallardo, and R. A. Broglia, 1987, Phys. Lett. B **198**, 19.
Baym, G., and C. Pethick, 1975, in *The Helium Liquids,* edited by J. G. M. Armitage and I. E. Farquhar (Academic, New York), p. 417.
Beck, E. M., J. C. Bacelar, M. A. Deleplanque, R. M. Diamond, F. S. Stephens, J. E. Draper, B. Herskind, A. Holm, and P. O. Tjøm, 1987, Nucl. Phys. A **464**, 472.
Bengtsson, R., 1980, J. Phys. (Paris) Colloq. C **10**, 84.
Bengtsson, R., Y. S. Chen, J.-Y. Zhang, and S. Åberg, 1983, Nucl. Phys. A **405**, 221.
Bengtsson, R., and S. Frauendorf, 1979, Nucl. Phys. A **327**, 139.
Bengtsson, R., S. Frauendorf, and F.-R. May, 1986, At. Data Nucl. Data Tables **35**, 15.
Bengtsson, R., and J. D. Garrett, 1984, in *Collective Phenomena in Atomic Nuclei,* International Review of Nuclear Physics, Vol. 2, edited by T. Engeland, J. Rekstad, and J. S. Vaagen (World Scientific, Singapore), p. 193.
Bengtsson, R., and H. B. Häkansson, 1981, Nucl. Phys. A **357**, 61.
Bengtsson, R., I. Hamamoto, and R. H. Ibarra, 1978, Phys. Scr. **17**, 583.
Bengtsson, R., and J.-Y. Zhang, 1984, Phys. Lett. **135**, 358.
Bengtsson, T., and I. Ragnarsson, 1985, Nucl. Phys. A **436**, 14.
Bertsch, G. F., R. A. Broglia, and J. R. Schrieffer, 1988, Nuovo Cimento A **100**, 283.
Bés, D. R., and R. A. Broglia, 1966, Nucl. Phys. A **80**, 289.
Bés, D. R., R. A. Broglia, J. Dudek, W. Nazarewicz, and Z. Szymański, 1988, Ann. Phys. (N.Y.) **182**, 237.
Bés, D. R., R. A. Broglia, R. P. J. Perazzo, and K. Kumar, 1970, Nucl. Phys. A **143**, 1.
Bjerregaard, J. H., O. Hansen, O. Nathan, and S. Hinds, 1966, Nucl. Phys. **89**, 337.
Blume, K. P., H. Hübel, M. Murzel, J. Recht, K. Theine, H. Kluge, A. Kuhnert, K. H. Maier, A. Maj, M. Guttormsen, and A. P. DeLima, 1987, Nucl. Phys. A **464**, 445.
Bohr, A., 1976, in *Elementary Modes of Excitation in Nuclei,* edited by A. Bohr and R. A. Broglia (North-Holland, Amsterdam), p. 3.
Bohr, A., and B. R. Mottelson, 1969, *Nuclear Structure* (Benjamin, New York), Vol. I, p. 169.
Bohr, A., and B. R. Mottelson, 1975, *Nuclear Structure* (Benjamin, Reading, MA), Vol. II, Chap. 6.
Bohr, A., and B. R. Mottelson, 1981, Phys. Scr. **24**, 71.
Bohr, A., B. R. Mottelson, and D. Pines, 1958, Phys. Rev. **110**, 936.
Bortignon, P. F., R. A. Broglia, D. R. Bés, and R. Liotta, 1977, Phys. Rep. **30C**, 305.
Broglia, R. A., 1985, in *Theory of Nuclear Structure and Reactions,* edited by M. Lozano and G. Madurga (World Scientific, Singapore), p. 133.
Broglia, R. A., D. R. Bés, and B. Nilsson, 1974, Phys. Lett. B **50**, 213.
Broglia, R. A., M. Diebel, S. Frauendorf, and F. Barranco, 1985, in *Proceedings of the XXIII Winter Meeting on Nuclear Physics, Bormio, Italy,* edited by I. Iori (Ricerca Scientifica ed Educazione Permanente, Milano), p. 1.
Broglia, R. A., M. Diebel, S. Frauendorf, and M. Gallardo, 1986, Phys. Lett. B **166**, 252.
Broglia, R. A., and M. Gallardo, 1985, Nucl. Phys. A **447**, 489c.
Broglia, R. A., O. Hansen, and C. Riedel, 1973, Adv. Nucl. Phys. **6**, 287.
Broglia, R. A., C. Riedel, and B. Sørensen, 1968, Nucl. Phys. A **107**, 1.
Butler, P. A., C. Baktash, C. R. Bingham, M. Carpenter, D. Cline, B. Cox, M. W. Guidry, S. Juutinen, A. E. Kavka, W. J. Kernan, R. W. Kincaid, A. Larabee, I. Y. Lee, X. T. Liu, S. P. Sorensen, E. Vogt, and C. Y. Wu, 1987, Phys. Lett. B **191**, 333.
Canto, L. F., R. Donangelo, R. S. Nikam, and P. Ring, 1987, Phys. Lett. B **192**, 4.
Canto, L. F., P. Ring, and J. O. Rasmussen, 1985, Phys. Lett. B **161**, 21.
Chapman, R., J. C. Lisle, J. N. Mo, J. D. Garrett, G. B. Hagemann, and B. Herskind, 1986, in *Proceedings of the International Nuclear Physics Conference, Harrogate, U.K. . . . 1986,* edited by J. L. Durell, J. M. Irvine, and G. C. Morrison (Institute of Physics, Bristol), Vol. 1, p. 161.
Chapman, R., J. C. Lisle, J. N. Mo, E. Paul, J. C. Willmott, J. R. Leslie, H. G. Price, P. M. Walker, J. C. Bacelar, J. D. Garrett, G. B. Hagemann, B. Herskind, A. Holm, and P. J. Nolan, 1983, Phys. Rev. Lett. **51**, 2265.
Chu, S. Y., E. R. Marshalek, P. Ring, J. Krumlinde, and J. O. Rasmussen, 1975, Phys. Rev. C **12**, 1017.
Dasso, C. H., S. Landowne, R. A. Broglia, and A. Winther, 1984, Z. Phys. A **317**, 187.
Deleplanque, M. A., J. C. Bacelar, E. M. Beck, R. M. Diamond, J. E. Draper, R. J. McDonald, and F. S. Stephens, 1987, Phys. Lett. B **193**, 422.
Diebel, M., 1984, Nucl. Phys. A **419**, 221.
Dracoulis, G. D., H. Hubel, A. P. Byrne, and R. F. Davies, 1983, Nucl. Phys. A **405**, 363.
Dudek, J., A. Majhofer, and J. Skalski, 1980, J. Phys. G **6**, 447.
Egido, J. L., H. J. Mang, and P. Ring, 1980a, Nucl. Phys. A **339**, 390.
Egido, J. L., H. J. Mang, and P. Ring, 1980b, Nucl. Phys. A **341**, 229.
Egido, J. L., and J. O. Rasmussen, 1987, Phys. Rev. C **36**, 316.
Egido, J. L., and P. Ring, 1982a, Nucl. Phys. A **383**, 189.
Egido, J. L., and P. Ring, 1982b, Nucl. Phys. A **388**, 19.
Egido, J. L., and P. Ring, 1984, Nucl. Phys. A **423**, 93.
Egido, J. L., P. Ring, S. Iwasaki, and H. J. Mang, 1985, Phys. Lett. B **154**, 1.
Egido, J. L., P. Ring, and H. J. Mang, 1986, Nucl. Phys. A **451**, 77.
Faessler, A., K. R. Sandhya Devi, F. Grümmer, K. W. Schmid, and R. R. Hilton, 1976, Nucl. Phys. A **256**, 106.
Fetter, A. L., and J. D. Walecka, 1971, *Quantum Theory of Many-Particle Systems (McGraw-Hill, New York).*
Frandsen, P., J. D. Garrett, G. B. Hagemann, B. Herskind, M. A. Riley, R. Chapman, J. C. Lisle, J. N. Mo, L. Carlen, J. Lyttkens, H. Ryde, and P. M. Walker, 1986, Phys. Lett. B **177**, 287.
Frauendorf, S., 1981, Phys. Scr. **24**, 349.
Frauendorf, S., 1982, in *Nuclear Physics, Proceedings of the Nuclear Physics Workshop, ICTP, Trieste . . . 1981,* edited by C.

H. Dasso, R. A. Broglia, and A. Winther (North-Holland, Amsterdam), p. 111.
Frauendorf, S., 1984, in *Proceedings of Fifth Nordic Meeting on Nuclear Physics, Jyväskylä, Finland* (University of Jyväskylä, Jyväskylä), p. 19.
Garrett, J. D., 1982, in *Proceedings of the XX International Winter Meeting on Nuclear Physics, Bormio, Italy,* edited by I. Iori (Ricerca Scientifica ed Educazione Permanente, Milano), p. 1.
Garrett, J. D., 1983, Nucl. Phys. A **409**, 259c.
Garrett, J. D., 1984, Nucl. Phys. A **421**, 313c.
Garrett, J. D., 1985a, J. Phys. Soc. Jpn. **54**, Suppl., 456.
Garrett, J. D., 1985b, in *Nuclear Structure 1985,* edited by R. A. Broglia, G. B. Hagemann, and B. Herskind (North-Holland, Amsterdam), p. 111.
Garrett, J. D., 1988, in *The Response of Nuclei Under Extreme Conditions,* edited by R. A. Broglia and G. F. Bertsch (Plenum, New York), p. 1.
Garrett, J. D., O. Andersen, J. J. Gaardhøje, G. B. Hagemann, B. Herskind, J. Kownacki, J. C. Lisle, L. L. Riedinger, W. Waluś, N. Roy, S. Jönsson, H. Ryde, M. Guttormsen, and P. O. Tjøm, 1981, Phys. Rev. Lett. **47**, 75.
Garrett, J. D., G. B. Hagemann, B. Herskind, J. C. Bacelar, R. Chapman, J. C. Lisle, J. N. Mo, A. Simcock, J. C. Willmott, and H. G. Price, 1982, Phys. Lett. B **118**, 297.
Garrett, J. D., J. Nyberg, C. H. Yu, J. M. Espino, and M. J. Godfrey, 1988, in *Contemporary Topics in Nuclear Structure Physics,* edited by R. F. Casten *et al.* (World Scientific, Singapore), p. 699.
Gollub, J. P., M. R. Beasley, R. S. Newbower, and M. Tinkham, 1969, Phys. Rev. Lett. **22**, 1288.
Goodman, A. L., 1974, Nucl. Phys. A **230**, 466.
Goswami, A., L. Lin, and G. L. Struble, 1967, Phys. Lett. B **25**, 451.
Grin, Y. T., 1974, Phys. Lett. B **52**, 135.
Grosse, E., F. S. Stephens, and R. M. Diamond, 1973, Phys. Rev. Lett. **31**, 840.
Guidry, M. W., 1986, in *Conference on Nuclear Structure with Heavy Ions,* edited by R. A. Ricci and C. Villi (Editrice Compositori, Bologna), p. 99.
Harris, S. M., 1965, Phys. Rev. **138**, 509B.
Herskind, B., 1984, Annals Israel Phys. Soc. **7**, 3.
Herskind, B., 1985, Nucl. Phys. A **447**, 395c.
Högaasen-Feldman, J., 1961, Nucl. Phys. **28**, 258.
Johnson, A., H. Ryde, and J. Sztarkier, 1971, Phys. Lett. B **34**, 605.
Jónsson, S., N. Roy, H. Ryde, W. Waluś, J. Kownacki, J. D. Garrett, G. B. Hagemann, B. Herskind, R. Bengtsson, and S. Åberg, 1986, Nucl. Phys. A **449**, 537.
Juutinen, S., X. T. Liu, S. Sørensen, B. Cox, R. W. Kincaid, C. R. Bingham, M. W. Guidry, W. J. Kernan, C. Y. Wu, E. Vogt, T. Czosnyka, D. Cline, M. L. Halbert, I. Y. Lee, and C. Baktash, 1987, Phys. Lett. B **192**, 307.
Kownacki, J., J. D. Garrett, J. J. Gaardhøje, G. B. Hagemann, B. Herskind, S. Jónsson, N. Roy, H. Ryde, and W. Waluś, 1983, Nucl. Phys. A **394**, 269.
Lin, L., 1974, Lett. Nuovo Cimento **11**, 51.
Mahaux, C., P. F. Bortignon, R. A. Broglia, and C. H. Dasso, 1985, Phys. Rep. **120**, 1.
Mang, H. J., 1975, Phys. Rep. **18**, 325.
Mo, J. N., S. Sergiwa, R. Chapman, J. C. Lisle, E. Paul, J. C. Willmott, J. Hattula, M. Jääskeläinen, J. Simpson, P. M. Walker, J. D. Garrett, G. B. Hagemann, B. Herskind, M. A. Riley, and G. Sletten, 1987, Nucl. Phys. A **472**, 295.
Mottelson, B. R., and J. G. Valatin, 1960, Phys. Rev. Lett. **5**, 511.
Mutz, U., and P. Ring, 1984, J. Phys. G **10**, L39.
Nazarewicz, W., J. Dudek, R. Bengtsson, T. Bengtsson, and I. Ragnarsson, 1987, Nucl. Phys. A **435**, 397.
Nazarewicz, W., J. Dudek, and Z. Szymański, 1985, Nucl. Phys. A **436**, 139.
Nazarewicz, W., Z. Szymański, and J. Dudek, 1987, Phys. Lett. B **196**, 404.
Neergård, K., H. Toki, M. Ploszajczak, and A. Faessler, 1977, Nucl. Phys. A **287**, 48.
Nikam, R. S., and P. Ring, 1987, Phys. Rev. Lett. **58**, 980.
Nikam, R. S., P. Ring, and L. F. Canto, 1986, Z. Phys. A **324**, 241.
Nikam, R. S., P. Ring, and L. F. Canto, 1987, Phys. Lett. B **185**, 269.
Nilsson, S. G., and O. Prior, 1961, K. Dan. Vidensk. Selsk. Mat. Fys. Medd. **32**, No. 16.
Nyberg J., J. M. Espino, J. Gascon, C.-H. Yu, and J. D. Garrett, 1988, private communication.
Pakkanen, A., Y. H. Chung, P. J. Daly, S. R. Faber, H. Helppi, J. Wilson, P. Chowdhury, T. L. Khoo, I. Ahmad, J. Borggreen, Z. W. Grabowski, and D. C. Radford, 1982, Phys. Rev. Lett. **48**, 1530.
Peterson, R. J., and J. D. Garrett, 1984, Nucl. Phys. A **414**, 59.
Pines, D., and P. Nozières, 1966, *The Theory of Quantum Liquids* (Benjamin, New York).
Price, H. G., C. J. Lister, B. J. Varley, W. Gelletly, and J. W. Olness, 1983, Phys. Rev. Lett. **51**, 1842.
Ragnarsson, I., and R. A. Broglia, 1976, Nucl. Phys. A **263**, 315.
Riedinger, L. L., O. Andersen, S. Frauendorf, J. D. Garrett, J. J. Gaardhøje, G. B. Hagemann, B. Herskind, Y. V. Makovetzky, J. C. Waddington, M. Guttormsen, and P. O. Tjøm, 1980, Phys. Rev. Lett. **44**, 568.
Riley, M. A., J. C. Bacelar, J. D. Garrett, G. B. Hagemann, B. Herskind, R. Chapman, J. C. Lisle, J. M. Mo, J. Simpson, and J. F. Sharpey-Schafer, 1987, in *Proceedings of the International Conference on Nuclear Shapes, Crete, 1987,* edited by G. Anagnostatos *et al.* (NRC Demokritos, Athens), Vol. 1, p. 76.
Riley, M. A., J. D. Garrett, J. Simpson, and J. F. Sharpey-Schafer, 1988, Phys. Rev. Lett. **60**, 553.
Riley, M. A., J. Simpson, R. Aryaeinejad, J. R. Cresswell, P. D. Forsyth, D. Howe, P. J. Nolan, B. M. Nyako, J. F. Sharpey-Schafer, P. J. Twin, J. Bacelar, J. D. Garrett, G. B. Hagemann, B. Herskind, and A. Holm, 1984, Phys. Lett. B **135**, 275.
Ring, P., and P. Schuck, 1980, *The Nuclear Many-Body Problem* (Springer, Berlin).
Roy, N., S. Jónsson, H. Ryde, W. Waluś, J. J. Gaardhøje, J. D. Garrett, G. B. Hagemann, and B. Herskind, 1982, Nucl. Phys. A **382**, 125.
Schrieffer, J. R., 1964, *Theory of Superconductivity* (Benjamin, New York).
Schuck, C., N. Bendjaballah, R. M. Diamond, Y. Ellis-Akovali, K. H. Lindenberger, J. O. Newton, F. S. Stephens, J. D. Garrett, and B. Herskind, 1984, Phys. Lett. B **142**, 253.
Schuck, C., F. Hannachi, R. Chapman, J. C. Lisle, J. N. Mo, E. Paul, D. J. G. Love, P. J. Nolan, A. H. Nelson, P. M. Walker, Y. Ellis-Akovali, N. R. Johnson, N. Bendjaballah, R. M. Diamond, M. A. Deleplanque, F. S. Stephens, G. Dines, and J. Draper, 1985, in *Proceedings of the XXIII International Winter Meeting on Nuclear Physics, Bormio, Italy, 1985* (Ricerca Scientifica ed Educazione Permanente, Milano), p. 294.
Shastry, S., J. C. Bacelar, J. D. Garrett, G. B. Hagemann, B.

Herskind, and J. Kownacki, 1987, Nucl. Phys. A **470**, 253.
Shimizu, Y. R., 1987, in *Proceedings of the International Conference on Nuclear Shape, Crete, Greece, 1987,* edited by J. D. Garrett *et al.* (World Scientific, Singapore), p. 395.
Shimizu, Y. R., and R. A. Broglia, 1988, Nucl. Phys. A **476**, 228.
Shimizu, Y. R., and K. Matsuyanagi, 1982, Prog. Theor. Phys. **67**, 1641.
Shimizu, Y. R., and K. Matsuyanagi, 1983, Prog. Theor. Phys. **70**, 144.
Shimizu, Y. R., and K. Matsuyanagi, 1984a, Prog. Theor. Phys. **71**, 960.
Shimizu, Y. R., and K. Matsuyanagi, 1984b, Prog. Theor. Phys. **72**, 1017.
Shimizu, Y. R., and K. Matsuyanagi, 1985, Prog. Theor. Phys. **74**, 1346.
Shimizu, Y. R., and K. Matsuyanagi, 1986, Prog. Theor. Phys. **75**, 1161.
Shimizu, Y. R., E. Vigezzi, and R. A. Broglia, 1987, Phys. Lett. B **198**, 33
Simpson, J., P. A. Butler, P. D. Forsyth, J. F. Sharpey-Schafer, J. D. Garrett, G. B. Hagemann, B. Herskind, and L. P. Ekström, 1984, J. Phys. G **10**, 383.
Simpson, J., M. A. Riley, J. R. Cresswell, D. V. Elenkov, P. D. Forsyth, G. B. Hagemann, D. Howe, B. M. Nyako, L. Ogaza, J. C. Lisle, and J. F. Sharpey-Schafer, 1987, J. Phys. G **13**, 847.
Simpson, J., M. A. Riley, A. M. James, A. R. Mokhtar, H. W. Cranmer-Gordon, P. D. Forsyth, A. J. Kirwan, D. Howe, J. D. Morrison, and J. F. Sharpey-Schafer, 1987, J. Phys. G **13**, L235.
Stephens, F. S., and R. S. Simon, 1972, Nucl. Phys. A **183**, 257.
Sugawara-Tanabe, K., K. Tanabe, and H. J. Mang, 1981, Nucl. Phys. A **357**, 45.
Szymański, Z., 1985, in *Nuclear Structure 1985,* edited by R. A. Broglia, G. B. Hagemann, and B. Herskind (North-Holland, Amsterdam), p. 343.
Twin, P. J., P. J. Nolan, R. Aryaeinejad, D. J. G. Love, A. H. Nelson, and A. Kirwan, 1983, Nucl. Phys. A **409**, 343c.
Vigezzi, E., D. R. Bés, R. A. Broglia, and S. Frauendorf, 1988, Phys. Rev. C **38**, 1448.
Von Oertzen, W., H. G. Bohlen, B. Gebauer, R. Künkel, F. Pühlhofer, and D. Schüll, 1987, Z. Phys. A **326**, 463.
Wakai, M., and A. Faessler, 1978, Nucl. Phys. A **295**, 86.
Waluś, W., N. Roy, S. Jónsson, L. Carlén, H. Ryde, G. B. Hagemann, B. Herskind, J. D. Garrett, Y. S. Chen, J. Almberger, and G. Leander, 1981, Phys. Scr. **24**, 324.
Wapstra, A. H., and G. Audi, 1985, Nucl. Phys. A **432**, 1.
Wu, C. Y., X. T. Liu, S. P. Sorensen, R. W. Kincaid, M. W. Guidry, D. Cline, W. J. Kernan, E. Vogt, T. Czosnyka, A. E. Kavka, and B. Kotlinski, 1988, Phys. Rev. C (in press).
Wu, C. Y., X. T. Liu, S. P. Sorensen, R. W. Kincaid, M. W. Guidry, D. Cline, W. J. Kernan, E. Vogt, T. Czosnyka, A. E. Kavka, M. A. Stoyer, J. O. Rasmussen, and M. L. Halbert, 1987, Phys. Lett. B **188**, 25.
Zhang, J.-Y., J. D. Garrett, J. C. Bacelar, and S. Frauendorf, 1986, Nucl. Phys. A **453**, 104.